UNIVERSITY OF TWENTE.

The influence of a target motion model on the exact Bayesian filter recursion; research by particle filtering

Master thesis - Applied Mathematics - August 2010

J.J. van der Valk

Supervisors:
H.A.P. Blom - National Aerospace Laboratory NLR
A.A. Stoorvogel - University of Twente

Written by Aniek van der Valk
Master Thesis
August 2010

The influence of a target motion model on the exact Bayesian filter recursion; research by particle filtering

Supervisors:
Prof. Dr. Anton A. Stoorvogel (University of Twente, the Netherlands)
Dr. ir. Henk A. P. Blom (National Aerospace Laboratory NLR, the Netherlands)

UNIVERSITY OF TWENTE.

University of Twente
Department of Applied Mathematics
Mathematical System and Control Theory
P.O. Box 217
7500 AE Enschede
The Netherlands

Host organisation
National Aerospace Laboratory NLR
Department ATSI
Anthony Fokkerweg 2
1059CM Amsterdam

Preface

This is my thesis for the Master 'Applied Mathematics' at University of Twente, carried out at National Aerospace Laboratory NLR. The aim of my thesis is to investigate the influence of a target motion model on the exact Bayesian filter equations. Particle filtering will be used as tool to get more insight in the Bayesian filter recursion.

NLR is a Dutch organization that identifies, develops and applies high-tech knowledge in the aviation and aerospace sectors. At NLR I performed my research at the Air Transport Safety Institute (ATSI). NLR-ATSI is a consultancy and research organization that develops and applies world-class knowledge and expertise to improve air transport safety. NLR-ATSI supports worldwide stakeholders in air transport to understand and resolve complex safety implications of the new technologies and operations necessary to accommodate growth in air transport. Amongst customers of the safety institute are air navigation service providers, aviation authorities, airports and airlines.

I would like to thank my supervisors Dr. ir. Henk A. P. Blom at NLR and Prof. dr. Anton A. Stoorvogel at University of Twente for their supervision and support during my research. Henk, I enjoyed working with you very much and I appreciate a lot that you always found time to answer my questions. Anton, during our meetings you have given me a lot of new insights by approaching from another perspective. I would also like to thank Dr. Jaroslav Krystul for his willingness to be in the graduation committee.
I am very grateful to NLR for giving me the opportunity to perform my research. I would like to thank the members of ATSI for their interesting conversations during the lunch colloquia. Special thanks to Dr. ir. Mariken Everdij for her help with LateX and to ir. Edwin Bloem for his help with Matlab. Thanks to the members of NLR-ATTS for their interesting conversations during lunch, and also for letting me assist them with their experiments on NLR simulators as an F16 pilot, helicopter pilot or UAV operator. Many thanks to my colleagues Stefan, Waldo, Fedde, Frank, Anneloes, Veronica and Andrew for the great time we had, for the good talks and the fun with ping pong or rugby. Above all, I would like to thank Kelvin and my family and friends for their support and inspiration.

Aniek van der Valk BSc.
August 31, 2010

Summary

The goal of this thesis is to find out what role the underlying target motion model plays in tracking problems with S-turns. The target motion model is a hybrid stochastic dynamic model taking into account the state of the object and its mode. Furthermore, the observation process also satisfies a hybrid stochastic dynamic model.

To achieve this goal we derive the exact Bayesian filter recursion for several motion models and observation processes. We use Particle filtering to evaluate the Bayesian filter equations numerically.

In this thesis results are given of Monte Carlo simulations for the Hybrid Particle filter and the IMM filter algorithm for several different target motion models. Results show that all filters perform relatively well, when the target is switching between acceleration and deceleration. The results show no effect of the tracking problems caused by S-turns we expected.

For all tested filter scenarios IMM performs better than HPF. In most of the filter scenarios, IMM and HPF using the target motion model with three modes perform better than IMM and HPF using the target motion model with two modes.

Furthermore, results of two models with three modes show that the choice for a target motion model does effect the performance of HPF. We used a target motion model that permits the target to have a positive acceleration in deceleration mode because the prior deceleration value is assumed to satisfy a Gaussian distribution. The HPF filter using this model performs worse than the HPF filter using a model that does not permit the target to have a positive acceleration in deceleration mode.

We recommend to do further research to make a better target motion model that does not permit the target to have a positive acceleration in deceleration mode. Future work could be done to increase the amount of modes in the target motion model. More research could also be done to decrease the hight of the first peak in position RMS error, by making sure that the error cannot converge below a certain low value.

List of abbreviations

Abs HPF	HPF using the model with non-Gaussian acceleration noise from section 8.4
ARTAS	ATC Radar Tracker and Server
ATC	air traffic control
ATSI	Air Transport Safety Institute
CKB	Chapman-Kolmogorov-Bayes
HPF	Hybrid Particle Filter
i.i.d.	independent and identically distributed
IMM	Interacting Multiple Model
IS	importance sampling
MC	Monte Carlo
NLR	National Aerospace Laboratory NLR
PF	Particle Filter
SIR	Sampling Importance Resampling
UAV	Unmanned Aerial Vehicle

List of symbols

a	measurable function
abs	absolute value
A_1	measurable function
A_2	measurable function
B_1	measurable function
B_2	measurable function
c_t	constant with respect to (x, η)
C_1	measurable function
C_2	measurable function
χ	$0-1$ indicator
δ	Dirac *delta*-function
exp	Exponential function
$\eta \in \mathbb{M}$	parameter
$F \in \mathbb{R}^{n \times n}$	constant
$f_Y(y)$	probability density function of $Y = y$
$f_{X,Y}(x, y)$	joint probability density function of $(X, Y) = (x, y)$
$f_{X\|Y}(x\|y)$	conditional probability density of $X = x$ given $Y = y$
g	measurable function
$G \in \mathbb{R}^{m \times m'}$	measurable function
h	measurable function
$H \in \mathbb{R}^{n \times m}$	measurable function
$i \in \mathbb{N}$	parameter
$I(f_k)$	expectation of f_k
∞	infinity

$j \in \mathbb{N}$	parameter
$k \in \mathbb{N}$	parameter
$K \in \mathbb{R}$	constant
K_k	measurable function
$L \in \mathbb{R}^{n \times n}$	constant
m	dimension of y_k
m'	dimension of the measurement noise
$M \in \mathbb{N}$	constant
$\mathbb{M}$	set of M discrete modes
$\mu \in \mathbb{R}^n$	mean of the process $\{x_k = x \mid Y_k\}$
$\mu_0^{\theta,j}$	initial weight of particle j in mode θ
n	dimension of x_k
n'	dimension of the acceleration noise
N_p	number of particles
N_{eff}	effective sample size
N_{thres}	threshold sample size
$\mathcal{N}_{E,V}$	Gaussian distribution on $\mathbb{R}^n$ with parameters E and V
$\nu_i^{\theta,j}$	i.i.d. standard Gaussian variables of dimension one, independent of θ, j
$p_{x_k}(x)$	probability density function of $x_k = x$
$p_{X_k}(X)$	probability density function of $X_k = X$
$p_{x_k \mid Y_k}(x_k)$	conditional density of $x_k = x$ given Y_k
$p_{x_{k+1}, x_k \mid Y_k}(x, x')$	joint conditional probability density function of $(x_{k+1}, x_k) = (x, x')$ given Y_k
$p_{y_{k+1} \mid x_{k+1}}(y_{k+1} \mid x)$	conditional likelihood of the realization $y_{k+1} \in \mathbb{R}^m$ of the process $\{y_k\}$ at moment $k+1$ given $x_{k+1} = x \in \mathbb{R}^n$
p_k	measurable function
p_0^θ	initial mode probability of mode θ
$p\{X = x\}$	probability that $X = x$
$\pi_{\theta\eta}$	probability that the process $\{\theta_k\}$ at moment $k+1$ equals η, i.e. $\theta_{k+1} = \eta$, given that at moment k the process $\{\theta_k\}$ equals θ, i.e. $\theta_k = \theta$
Π	transition probability matrix with components $\pi_{\theta\eta}$
$q \in \mathbb{R}$	constant
$Q \in \mathbb{R}^{n \times n}$	covariance matrix of the process $\{w_k\}$
Q_k	measurable function
$r \in \mathbb{R}^n$	constant
$r_1 \in \mathbb{R}$	constant
$r_2 \in \mathbb{R}$	constant
r_n	amount of simulation runs
R_k	measurable function
$\mathbb{R}$	set of real numbers
$S \in \mathbb{R}^{n \times n}$	constant
σ_a	standard deviation of the acceleration noise
σ_m	standard deviation of the measurement error
$\Sigma \in \mathbb{R}^{n \times n}$	variance of the process $\{x_k = x \mid Y_k\}$
$T \in \mathbb{N}$	constant
$\theta \in \mathbb{M}$	parameter
$\{\theta_k\}$	discrete valued Markov process with transition probability matrix Π

$\{v_k\}$	sequence of i.i.d. standard Gaussian variables of dimension m, independent of $\{w_k\}$
$\{w_k\}$	zero mean Gaussian white noise process with covariance Q
$x \in \mathbb{R}^n$	parameter
$x' \in \mathbb{R}^n$	parameter
$X \in \mathbb{R}^n$	random vector
x_0	exact initial state
$x_0^{\theta,j}$	initial state of particle j in mode θ
$\{x_k\}$	Euclidean valued stochastic process
$\hat{x}_{k,i}$	filter estimation of x_k in run i at moment k
$\hat{x}_k^{HPF}$	output of the HPF cycle
$X_k = \{x_s; s \leq k\}$	the realization of the process $\{x_k\}$ up to and including moment k
$\{y_k\}$	observation process which observes the state x_k
$Y \in \mathbb{R}^n$	random vector
$Y_k = \{y_s; s \leq k\}$	the realization of the process $\{y_k\}$ up to and including moment k
z_k	measurable function
Z_k	measurable function

Contents

1 Introduction

In air traffic control (ATC), ARTAS (ATC Radar Tracker and Server) forms a critical link between the radars and the air traffic controller. ARTAS is a system designed to establish an accurate air situation picture of all traffic over a well-defined geographical area (e.g. the European Civil Aviation Conference), and to distribute the relevant surveillance information to a community of user systems. Amongst other techniques, ARTAS makes use of the Interacting Multiple Model (IMM) filter algorithm and a heuristic such that S-turns of objects are well processed. The question is; is this heuristic necessary because the IMM is an approximation or is this heuristic necessary because the underlying model causes a problem?

The goal of this research is to find out what role the underlying model plays in tracking problems with S-turns. The type of underlying model considered is as follows. For an aircraft a motion model is assumed. This motion model is a hybrid stochastic dynamic model taking into account the state (x-coordinate, y-coordinate, velocity, etc.) of the aircraft and its mode (turn left, straight ahead or turn right). Furthermore, the observation process also satisfies a hybrid stochastic dynamic model.

Rather than continuing with an approximate filter, in this study we use an exact Bayesian filter for the motion model and the observation process. Then we will use particle filtering to evaluate the Bayesian filter equations numerically. If we then find the same phenomenon, we know that the nature of the problem lies in the motion model and observation process.

Thus, this thesis is about the influence of the motion model on the exact Bayesian filter equations. The research question is: 'How does the choice for a certain motion model affect the exact Bayesian filter equations?'

The outline of this thesis will be as follows. First we will derive exact Bayesian filter recursions for several models. Section 2 presents an exact filter recursion for an Euclidean valued state model. In section 3 the exact Bayesian filer recursion for a hidden Markov model is derived. In section 4 we derive the exact Bayesian filter recursion for a hidden Markov model with observer.
To evaluate the exact Bayesian filter equations numerically, we will use particle filtering. Section 5 will address particle filters and their convergence. In section 6 we discuss particle filters for a system with state depending on the mode values at two different moments in time.
Section 7 will address the generalized IMM algorithm. Section 8 presents one-dimensional target motion models. In section 9 results are given of MC simulations for the Hybrid Particle filter and the IMM filter algorithm for the models given in section 8. Conclusions and recommendations are presented in section 10.

2 Exact filter recursion for Euclidean state model

Consider the Euclidean valued stochastic process $\{x_k\}$. The system considered satisfies a stochastic dynamical model of the form:

$$x_{k+1} = Fx_k + w_k \tag{1}$$

with $\{w_k\}$ is a zero mean, Gaussian white noise process with covariance Q. Furthermore, $x_k \in \mathbb{R}^n$, $w_k \in \mathbb{R}^{n'}$ and constant $F \in \mathbb{R}^{n\times n}$.

Consider the process $\{y_k\}$ which observes the state x_k. $\{y_k\}$ satisfies the following equation:

$$y_k = h(x_k) + g(x_k)v_k \tag{2}$$

where $\{v_k\}$ is a sequence of i.i.d. (independent and identically distributed) standard Gaussian variables and independent of w_k. Further, $y_k \in \mathbb{R}^m$, $v_k \in \mathbb{R}^{m'}$, and h and g are measurable mappings of $\mathbb{R}^n$ into $\mathbb{R}^m$.

The filtering problem is to estimate the conditional density $p_{x_k|Y_k}(x)$, $x \in \mathbb{R}^n$, of x_k given $Y_k = \{y_s; s \leq k\}$, i.e. Y_k denotes the realization of the process $\{y_k\}$ up to and including moment k. Following [Blom & Bar-Shalom, 2009], we develop the exact recursive equations for $p_{x_k|Y_k}(x)$. The characterization of this conditional density consists of two steps. In those two steps, we make use of Bayes' rule [Bagchi, 1993]. Bayes' rule states that for two random vectors $X = [X_1, ..., X_n]^T$ and $Y = [Y_1, ..., Y_n]^T$, with joint probability density function $f_{X,Y}(x, y)$ and $f_Y(y) \neq 0$, the conditional probability density of X given Y is defined by

$$f_{X|Y}(x|y) = \frac{f_{X,Y}(x, y)}{f_Y(y)} \tag{3}$$

The first step is a Chapman-Kolmogorov equation [Bagchi, 1993] for the evolution of x_k from k to $k+1$, i.e. the characterization of $p_{x_{k+1}|Y_k}(x)$ as a function of $p_{x_k|Y_k}(x)$. Let $p_{x_{k+1},x_k|Y_k}(x, x')$ denote the conditional density of $x_{k+1} = x$ and $x_k = x'$ given the realization Y_k:

$$\begin{aligned} p_{x_{k+1}|Y_k}(x) &= \int_{x'\in\mathbb{R}^n} p_{x_{k+1},x_k|Y_k}(x, x')dx' \\ &= \int_{x'\in\mathbb{R}^n} p_{x_{k+1}|x_k,Y_k}(x|\, x')p_{x_k|Y_k}(x')dx' \\ &= \int_{x'\in\mathbb{R}^n} p_{x_{k+1}|x_k}(x|\, x')p_{x_k|Y_k}(x')dx' \end{aligned} \tag{4}$$

Note that equation (4) uses the transition density $p_{x_{k+1}|x_k}(x|\, x')$. This transition density can be expressed as follows. Since $x_k = x'$ is given, the expression Fx' is deterministic. Now w_k is zero mean Gaussian white noise with covariance Q, thus x_{k+1} given $x_k = x'$ is a Gaussian process with mean Fx' and covariance Q. This leads to the following multivariate normal

distribution for x_{k+1} given $x_k = x'$:

$$p_{x_{k+1}|x_k}(x|\ x') = \frac{\exp\left\{-\frac{1}{2}[x - Fx']^T Q^{-1}[x - Fx']\right\}}{\text{Det}\left\{2\pi Q\right\}^{1/2}} \tag{5}$$

Substituting this in (4) yields:

$$p_{x_{k+1}|Y_k}(x) = \int\limits_{x' \in \mathbb{R}^n} \frac{\exp\left\{-\frac{1}{2}[x - Fx']^T Q^{-1}[x - Fx']\right\}}{\text{Det}\left\{2\pi Q\right\}^{1/2}}\ p_{x_k|Y_k}(x')dx' \tag{6}$$

The second step is the Bayes measurement update, i.e. the characterization of $p_{x_{k+1}|Y_{k+1}}(x)$ as a function of $p_{x_{k+1}|Y_k}(x)$. In the evaluation of this step, we use Bayes' rule.

$$\begin{aligned} p_{x_{k+1}|Y_{k+1}}(x) &= \frac{p_{x_{k+1},y_{k+1}|Y_k}(x, y_{k+1})}{p_{y_{k+1}|Y_k}(y_{k+1})} \\ &= \frac{p_{y_{k+1}|x_{k+1},Y_k}(y_{k+1}|x)p_{x_{k+1}|Y_k}(x)}{p_{y_{k+1}|Y_k}(y_{k+1})} \\ &= \frac{p_{y_{k+1}|x_{k+1}}(y_{k+1}|x)p_{x_{k+1}|Y_k}(x)}{p_{y_{k+1}|Y_k}(y_{k+1})} \end{aligned} \tag{7}$$

Now $\{v_k\}$ in (2) is a sequence of i.i.d. standard Gaussian variables. Thus the mean of v_k equals zero and the variance of v_k equals the $m' \times m'$ identity matrix. For given $x_k = x$, the expression $h(x_k)$ in (2) is deterministic. This means that $\{y_k|x_k = x\}$ is a Gaussian process with mean $h(x)$ and variance $g(x)g(x)^T$. This leads to the following multivariate normal distribution for y_k given $x_k = x$:

$$p_{y_k|x_k}(y|x) = \frac{\exp\left\{-\frac{1}{2}[y - h(x)]^T[g(x)g(x)^T]^{-1}[y - h(x)]\right\}}{\text{Det}\left\{2\pi g(x)g(x)^T\right\}^{1/2}} \tag{8}$$

The conditional likelihood $p_{y_{k+1}|x_{k+1}}(y_{k+1}, x)$ of the realization $y_{k+1} \in \mathbb{R}^m$ of the process $\{y_k\}$ at moment $k+1$ given $x_{k+1} = x$, is in this case a function of x;

$$p_{y_{k+1}|x_{k+1}}(y_{k+1}|x) = \frac{\exp\left\{-\frac{1}{2}[y_{k+1} - h(x)]^T[g(x)g(x)^T]^{-1}[y_{k+1} - h(x)]\right\}}{\text{Det}\left\{2\pi g(x)g(x)^T\right\}^{1/2}} \tag{9}$$

Further the conditional likelihood $p_{y_{k+1}|Y_k}(y_{k+1})$ of the realization $y_{k+1} \in \mathbb{R}^m$ of the process $\{y_k\}$ at moment $k+1$ given $Y_k = \{y_s; s \leq k\}$, is x-invariant. This constant with respect to x can be found for example through normalization of the conditional density $p_{x_k|Y_k}(x)$. We denote the conditional likelihood $p_{y_{k+1}|Y_k}(y_{k+1})$ by c_t, because the likelihood could depend on other variables e.g. time. Thus,

$$p_{y_{k+1}|Y_k}(y_{k+1}) = c_t \tag{10}$$

Now substituting (9) into (7) yields:

$$p_{x_{k+1}|Y_{k+1}}(x) = \frac{\exp\left\{-\frac{1}{2}[y_{k+1} - h(x)]^T[g(x)g(x)^T]^{-1}[y_{k+1} - h(x)]\right\}}{c_t \text{Det}\left\{2\pi g(x)g(x)^T\right\}^{1/2}}\ p_{x_{k+1}|Y_k}(x) \tag{11}$$

Substituting (6) into (11) yields:

$$\begin{aligned} & p_{x_{k+1}|Y_{k+1}}(x) \\ = & \frac{\exp\left\{-\frac{1}{2}[y_{k+1}-h(x)]^T[g(x)g(x)^T]^{-1}[y_{k+1}-h(x)]\right\}}{c_t \mathrm{Det}\left\{2\pi g(x)g(x)^T\right\}^{1/2}} \\ & \cdot \int\limits_{x'\in\mathbb{R}^n} \frac{\exp\left\{-\frac{1}{2}[x-Fx']^TQ^{-1}[x-Fx']\right\}}{\mathrm{Det}\left\{2\pi Q\right\}^{1/2}} \; p_{x_k|Y_k}(x')dx' \end{aligned} \tag{12}$$

This is a recursive equation for $p_{x_k|Y_k}(x)$.

Note that if $h(x) = Hx$ and $g(x) = G$, the system is linear and we can use the Kalman filter to estimate the state x_k from the observations $Y_k = \{y_s; s \leq k\}$ [Bagchi, 1993]. We choose to use the recursive equation for the conditional density $p_{x_k|Y_k}(x)$, because we want to investigate the exact filter equations.

2.1 Further evaluation

In general analytical reduction of (12) is not feasible. An exceptional case however is when $h(x) = Hx$ and $g(x) = G$ and the conditional density $p_{x_k|Y_k}(x)$ is Gaussian with mean μ and variance Σ. In that case we can further evaluate recursive equation (12);

$$\begin{aligned} & p_{x_{k+1}|Y_{k+1}}(x) \\ = & \frac{\exp\left\{-\frac{1}{2}[y_{k+1}-Hx]^T[GG^T]^{-1}[y_{k+1}-Hx]\right\}}{c_t \mathrm{Det}\left\{2\pi GG^T\right\}^{1/2}} \\ & \cdot \int\limits_{x'\in\mathbb{R}^n} \frac{\exp\left\{-\frac{1}{2}[x-Fx']^TQ^{-1}[x-Fx']\right\}}{\mathrm{Det}\left\{2\pi Q\right\}^{1/2}} \; \frac{\exp\left\{-\frac{1}{2}(x'-\mu)^T\Sigma^{-1}(x'-\mu)\right\}}{\mathrm{Det}\left\{2\pi\Sigma\right\}^{1/2}} dx' \end{aligned} \tag{13}$$

The integral in equation (13) can be written as:

$$\begin{aligned} & \int\limits_{x'\in\mathbb{R}^n} \frac{\exp\left\{-\frac{1}{2}[x-Fx']^TQ^{-1}[x-Fx']\right\}}{\mathrm{Det}\left\{2\pi Q\right\}^{1/2}} \; \frac{\exp\left\{-\frac{1}{2}(x'-\mu)^T\Sigma^{-1}(x'-\mu)\right\}}{\mathrm{Det}\left\{2\pi\Sigma\right\}^{1/2}} dx' \\ = & \int\limits_{x'\in\mathbb{R}^n} \exp\left\{-\frac{1}{2}[x'-p]^TS[x'-p]\right\} \frac{\exp\left\{-\frac{1}{2}q\right\}}{\mathrm{Det}\left\{2\pi Q\right\}^{1/2}\mathrm{Det}\left\{2\pi\Sigma\right\}^{1/2}} dx' \end{aligned} \tag{14}$$

with

$$S = F^TQ^{-1}F + \Sigma^{-1} \tag{15}$$

$$p = S^{-1}(F^TQ^{-1}x + \Sigma^{-1}\mu) \tag{16}$$

$$q = x^TQ^{-1}x + \mu^T\Sigma^{-1}\mu - p^TSp \tag{17}$$

Note that the inverse of S does exist because S is positive definite since $F^TQ^{-1}F \geq 0$ and $\Sigma^{-1} > 0$. Now equation (14) yields:

$$\begin{aligned} & \int_{x' \in \mathbb{R}^n} \exp\left\{-\frac{1}{2}[x'-p]^T S[x'-p]\right\} \frac{\exp\left\{-\frac{1}{2}q\right\}}{\mathrm{Det}\left\{2\pi Q\right\}^{1/2}\mathrm{Det}\left\{2\pi\Sigma\right\}^{1/2}} dx' \\ = & \frac{\exp\left\{-\frac{1}{2}q\right\}}{\mathrm{Det}\left\{2\pi Q\right\}^{1/2}\mathrm{Det}\left\{2\pi\Sigma\right\}^{1/2}} \cdot \mathrm{Det}\left\{2\pi S^{-1}\right\}^{1/2} \end{aligned} \tag{18}$$

and equation (13) yields:

$$\begin{aligned} & p_{x_{k+1}|Y_{k+1}}(x) \\ = & \frac{\exp\left\{-\frac{1}{2}[y_{k+1}-Hx]^T[GG^T]^{-1}[y_{k+1}-Hx]\right\}}{c_t \mathrm{Det}\left\{2\pi GG^T\right\}^{1/2}} \frac{\exp\left\{-\frac{1}{2}q\right\}\mathrm{Det}\left\{2\pi S^{-1}\right\}^{1/2}}{\mathrm{Det}\left\{2\pi Q\right\}^{1/2}\mathrm{Det}\left\{2\pi\Sigma\right\}^{1/2}} \\ = & K \cdot \exp\left\{-\frac{1}{2}[x-r]^T L[x-r]\right\} \end{aligned} \tag{19}$$

with

$$S = F^TQ^{-1}F + \Sigma^{-1}$$

$$L = Q^{-1} - Q^{-1}FS^{-1}F^TQ^{-1} + H^T(GG^T)^{-1}H \tag{20}$$

$$r = L^{-1}[Q^{-1}FS^{-1}\Sigma^{-1}\mu + H^T(GG^T)^{-1}y_{k+1}] \tag{21}$$

$$K = \frac{\exp\left\{-\frac{1}{2}\left[\mu^T\Sigma^{-1}\mu - \mu^T\Sigma^{-1}S^{-1}\Sigma^{-1}\mu + y_{k+1}^T(GG^T)^{-1}y_{k+1} - r^TLr\right]\right\}\mathrm{Det}\left\{2\pi S^{-1}\right\}^{1/2}}{c_t\ \mathrm{Det}\left\{2\pi GG^T\right\}^{1/2}\mathrm{Det}\left\{2\pi Q\right\}^{1/2}\mathrm{Det}\left\{2\pi\Sigma\right\}^{1/2}} \tag{22}$$

Note that the inverse of L does exist because L is positive definite since $Q^{-1} > 0$, $Q^{-1}FS^{-1}F^TQ^{-1} \geq 0$ and $H^T(GG^T)^{-1}H \geq 0$. We can rewrite L as (see Appendix A.1):

$$L = [F\Sigma F^T + Q]^{-1} + H^T(GG^T)^{-1}H \tag{23}$$

Because (see Appendix A.2):

$$Q^{-1}FS^{-1}\Sigma^{-1}\mu = [F\Sigma F^T + Q]^{-1}F\mu \tag{24}$$

We can rewrite r as:

$$\begin{aligned} r &= L^{-1}[Q^{-1}FS^{-1}\Sigma^{-1}\mu + H^T(GG^T)^{-1}y_{k+1}] \\ &= \left([F\Sigma F^T + Q]^{-1} + H^T(GG^T)^{-1}H\right)^{-1}\left([F\Sigma F^T + Q]^{-1}F\mu + H^T(GG^T)^{-1}y_{k+1}\right) \end{aligned} \tag{25}$$

Because $p_{x_{k+1}|Y_{k+1}}(x)$ is a density, the integral over this density should equal 1. Thus K can also be found by normalizing the density. That is K should be equal to $\mathrm{Det}\{2\pi L^{-1}\}^{-1/2}$. And c_t can be found in two ways, by using K or by evaluating $p_{y_{k+1}|Y_k}(y_{k+1})$. If we look at the expression for the new mean r, we see that it uses the previous mean μ, the previous

variance Σ and the measurement y_{k+1}.

From equation (19) we see that $p_{x_{k+1}|Y_{k+1}}(x)$ is a Gaussian distribution with mean r and variance L^{-1}. Thus when $p_{x_k|Y_k}(x)$ is Gaussian this leads to $p_{x_{k+1}|Y_{k+1}}(x)$ being Gaussian.

3 Exact Bayesian filter recursion for a hidden Markov model

Consider a two-component Markov process $\{x_k, \theta_k\}$, with $\{x_k\}$ an Euclidean valued stochastic process and $\{\theta_k\}$ a discrete valued process. The system considered satisfies a hybrid stochastic dynamical model of the form:

$$x_{k+1} = a(\theta_{k+1}, x_k) + b(\theta_{k+1})w_k \tag{26}$$

where w_k is a zero mean, Gaussian white noise process with covariance Q. Further, $\{\theta_k\}$ is an $\mathbb{M}$-valued Markov chain with transition probability matrix Π with components $\pi_{\theta\eta} = p\{\theta_{k+1} = \eta |\ \theta_k = \theta\}$.

The filtering problem is to estimate the conditional density $p_{\theta_k|X_k}(\theta)$ with $\theta \in \mathbb{M}$ of θ_k given $X_k = \{x_s; s \leq k\}$, i.e. the realization of the process $\{x_k\}$ up to and including moment k. Following [Blom & Bar-Shalom, 2009], we develop the exact recursive equations for $p_{\theta_k|X_k}(\theta)$. The characterization of this conditional density consists of two steps.

The first step is to characterize the Chapman-Kolmogorov equation for the evolution of x_k from k to $k+1$, i.e. the characterization of $p_{\theta_{k+1}|X_k}(\theta)$ as a function of $p_{\theta_k|X_k}(\theta)$:

$$p_{\theta_{k+1}|X_k}(\eta) = \sum_{\theta\in\mathbb{M}} p_{\theta_{k+1},\theta_k|X_k}(\eta,\theta) = \sum_{\theta\in\mathbb{M}} p_{\theta_{k+1}|\theta_k,X_k}(\eta|\ \theta)p_{\theta_k|X_k}(\theta) = \sum_{\theta\in\mathbb{M}} \pi_{\theta\eta}p_{\theta_k|X_k}(\theta) \tag{27}$$

The second step is the Bayes measurement update, i.e. the characterization of $p_{\theta_{k+1}|X_{k+1}}(\theta)$ as a function of $p_{\theta_{k+1}|X_k}(\theta)$. Using Bayes' rule we have

$$\begin{aligned} p_{\theta_{k+1}|X_{k+1}}(\eta) &= \frac{p_{\theta_{k+1},x_{k+1}|X_k}(\eta, x_{k+1})}{p_{x_{k+1}|X_k}(x_{k+1})} \\ &= \frac{p_{x_{k+1}|\theta_{k+1},X_k}(x_{k+1}|\eta)p_{\theta_{k+1}|X_k}(\eta)}{p_{x_{k+1}|X_k}(x_{k+1})} \\ &= \frac{p_{x_{k+1}|\theta_{k+1},x_k}(x_{k+1}|\eta, x_k)p_{\theta_{k+1}|X_k}(\eta)}{p_{x_{k+1}|X_k}(x_{k+1})} \end{aligned} \tag{28}$$

Note that equation (28) uses the conditional density $p_{x_{k+1}|\theta_{k+1},x_k}(x|\eta, x')$. Given the pair $(\theta_{k+1} = \eta, x_k = x')$ the expression $a(\eta, x')$ is deterministic and w_k is a zero mean Gaussian white noise process with covariance Q. Therefore, the process $\{x_{k+1}|\theta_{k+1} = \eta, x_k = x'\}$ is a Gaussian process with mean $a(\eta, x')$ and covariance $b(\eta)Qb(\eta)^T$. Now the conditional density $p_{x_{k+1}|\theta_{k+1},x_k}(x|\eta, x')$ can be expressed as follows:

$$p_{x_{k+1}|\theta_{k+1},x_k}(x|\eta, x') = \frac{\exp\left\{-\frac{1}{2}[x - a(\eta, x')]^T(b(\eta)Qb(\eta)^T)^{-1}[x - a(\eta, x')]\right\}}{\mathrm{Det}\{2\pi b(\eta)Qb(\eta)^T\}^{1/2}} \tag{29}$$

The conditional likelihood $p_{x_{k+1}|\,\theta_{k+1},x_k}(x_{k+1}|\eta,x_k)$ of the realization of $x_{k+1}\in\mathbb{R}^n$ of the process $\{x_k\}$ at moment $k+1$, given the realization of $x_k\in\mathbb{R}^n$ of the process $\{x_k\}$ at moment k, and $\theta_{k+1}=\eta$, is in this case a function of η:

$$p_{x_{k+1}|\theta_{k+1},x_k}(x_{k+1}|\eta,x_k)=\frac{\exp\left\{-\frac{1}{2}[x_{k+1}-a(\eta,x_k)]^T(b(\eta)Qb(\eta)^T)^{-1}[x_{k+1}-a(\eta,x_k)]\right\}}{\mathrm{Det}\{2\pi b(\eta)Qb(\eta)^T\}^{1/2}} \quad (30)$$

Further, the conditional likelihood $p_{x_{k+1}|X_k}(x_{k+1})$ of the realization $x_{k+1}\in\mathbb{R}^n$ of the process $\{x_k\}$ at moment $k+1$, given $X_k=\{x_s;s\leq k\}$, is (x,η)-invariant. This constant with respect to (x,η) can be found for example through normalization of the conditional density $p_{\theta_k|X_k}(\theta)$. We denote the conditional likelihood $p_{x_{k+1}|X_k}(x_{k+1})$ by c_t, because the likelihood could depend on other variables e.g. time. Thus,

$$p_{x_{k+1}|X_k}(x_{k+1})=c_t \quad (31)$$

Now substituting (30) and (31) into (28) yields:

$$p_{\theta_{k+1}|X_{k+1}}(\eta)=\frac{\exp\left\{-\frac{1}{2}[x_{k+1}-a(\eta,x_k)]^T(b(\eta)Qb(\eta)^T)^{-1}[x_{k+1}-a(\eta,x_k)]\right\}}{c_t\ \mathrm{Det}\{2\pi b(\eta)Qb(\eta)^T\}^{1/2}}\ p_{\theta_{k+1}|X_k}(\eta) \quad (32)$$

Substituting (27) into (32) yields:

$$p_{\theta_{k+1}|X_{k+1}}(\eta)=\frac{\exp\left\{-\frac{1}{2}[x_{k+1}-a(\eta,x_k)]^T(b(\eta)Qb(\eta)^T)^{-1}[x_{k+1}-a(\eta,x_k)]\right\}}{c_t\ \mathrm{Det}\{2\pi b(\eta)Qb(\eta)^T\}^{1/2}}\ \sum_{\theta\in\mathbb{M}}\pi_{\theta\eta}p_{\theta_k|X_k}(\theta) \quad (33)$$

This is a recursive equation for $p_{\theta_k|X_k}(\theta)$.

4 Exact Bayesian filter recursion for a hidden Markov model with observer

Consider a two-component Markov process $\{x_k, \theta_k\}$ with $\{x_k\}$ an Euclidean valued stochastic process and $\{\theta_k\}$ a discrete valued process. The system considered satisfies a hybrid stochastic dynamical model of the form:

$$x_{k+1} = a(\theta_{k+1}, x_k) + b(\theta_{k+1})w_k \tag{34}$$

where w_k is a zero mean, Gaussian white noise process with covariance Q. Further, $\{\theta_k\}$ is an $\mathbb{M}$-valued Markov chain with transition probability matrix Π with components $\pi_{\theta\eta} = p\{\theta_{k+1} = \eta |\ \theta_k = \theta\}$.

Consider the process $\{y_k\}$ which observes the state x_k. $\{y_k\}$ satisfies the following equation:

$$y_k = h(\theta_k, x_k) + g(\theta_k, x_k)v_k \tag{35}$$

where $\{v_k\}$ is a sequence of i.i.d. standard Gaussian variables of dimension m' and independent of w_k.

The filtering problem is to estimate the joint conditional density $p_{x_k,\theta_k|Y_k}(x,\theta)$, $x \in \mathbb{R}^n$, $\theta \in \mathbb{M}$, of the pair (x_k, θ_k) given $Y_k = \{y_s; s \leq k\}$, i.e. the realization of the process $\{y_k\}$ up to and including moment k. Following [Blom & Bar-Shalom, 2009], we develop the exact recursive equations for $p_{x_k,\theta_k|Y_k}(x,\theta)$. The characterization of this conditional density consists of two steps.

The first step is to characterize the Chapman-Kolmogorov equation for the evolution of the pair (x_k, θ_k) from k to $k+1$, i.e. the characterization of $p_{x_{k+1},\theta_{k+1}|Y_k}(x,\theta)$ as a function of $p_{x_k,\theta_k|Y_k}(\theta)$:

$$\begin{aligned}
p_{x_{k+1},\theta_{k+1}|Y_k}(x,\eta) &= \int\limits_{x'\in\mathbb{R}^n} p_{x_{k+1},x_k,\theta_{k+1}|Y_k}(x,x',\eta)dx' \\
&= \int\limits_{x'\in\mathbb{R}^n} p_{x_{k+1},\theta_{k+1}|x_k,Y_k}(x,\eta|x')p_{x_k|Y_k}(x')dx' \\
&= \int\limits_{x'\in\mathbb{R}^n} \sum_{\theta\in\mathbb{M}} p_{x_{k+1},\theta_{k+1},\theta_k|x_k,Y_k}(x,\eta,\theta|x')p_{x_k|Y_k}(x')dx' \\
&= \int\limits_{x'\in\mathbb{R}^n} \sum_{\theta\in\mathbb{M}} p_{x_{k+1},\theta_{k+1}|x_k,\theta_k,Y_k}(x,\eta|x',\theta)p_{\theta_k|Y_k}(\theta)p_{x_k|Y_k}(x')dx' \\
&= \int\limits_{x'\in\mathbb{R}^n} \sum_{\theta\in\mathbb{M}} p_{x_{k+1},\theta_{k+1}|x_k,\theta_k}(x,\eta|x',\theta)p_{x_k,\theta_k|Y_k}(x',\theta)dx'
\end{aligned} \tag{36}$$

Note that equation (36) uses the transition density $p_{x_{k+1},\theta_{k+1}|x_k,\theta_k}(x,\eta|x',\theta)$. This transition density can be expressed as follows:

$$\begin{aligned} p_{x_{k+1},\theta_{k+1}|x_k,\theta_k}(x,\eta|x',\theta) &= p_{x_{k+1}|\theta_{k+1},x_k,\theta_k}(x|\eta,x',\theta)p_{\theta_{k+1}|x_k,\theta_k}(\eta|x',\theta) \\ &= p_{x_{k+1}|\theta_{k+1},x_k}(x|\eta,x')p_{\theta_{k+1}|\theta_k}(\eta|\theta) \\ &= p_{x_{k+1}|\theta_{k+1},x_k}(x|\eta,x')\pi_{\theta,\eta} \end{aligned} \tag{37}$$

For a given $(\theta_{k+1}=\eta, x_k=x')$, the expression $a(\eta,x')$ is deterministic. Now w_k is zero mean Gaussian white noise with covariance Q. Thus $\{x_{k+1}|\theta_{k+1}=\eta, x_k=x'\}$ is a Gaussian process with mean $a(\eta,x')$ and covariance $b(\eta)Qb(\eta)^T$. This leads to the following multivariate normal distribution for x_{k+1} given $(\theta_{k+1}=\eta, x_k=x')$:

$$p_{x_{k+1}|\theta_{k+1},x_k}(x|\eta,x') = \frac{\exp\left\{-\frac{1}{2}[x-a(\eta,x')]^T(b(\eta)Qb(\eta)^T)^{-1}[x-a(\eta,x')]\right\}}{\mathrm{Det}\{2\pi b(\eta)Qb(\eta)^T\}^{1/2}} \tag{38}$$

This leads to the following expression for $p_{x_{k+1},\theta_{k+1}|x_k,\theta_k}(x,\eta|x',\theta)$:

$$\begin{aligned} p_{x_{k+1},\theta_{k+1}|\,x_k,\theta_k}(x,\eta|\,x',\theta) &= p_{x_{k+1}|\theta_{k+1},x_k}(x|\eta,x')p_{\theta_{k+1}|\theta_k}(\eta|\theta) \\ &= \frac{\exp\left\{-\frac{1}{2}[x-a(\eta,x')]^T(b(\eta)Qb(\eta)^T)^{-1}[x-a(\eta,x')]\right\}}{\mathrm{Det}\{2\pi b(\eta)Qb(\eta)^T\}^{1/2}}\ \pi_{\theta\eta} \end{aligned} \tag{39}$$

Substituting this into (36) yields:

$$\begin{aligned} & p_{x_{k+1},\theta_{k+1}|Y_k}(x,\eta) \\ = & \int\limits_{x'\in\mathbb{R}^n}\sum_{\theta\in\mathbb{M}} \frac{\exp\left\{-\frac{1}{2}[x-a(\eta,x')]^T(b(\eta)Qb(\eta)^T)^{-1}[x-a(\eta,x')]\right\}}{\mathrm{Det}(2\pi b(\eta)Qb(\eta)^T)^{1/2}}\ \pi_{\theta\eta}\ \ p_{x_k,\theta_k|Y_k}(x',\theta)dx' \\ = & \int\limits_{x'\in\mathbb{R}^n} \frac{\exp\left\{-\frac{1}{2}[x-a(\eta,x')]^T(b(\eta)Qb(\eta)^T)^{-1}[x-a(\eta,x')]\right\}}{\mathrm{Det}(2\pi b(\eta)Qb(\eta)^T)^{1/2}}\ \sum_{\theta\in\mathbb{M}}\pi_{\theta\eta}\ \ p_{x_k,\theta_k|Y_k}(x',\theta)dx' \end{aligned} \tag{40}$$

The second step is the Bayes measurement update, i.e. the characterization of $p_{x_{k+1},\theta_{k+1}|Y_{k+1}}(x,\theta)$ as a function of $p_{x_{k+1},\theta_{k+1}|Y_k}$. Using Bayes' rule we have

$$p_{x_{k+1},\theta_{k+1}|Y_{k+1}}(x,\eta) = \frac{p_{y_{k+1}|x_{k+1},\theta_{k+1}}(y_{k+1}|x,\eta)p_{x_{k+1},\theta_{k+1}|Y_k}(x,\eta)}{p_{y_{k+1}|Y_k}(y_{k+1})} \tag{41}$$

Now $\{v_k\}$ in (83) is a sequence of i.i.d. standard Gaussian variables. Thus the mean of v_k equals zero and the variance of v_k equals the $m'\times m'$ identity matrix. For a given pair (x_k,θ_k), the expression $h(\theta_k,x_k)$ in (83) is known. This means that $\{y_{k+1}|x_{k+1}=x,\theta_{k+1}=\eta\}$ is a Gaussian process with mean $h(\eta,x)$ and variance $g(\eta,x)g(\eta,x)^T$. This leads to the following multivariate normal distribution for y_{k+1} given the pair $(x_{k+1}=x,\theta_{k+1}=\eta)$:

$$p_{y_{k+1}|x_{k+1},\theta_{k+1}}(y|x,\eta) = \frac{\exp\left\{-\frac{1}{2}[y-h(\eta,x)]^T(g(\eta,x)g(\eta,x)^T)^{-1}[y-h(\eta,x)]\right\}}{\mathrm{Det}\left\{2\pi g(x,\eta)g(x,\eta)^T\right\}^{1/2}} \tag{42}$$

$p_{y_{k+1}|x_{k+1},\theta_{k+1}}(y_{k+1}|x,\eta)$ is the conditional likelihood of the realization of $y_{k+1} \in \mathbb{R}^m$ of the process $\{y_k\}$ at moment $k+1$, given $x_{k+1} = x$ and $\theta_{k+1} = \eta$. The conditional likelihood $p_{y_{k+1}|x_{k+1},\theta_{k+1}}(y_{k+1}|x,\eta)$ is in this case a function of x and η:

$$p_{y_{k+1}|x_{k+1},\theta_{k+1}}(y_{k+1}|x,\eta) = \frac{\exp\left\{-\frac{1}{2}[y_{k+1} - h(\eta,x)]^T (g(\eta,x)g(\eta,x)^T)^{-1}[y_{k+1} - h(\eta,x)]\right\}}{\mathrm{Det}\left\{2\pi g(x,\eta)g(x,\eta)^T\right\}^{1/2}} \tag{43}$$

Further, the conditional likelihood $p_{y_{k+1}|Y_k}(y_{k+1})$ of the realization $y_{k+1} \in \mathbb{R}^m$ of the process $\{y_k\}$ at moment $k+1$, given $Y_k = \{y_s; s \leq k\}$, is a (x,η)-invariant. This constant with respect to (x,η) can be found for example through normalization of the conditional density $p_{x_k,\theta_k|Y_k}$. We denote the conditional likelihood $p_{y_{k+1}|Y_k}(y_{k+1})$ by c_t, because the likelihood could depend on other variables e.g. time. Thus,

$$p_{y_{k+1}|Y_k}(y_{k+1}) = c_t \tag{44}$$

Now substituting (43) into (41) yields:

$$\begin{aligned} & p_{x_{k+1},\theta_{k+1}|Y_{k+1}}(x,\eta) \\ = \; & \frac{\exp\left\{-\frac{1}{2}[y_{k+1} - h(\eta,x)]^T (g(\eta,x)g(\eta,x)^T)^{-1}[y_{k+1} - h(\eta,x)]\right\}}{c_t \ \mathrm{Det}\{2\pi g(x,\eta)g(x,\eta)^T\}^{1/2}} \ p_{x_{k+1},\theta_{k+1}|Y_k}(x,\eta) \end{aligned} \tag{45}$$

Substituting (40) into (45) yields:

$$\begin{aligned} & p_{x_{k+1},\theta_{k+1}|Y_{k+1}}(x,\eta) \\ = \; & \frac{\exp\left\{-\frac{1}{2}[y_{k+1} - h(\eta,x)]^T (g(\eta,x)g(\eta,x)^T)^{-1}[y_{k+1} - h(\eta,x)]\right\}}{c_t \ \mathrm{Det}\left\{2\pi g(x,\eta)g(x,\eta)^T\right\}^{1/2}} \\ & \cdot \int\limits_{x' \in \mathbb{R}^n} \frac{\exp\left\{-\frac{1}{2}[x - a(\eta,x')]^T (b(\eta)Qb(\eta)^T)^{-1}[x - a(\eta,x')]\right\}}{\mathrm{Det}\left\{2\pi b(\eta)Qb(\eta)^T\right\}^{1/2}} \ \sum_{\theta \in \mathbb{M}} \pi_{\theta\eta} \ p_{x_k,\theta_k|Y_k}(x',\theta)dx' \end{aligned} \tag{46}$$

This is a recursive equation for $p_{x_{k+1},\theta_{k+1}|Y_{k+1}}(x,\eta)$. We can rewrite this equation as follows (see Appendix A.3):

$$\begin{aligned} & p_{x_{k+1},\theta_{k+1}|Y_{k+1}}(x,\eta) \\ = \; & \int\limits_{x' \in \mathbb{R}^n} \frac{\exp\left\{-\frac{1}{2}\left(r_1 + r_2\right)\right\}}{c_t \left(\mathrm{Det}\left\{2\pi g(x,\eta)g(x,\eta)^T\right\} \mathrm{Det}\left\{2\pi b(\eta)Qb(\eta)^T\right\}\right)^{1/2}} \ \sum_{\theta \in \mathbb{M}} \pi_{\theta\eta} \ p_{x_k,\theta_k|Y_k}(x',\theta)dx' \end{aligned} \tag{47}$$

where

$$r_1 = [y_{k+1} - h(\eta,x)]^T (g(\eta,x)g(\eta,x)^T)^{-1}[y_{k+1} - h(\eta,x)] \tag{48}$$

$$r_2 = [x - a(\eta,x')]^T (b(\eta)Qb(\eta)^T)^{-1}[x - a(\eta,x')] \tag{49}$$

5 Particle filter

5.1 Introduction

To investigate the influence of a target motion model on the exact Bayesian filter equations, we may simulate this filtering process with a particle filter. Since their introduction in 1993 [Gordon et al., 1993], particle filters have become a very popular class of numerical methods for the solution of optimal estimation problems in non-linear non-Gaussian scenarios. In 1993 the particle filter was known as the bootstrap filter. Particle methods are a subset of the class of methods known as Sequential Monte Carlo methods. In comparison with the standard approximation methods, such as the Extended Kalman Filter, the principal advantage of particle methods is that they do not rely on any local liberalization technique or any functional approximation.

According to the strong law of large numbers, the approximation density almost sure converges to the exact conditional density if the number of particles used in the approximation is going to infinity [van der Merwe et al., 2000]. This is why a particle filter has been selected to investigate the influence of a target motion model on the exact conditional density. As many particles as necessary for a good enough approximation of the joint conditional density will be used. The purpose is not to decrease the number of particles but to investigate the joint conditional density with a particle filter as an arbitrary accurate numerical approximation technique.

5.2 The filtering problem

Following [Blom & Bloem, 2007], let $\{x_k, \theta_k\}$ be a hybrid state process, with x_k assuming values in $\mathbb{R}^n$ and θ_k assuming values in a finite set $\mathbb{M}$ of possible modes, be a hidden state process to be estimated from noisy observations $\{y_k\}$, with y_k assuming values in $\mathbb{R}^m$. Consider the following system of stochastic difference equations, on $[0, T]$, $T < \infty$,

$$x_k = a(\theta_k, x_{k-1}, w_k) \tag{50}$$

$$\theta_k = c(\theta_{k-1}, x_{k-1}, u_k) \tag{51}$$

$$y_k = h(\theta_k, x_k, v_k) \tag{52}$$

where the pair (x_k, θ_k) represents the hybrid system state, and y_k represents the observation at moment k, $\{w_k\}$ and $\{v_k\}$ are independent sequences of i.i.d. standard Gaussian variables of dimension n' and m' respectively, $\{u_k\}$ is an $\{w_k, v_k\}$-independent sequence of i.i.d. standard uniform random variables, $\{w_k, v_k, u_k\}$ is independent of the $\mathbb{R}^n \times \mathbb{M}$ valued initial condition (x_0, θ_0), with $\mathbb{M}$ a set of M discrete modes. Furthermore, a and h are measurable mappings of $\mathbb{M} \times \mathbb{R}^n \times \mathbb{R}^{n'}$ into $\mathbb{R}^n$ and $\mathbb{M} \times \mathbb{R}^n \times \mathbb{R}^{m'}$ into $\mathbb{R}^m$ respectively, and c is a measurable mapping of $\mathbb{M} \times \mathbb{R}^n \times [0, 1]$ into $\mathbb{M}$. The mappings a, c and h are time-invariant for notational simplicity only.

The filtering problem is to estimate the joint conditional density-probability $p_{x_k, \theta_k | Y_k}(x, \theta)$, $x \in \mathbb{R}^n$, $\theta \in \mathbb{M}$, of the pair (x_k, θ_k) given the sequence of observations $Y_k = \{y_s; s \leq k\}$.

5.3 SIR particle filter

A common particle filter used in nonlinear filtering studies is the Sampling Importance Resampling (SIR) particle filter. It has shown to form an elegant and general approach towards the numerical evaluation of the conditional density of the Chapman-Kolmogorov-Bayes (CKB) filter recursion. The SIR particle filter is also capable in approximating the CKB equations of a stochastic hybrid Markov process $\{x_k, \theta_k\}$, with x_k assuming values in $\mathbb{R}^n$, and θ_k assuming values in a finite set $\mathbb{M}$ of possible modes. Therefore the SIR particle filter shall be used.
The SIR particle filter uses N_p particles. Each particle j has two-components (x_k^j, θ_k^j) at moment k, with x_k^j assuming an Euclidean value and θ_k^j assuming a discrete value.

Now we will present the SIR particle filter cycle applied to the model given in section 5.2. Each SIR particle filter cycle from $k-1$ to k consists of three steps [Blom & Bloem, 2007]:

- **Evolution.** For each of the N_p particles at moment $k-1$, draw a new hybrid particle $(\bar{x}_k^j, \bar{\theta}_k^j)$ according to the Chapman-Kolmogorov transition kernel. That is for each particle sample a state at moment k given the state of that particle at moment $k-1$, the transition probability matrix Π for the $\mathbb{M}$-valued Markov chain $\{\theta_k\}$ and the hybrid stochastic dynamical model for the process $\{x_k\}$.
- **Correction.** For each of the N_p particles evaluate $\bar{\mu}_k^j$ as the likelihood of the measurement at moment k, given $(\bar{x}_k^j, \bar{\theta}_k^j)$ and normalize the resulting $\bar{\mu}_k^j$'s. In this way, each particle is given a weight on the basis of the measurement and the sampled state of the particle.
- **Resampling.** Draw N_p independently identically distributed (i.i.d.) hybrid particle values (x_k^j, θ_k^j), from the sum of $\bar{\mu}_k^j$ weighted Dirac measures at $(\bar{x}_k^j, \bar{\theta}_k^j)$. That is we draw N_p new particles and each particle $(\bar{x}_k^j, \bar{\theta}_k^j)$ is drawn with probability $\bar{\mu}_k^j$.

Table 1 gives an overview of the SIR particle filter cycle for the filter problem setting of equations (50)-(52). In this table, $\chi(\theta, \theta_{k-1}^j)$ is a $0-1$ indicator with $\chi(\theta, \theta_{k-1}^j) = 1$ if $\theta = \theta_{k-1}^j$. Note that $p_{y_k|x_k,\theta_k}(y_k|\bar{x}_k^j, \bar{\theta}_k^j)$ is the likelihood of the measurement at moment k given $(\bar{x}_k^j, \bar{\theta}_k^j)$. The table without step (3) resampling, i.e. $N_{tres} = 0$, is given by [Blom & Bloem, 2007]. Step (3) resampling is given by [Doucet, 1998] and shall be discussed further on in this section.

Table 1: SIR Particle Filter (SIR PF) cycle

SIR $\quad \tilde{p}_{x_{k-1},\theta_{k-1}|Y_{k-1}} \rightarrow \tilde{p}_{x_k,\theta_k|Y_k}$

(1) Particles $\quad \left\{\mu^j_{k-1} \in [0,1], \theta^j_{k-1} \in \mathbb{M}, x^j_{k-1} \in \mathbb{R}^n; j = 1, ..., N_p\right\}$

$$\tilde{p}_{x_{k-1},\theta_{k-1}|Y_{k-1}}(x,\theta) = \sum_{j=1}^{N_p} \mu^j_{k-1}\chi(\theta,\theta^j_{k-1})\delta(x - x^j_{k-1})$$

(2) For $j = 1, ..., N_p$:

(a) Generate w^j_k and u^j_k i.i.d. from $p_{w_k}(w)$ and $p_{u_k}(u)$

(b) Evolution:

$$\bar{\theta}^j_k = c(\theta^j_{k-1}, x^j_{k-1}, u^j_k)$$
$$\bar{x}^j_k = a(\bar{\theta}^j_k, x^j_{k-1}, w^j_k)$$

(c) Correction:

$$\bar{\mu}^j_k = \mu^j_{k-1} \cdot p_{y_k|x_k,\theta_k}(y_k|\bar{x}^j_k, \bar{\theta}^j_k)/c_t$$

with c_t such that $\sum_{j=1}^{N_p} \bar{\mu}^j_k = 1$

(3) Resampling:

Evaluate $\widehat{N_{eff}}$:

$$\widehat{N_{eff}} = \frac{1}{\sum_{j=1}^{N_p}(\bar{\mu}^j_k)^2}$$

If $\widehat{N_{eff}} \geq N_{tres}$

$$\mu^j_k = \bar{\mu}^j_k$$
$$(x^j_k, \theta^j_k) = (\bar{x}^j_k, \bar{\theta}^j_k)$$

Else i.e. $\widehat{N_{eff}} < N_{tres}$

$$\mu^j_k = 1/N_p$$
$$(x^j_k, \theta^j_k) \sim \sum_{j=1}^{N_p} \bar{\mu}^j_k \chi(\theta, \bar{\theta}^j_k)\delta(x - \bar{x}^j_k)$$

5.4 Convergence of a particle filter

This subsection explains from a theoretical point of view why the SIR particle filter gives a good estimation of the exact Bayesian filter equations.

5.4.1 Problem statement

Following [Doucet, 1998], we estimate recursively in time the distribution $p_{X_k,\Theta_k|Y_k}(X,\Theta)$, where $X_k = \{x_0, ..., x_k\}$, $\Theta_k = \{\theta_0, ..., \theta_k\}$ and $Y_k = \{y_0, ..., y_k\}$, and with $X \in \mathbb{R}^{(k+1)\times n}$, $\Theta \in \mathbb{M}^{k+1}$. Why we use this approach will be shown further on. From $p_{X_k,\Theta_k|Y_k}(X,\Theta)$ we obtain $p_{x_k,\theta_k|Y_k}(x,\theta)$ by marginalizing over the variables that are not of interest. Thus, for $p_{X_k,\Theta_k|Y_k}(X,\Theta) = p_{X_{k-1},x_k,\Theta_{k-1},\theta_k|Y_k}(X',x,\Theta',\theta)$:

$$p_{x_k,\theta_k|Y_k}(x,\theta) = \sum_{\Theta' \in \mathbb{M}^k} \int_{X' \in \mathbb{R}^{k\times n}} p_{X_{k-1},x_k,\Theta_{k-1},\theta_k|Y_k}(X',x,\Theta',\theta)dX' \tag{53}$$

This implies that we can estimate recursively in time the distribution $p_{x_k,\theta_k|Y_k}(x,\theta)$ from marginalizing the estimation of $p_{X_k,\Theta_k|Y_k}(X,\Theta)$.

Further, the filtering problem is also to estimate the expectation

$$I(f_k) \triangleq \mathbb{E}_{p_{X_k,\Theta_k|Y_k}(X,\Theta)}(f_k(X,\Theta)) = \sum_{\Theta \in \mathbb{M}^{k+1}} \int_{X \in \mathbb{R}^{(k+1)\times n}} f_k(X,\Theta) p_{X_k,\Theta_k|Y_k}(X,\Theta)dX \tag{54}$$

for any $p_{X_k,\Theta_k|Y_k}(X,\Theta)$-integrable $f_k : \mathbb{R}^{(n+1)\times n_x} \times \mathbb{M}^{k+1} \to \mathbb{R}$. In other words, for every function $f_k : \mathbb{R}^{(n+1)\times n_x} \times \mathbb{M}^{k+1} \to \mathbb{R}$ for which the integral of $f_k(X,\Theta)p_{X_k,\Theta_k|Y_k}(X,\Theta)$ with respect to X exists.

The reason why we use $p_{X_k,\Theta_k|Y_k}(X,\Theta)$ instead of $p_{x_k,\theta_k|Y_k}(x,\theta)$ is because $p_{X_k,\Theta_k|Y_k}(X,\Theta)$ can be expressed by a recursive formula. In the derivation of this recursive formula, we will use the following:

$$p_{A|B}(a,b) = \frac{p_{A,B}(a,b)}{p_B(b)} = \frac{p_{B|A}(b|a)p_A(a)}{p_B(b)} \tag{55}$$

Using this, $p_{X_k,\Theta_k|Y_k}(X,\Theta)$ can be expressed as follows:

$$p_{X_{k+1},\Theta_{k+1}|Y_{k+1}}(X,\Theta) = \frac{p_{Y_{k+1}|X_{k+1},\Theta_{k+1}}(Y_{k+1}|X,\Theta)p_{X_{k+1},\Theta_{k+1}}(X,\Theta)}{p_{Y_{k+1}}(Y_{k+1})} \tag{56}$$

Due to the stochastic differential equations (50), (51) and (52) of the system, $p_{X_{k+1},\Theta_{k+1}}(X,\Theta)$ yields:

$$
\begin{aligned}
p_{X_{k+1},\Theta_{k+1}}(X,\Theta) &= p_{x_{k+1},\theta_{k+1},X_k,\Theta_k}(x,\eta,X',\Theta') \\
&= p_{x_{k+1},\theta_{k+1}|X_k,\Theta_k}(x,\eta|X',\Theta')p_{X_k,\Theta_k}(X',\Theta') \\
&= p_{x_{k+1},\theta_{k+1}|x_k,\theta_k}(x,\eta|x',\theta)p_{X_k,\Theta_k}(X',\Theta') \qquad (57)
\end{aligned}
$$

Further, $p_{Y_{k+1}|X_{k+1},\Theta_{k+1}}(Y_{k+1}|X,\Theta)$ can be expressed as:

$$
\begin{aligned}
p_{Y_{k+1}|X_{k+1},\Theta_{k+1}}(Y_{k+1}|X,\Theta) &= p_{y_{k+1},Y_k|X_{k+1},\Theta_{k+1}}(y_{k+1},Y_k|X,\Theta) \\
&= p_{y_{k+1}|Y_k,X_{k+1},\Theta_{k+1}}(y_{k+1}|Y_k,X,\Theta)p_{Y_k|X_{k+1},\Theta_{k+1}}(Y_k|X,\Theta) \\
&= p_{y_{k+1}|x_{k+1},\theta_{k+1}}(y_{k+1}|x,\eta)p_{Y_k|X_k,\Theta_k}(Y_k|X',\Theta') \qquad (58)
\end{aligned}
$$

$p_{Y_{k+1}}(Y_{k+1})$ satisfies:

$$
p_{Y_{k+1}}(Y_{k+1}) = p_{y_{k+1},Y_k}(y_{k+1},Y_k) = p_{y_{k+1}|Y_k}(y_{k+1}|Y_k)p_{Y_k}(Y_k) \qquad (59)
$$

Using (56), (57), (58) and (59) we have:

$$
\begin{aligned}
& p_{X_{k+1},\Theta_{k+1}|Y_{k+1}}(X,\Theta) \\
= \; & \frac{p_{Y_{k+1}|X_{k+1},\Theta_{k+1}}(Y_{k+1}|X,\Theta)p_{X_{k+1},\Theta_{k+1}}(X,\Theta)}{p_{Y_{k+1}}(Y_{k+1})} \\
= \; & \frac{p_{X_k,\Theta_k}(X',\Theta')p_{X_k,\Theta_k}(X',\Theta')}{p_{Y_k}(Y_k)} \quad \frac{p_{x_{k+1},\theta_{k+1}|x_k,\theta_k}(x,\eta|x',\theta)p_{x_{k+1},\theta_{k+1}|x_k,\theta_k}(x,\eta|x',\theta)}{p_{y_{k+1}|Y_k}(y_{k+1}|Y_k)} \\
= \; & p_{X_k,\Theta_k|Y_k}(X',\Theta') \quad \frac{p_{y_{k+1}|x_{k+1},\theta_{k+1}}(y_{k+1}|x,\theta)p_{x_{k+1},\theta_{k+1}|x_k,\theta_k}(x,\eta|x',\theta)}{p_{y_{k+1}|Y_k}(y_{k+1}|Y_k)} \qquad (60)
\end{aligned}
$$

5.4.2 Approximation of a density through particles

Let us assume that we are able to simulate N_p i.i.d. random samples $\{(X_k^j,\Theta_k^j); j = 1,...,N_p\}$ according to $p_{X_k,\Theta_k|Y_k}(X,\Theta)$. An approximation $\widetilde{p}_{X_k,\Theta_k|Y_k}(X,\Theta)$ of $p_{X_k,\Theta_k|Y_k}(X,\Theta)$ is given by:

$$
\widetilde{p}_{X_k,\Theta_k|Y_k}(X,\Theta) = \frac{1}{N_p}\sum_{j=1}^{N_p}\chi(\Theta,\Theta_k^j)\delta(X - X_k^j) \qquad (61)
$$

where $\chi(\Theta,\Theta_k^j)$ is a $0-1$ indicator with $\chi(\Theta,\Theta_k^j) = 1$ if $\Theta = \Theta_k^j$ and with $\delta(.)$ the Dirac δ-function. Given the approximated distribution function in (61), one obtains the following approximation of $I(f_k)$:

$$\widetilde{I}_{N_p}(f_k) = \sum_{\Theta \in \mathbb{M}^{k+1}} \int_{X \in \mathbb{R}^{(k+1)\times n}} f_k(X,\Theta)\hat{p}_{X_k,\Theta_k|Y_k}(X,\Theta)dX = \frac{1}{N_p}\sum_{j=1}^{N_p} f_k(X_k^j,\Theta_k^j) \tag{62}$$

From the strong law of large numbers [Ross, 1996],

$$P\left\{\lim_{N_p\to\infty} \overline{I}_{N_p}(f_k) = I(f_k)\right\} = 1 \tag{63}$$

i.e. $\overline{I}_{N_p}(f_k)$ converges almost sure to $I(f_k)$ when $N_p \to \infty$.

A problem arises when $p_{X_k,\Theta_k|Y_k}(X,\Theta)$ is unknown, because then we cannot sample from $p_{X_k,\Theta_k|Y_k}(X,\Theta)$. In that case we may use importance sampling (IS). The basic idea of IS is to choose a so-called importance function $\pi_k(X,\Theta)$, which is a probability distribution from which one can easily sample. Further, the importance function $\pi_k(X,\Theta)$ should satisfy $\pi_k(X,\Theta) > 0$ whenever $p_{X_k,\Theta_k|Y_k}(X,\Theta) > 0$. Now we can write:

$$\begin{aligned} I(f_k) &= \sum_{\Theta \in \mathbb{M}^{k+1}} \int_{X \in \mathbb{R}^{(k+1)\times n}} f_k(X,\Theta)\frac{p_{X_k,\Theta_k|Y_k}(X,\Theta)}{\pi_k(X,\Theta)} \quad \pi_k(X,\Theta)dX & (64)\\ &= \mathbb{E}_{\pi_k(X,\Theta)}[f_k(X,\Theta)w_k^*(X,\Theta)] & (65)\end{aligned}$$

where

$$w_k^*(X,\Theta) = \frac{p_{X_k,\Theta_k|Y_k}(X,\Theta)}{\pi_k(X,\Theta)} \tag{66}$$

Thus if we simulate N_p i.i.d. samples $\{(X_k^j,\Theta_k^j); j = 1,...,N_p\}$ according to $\pi_k(X,\Theta)$, an approximation of $I(f_k)$ is:

$$\widehat{I}_{N_p}^*(f_k) = \frac{1}{N_p}\sum_{j=1}^{N_p} f_k(X_k^j,\Theta_k^j)w_k^{*(j)} \tag{67}$$

where the importance weights $\{w_k^{*(j)}, j = 1,...,N_p\}$ are equal to:

$$w_k^{*(j)} = w_k^*(X_k^{(j)},\Theta_k^{(j)}) = \frac{p_{X_k,\Theta_k|Y_k}(X_k^{(j)},\Theta_k^{(j)})}{\pi_k(X_k^{(j)},\Theta_k^{(j)})} = \frac{p_{Y_k|X_k,\Theta_k}(Y_k|X_k^{(j)},\Theta_k^{(j)})p_{X_k,\Theta_k}(X_k^{(j)},\Theta_k^{(j)})}{p_{Y_k}(Y_k)\pi_k(X_k^{(j)},\Theta_k^{(j)})} \tag{68}$$

The estimate $\widehat{I}_{N_p}^*(f_k)$ is unbiased, i.e. $\mathbb{E}[\widehat{I}_{N_p}^*(f_k)|I(f_k)] = I(f_k)$ [Ross, 1996], and converges almost sure according to the strong law of large numbers toward $I(f_k)$ when $N_p \to \infty$ [Doucet, 1998].

Note that $p_{Y_k}(Y_k)$ is (X,Θ)-invariant and therefore it can be found by normalization. Let $w_k^{(j)}$ be defined as follows:

$$w_k^{(j)} \triangleq p_{Y_k}(Y_k)w_k^{*(j)} \tag{69}$$

Then substitution of (68) yields

$$w_k^{(j)} = \frac{p_{Y_k|X_k,\Theta_k}(Y_k|X_k^{(j)},\Theta_k^{(j)})p_{X_k,\Theta_k}(X_k^{(j)},\Theta_k^{(j)})}{\pi_k(X_k^{(j)},\Theta_k^{(j)})} \tag{70}$$

Using $w_k^{(j)}$ rather than $w_k^{*(j)}$, then an estimate of $I(f_k)$ becomes:

$$\widehat{I}_{N_p}(f_k) = \frac{1}{c_k}\sum_{j=1}^{N_p} f_k(X_k^j,\Theta_k^j)w_k^{(j)} \tag{71}$$

with

$$c_k = p_{Y_k}(Y_k) \tag{72}$$

Assumption 1

- $\left\{(X_k^{(j)},\Theta_k^{(j)}); j = 1,...,N_p\right\}$ is a set of i.i.d. vectors distributed according to $\pi_k(X,\Theta)$.
- $\pi_k(X,\Theta) > 0$ for all $(X,\Theta) \in (\mathbb{R}^{(k+1)\times n}, \mathbb{M}^{k+1})$ for which $p_{X_k,\Theta_k|Y_k}(X,\Theta) > 0$.
- $I(f_k)$ exists and is finite.

For N_p finite, $\widehat{I}_{N_p}(f_k)$ is biased, but under assumption 1, asymptotically the strong law of large numbers yields:

$$P\left\{\lim_{N_p\to\infty}\widehat{I}_{N_p}(f_k) = I(f_k)\right\} = 1 \tag{73}$$

i.e. $\widehat{I}_{N_p}(f_k)$ converges almost sure to $I(f_k)$ when $N_p \to \infty$ [Doucet, 1998].

In order to get the SIR particle filter, we choose the following importance function:

$$\pi_k(X,\Theta) = p_{X_k,\Theta_k}(X,\Theta) \tag{74}$$

Note that $p_{X_k,\Theta_k}(X,\Theta)$ should satisfy assumption 1.

Now $w_k^{(j)}$ satisfies:

$$w_k^{(j)} = p_{Y_k|X_k,\Theta_k}(Y_k|X_k^{(j)},\Theta_k^{(j)}) \tag{75}$$

Using (58), $w_{k+1}^{(j)}$ can be expressed as:

$$\begin{aligned} w_{k+1}^{(j)} &= p_{Y_{k+1}|X_{k+1},\Theta_{k+1}}(Y_{k+1}|X_{k+1}^{(j)},\Theta_{k+1}^{(j)}) \\ &= p_{Y_k|X_k,\Theta_k}(Y_k|X_k^{(j)},\Theta_k^{(j)})p_{y_{k+1}|x_{k+1},\theta_{k+1}}(y_{k+1}|x_{k+1}^{(j)},\theta_{k+1}^{(j)}) \\ &= w_k^{(j)}p_{y_{k+1}|x_{k+1},\theta_{k+1}}(y_{k+1}|x_{k+1}^{(j)},\theta_{k+1}^{(j)}) \end{aligned} \tag{76}$$

5.4.3 Algorithm

The algorithm in table 1 without the resampling step follows from recursive equation (60) in section 5.4.1 and from the approximation of a density through particles in section 5.4.2. We show this in more detail below.

First we sample N_p particles according to the importance function $\pi_0(x,\theta) = p_{x_0,\theta_0}(x,\theta)$. This is step 1 in table 1.

Then we start the SIR particle filter cycle. During the evolution step, we sample $(\bar{x}_k^{(j)}, \bar{\theta}_k^{(j)})$ according to the importance function $\pi_k(x_k,\theta_k|X_{k-1},\Theta_{k-1}) = p_{x_k,\theta_k|X_{k-1},\Theta_{k-1}}(x,\eta|X_{k-1}^{(j)},\Theta_{k-1}^{(j)})$ for $j = 1,...,N_p$, equation (74). These are step $2a$ and step $2b$ in table 1.

During the correction step, we evaluate the weights for the particles using equation (76). That is, $w_{k+1}^{(j)} = w_k^{(j)} p_{y_{k+1}|x_{k+1},\theta_{k+1}}(y_{k+1}|\bar{x}_{k+1}^{(j)},\bar{\theta}_{k+1}^{(j)})/c_{N_p}$ with c_{N_p} such that $\sum_{j=1}^{N_p} w_{k+1}^{(j)} = 1$. This is step $2c$ in table 1.

After each cycle, at time k we have the following approximation for $p_{X_k,\Theta_k|Y_k}(X,\Theta)$:

$$\hat{p}_{X_k,\Theta_k|Y_k}(X,\Theta) = \sum_{j=1}^{N_p} w_k^{(j)} \chi(\Theta,\Theta_k^j)\delta(X - X_k^j) \tag{77}$$

The approximation for $p_{x_k,\theta_k|Y_k}(x,\theta)$ can be obtained by marginalizing $\hat{p}_{X_k,\Theta_k|Y_k}(X,\Theta)$ over the variables that are not of interest. Note that:

$$\begin{aligned}
\hat{p}_{X_k,\Theta_k|Y_k}(X,\Theta) &= \hat{p}_{X_{k-1},x_k,\Theta_{k-1},\theta_k|Y_k}(X',x,\Theta',\theta) \\
&= \sum_{j=1}^{N_p} w_k^{(j)} \chi(\Theta',\Theta_{k-1}^j)\chi(\theta,\theta_k^j)\delta(X' - X_{k-1}^j)\delta(x - x_k^j)
\end{aligned} \tag{78}$$

Marginalizing over all X_{k-1} and Θ_{k-1} yields:

$$\begin{aligned}
\hat{p}_{x_k,\theta_k|Y_k}(x,\theta) &= \sum_{\Theta'\in\mathbb{M}^k} \int_{X'\in\mathbb{R}^{k\times n}} \hat{p}_{X_{k-1},x_k,\Theta_{k-1},\theta_k|Y_k}(X',x,\Theta',\theta)dX' \\
&= \sum_{\Theta'\in\mathbb{M}^k} \int_{X'\in\mathbb{R}^{k\times n}} \sum_{j=1}^{N_p} w_k^{(j)} \chi(\Theta',\Theta_{k-1}^j)\chi(\theta,\theta_k^j)\delta(X' - X_{k-1}^j)\delta(x - x_k^j)dX' \\
&= \sum_{j=1}^{N_p} w_k^{(j)} \chi(\theta,\theta_k^j)\delta(x - x_k^j) \sum_{\Theta'\in\mathbb{M}^k} \chi(\Theta',\Theta_{k-1}^j) \int_{X'\in\mathbb{R}^{k\times n}} \delta(X' - X_{k-1}^j)dX' \\
&= \sum_{j=1}^{N_p} w_k^{(j)} \chi(\theta,\theta_k^j)\delta(x - x_k^j)
\end{aligned} \tag{79}$$

5.4.4 Resampling

The basic idea of resampling methods consists of eliminating the trajectories which have weak normalized importance weights and to multiply trajectories with strong importance weights [Doucet, 1998]. Without resampling, at some point some particles will have very small weights while others will have very large weights. Those particles with large weight will have a big influence. This leads to degeneracy of the algorithm. We adopt as a measure of degeneracy of the algorithm the effective sample size N_{eff}. When the estimation of the effective sample size $\widehat{N_{eff}}$ is below a fixed threshold N_{thres}, we use a resampling procedure. The most popular resampling scheme is the SIR algorithm. This scheme is based on two steps: a first step is an IS step, the second step is a sampling step based on the obtained discrete distribution. That is if $\widehat{N_{eff}} < N_{thres}$ then, for $j = 1, ..., N_p$ sample an index $i(j)$ distributed according to the discrete distribution with N_p elements satisfying $P\{i(j) = l\} = w_k^{(l)}$ for $l = 1, ..., N_p$. Thus we sample N_p values from a discrete distribution that approximates the exact distribution $p_{X_k,\Theta_k|Y_k}(X, \Theta)$. It seems plausible that for $N_p \to \infty$ the obtained discrete distribution approximates the exact distribution $p_{X_k,\Theta_k|Y_k}(X, \Theta)$ as well.

An estimate $\widehat{N_{eff}}$ of N_{eff} is given by [Doucet, 1998]:

$$\widehat{N_{eff}} = \frac{1}{\sum_{j=1}^{N_p} \left(\widetilde{w}_k^{(j)}\right)^2} \tag{80}$$

When the resampling step is applied at each iteration, i.e. for N_{thres} very big, a central limit theorem for the estimate of $I(f_k)$ has been established [Berzuini et al., 1997]. This is step 3 in table 1.

6 Particle filters for a system with state depending on θ_{k-1} and θ_k

6.1 The filtering problem

Let $\{x_k, \theta_k\}$ be a hybrid state process, with x_k assuming values in $\mathbb{R}^n$ and θ_k assuming values in a finite set $\mathbb{M}$ of possible modes, be a hidden state process to be estimated from noisy observations $\{y_k\}$, with y_k assuming values in $\mathbb{R}^m$. Consider the following system of stochastic difference equations, on $[0, T]$, $T < \infty$,

$$\begin{aligned} x_k &= a(\theta_k, \theta_{k-1}, x_{k-1}, w_k) \\ \theta_k &= c(\theta_{k-1}, x_{k-1}, u_k) \\ y_k &= h(\theta_k, x_k, v_k) \end{aligned} \tag{81}$$

where the pair (x_k, θ_k) represents the hybrid system state, and y_k represents the observation at moment k, $\{w_k\}$ and $\{v_k\}$ are independent sequences of i.i.d. standard Gaussian variables of dimension n' and m' respectively, $\{u_k\}$ is an $\{w_k, v_k\}$-independent sequence of i.i.d. standard uniform random variables, $\{w_k, v_k, u_k\}$ is independent of the $\mathbb{R}^n \times \mathbb{M}$ valued initial condition (x_0, θ_0), with $\mathbb{M}$ a set of M discrete modes. Furthermore, a and h are measurable mappings of $\mathbb{M} \times \mathbb{R}^n \times \mathbb{R}^{n'}$ into $\mathbb{R}^n$ and $\mathbb{M} \times \mathbb{R}^n \times \mathbb{R}^{m'}$ into $\mathbb{R}^m$ respectively, and c is a measurable mapping of $\mathbb{M} \times \mathbb{R}^n \times [0, 1]$ into $\mathbb{M}$. The mappings a, c and h are time-invariant for notational simplicity only.

Thus the difference between this model and the model studied in section 5 is that the stochastic difference equation for the state is now also dependant on θ_{k-1}.

The filtering problem is to estimate the joint conditional density-probability $p_{x_k, \theta_k | Y_k}(x, \theta)$, $x \in \mathbb{R}^n$, $\theta \in \mathbb{M}$, of the pair (x_k, θ_k) given the sequence of observations $Y_k = \{y_s; s \leq k\}$.

6.2 The SIR particle filter for a system with state depending on θ_{k-1} and θ_k

Table 2 gives an overview of the SIR particle filter cycle for the model in section 6.1. This table is based on table 1 in section 5. Only the evolution step in table 2 is different from the evolution step in table 1. In table 2, $\chi(\theta, \theta_{k-1}^j)$ is a $0-1$ indicator with $\chi(\theta, \theta_{k-1}^j) = 1$ if $\theta = \theta_{k-1}^j$. Note that $p_{y_k | x_k, \theta_k}(y_k | \bar{x}_k^j, \bar{\theta}_k^j)$ is the likelihood of the measurement at moment k given $(\bar{x}_k^j, \bar{\theta}_k^j)$.

Table 2: SIR Particle Filter (SIR PF) cycle; state dependant on θ_{k-1} and θ_k.

SIR	$\tilde{p}_{x_{k-1},\theta_{k-1}\|Y_{k-1}} \rightarrow \tilde{p}_{x_k,\theta_k\|Y_k}$
(1)	Particles $\left\{\mu^j_{k-1} \in [0,1], \theta^j_{k-1} \in \mathbb{M}, x^j_{k-1} \in \mathbb{R}^n; j = 1, ..., N_p\right\}$ $\tilde{p}_{x_{k-1},\theta_{k-1}\|Y_{k-1}}(x,\theta) = \sum_{j=1}^{N_p} \mu^j_{k-1}\chi(\theta,\theta^j_{k-1})\delta(x - x^j_{k-1})$
(2)	For $j = 1, ..., N_p$:
(a)	Generate w^j_k and u^j_k i.i.d. from $p_{w_k}(w)$ and $p_{u_k}(u)$
(b)	Evolution: $\bar{\theta}^j_k = c(\theta^j_{k-1}, x^j_{k-1}, u^j_k)$ $\bar{x}^j_k = a(\bar{\theta}^j_k, \theta^j_{k-1}, x^j_{k-1}, w^j_k)$
(c)	Correction: $\bar{\mu}^j_k = \mu^j_{k-1} \cdot p_{y_k\|x_k,\theta_k}(y_k\|\bar{x}^j_k, \bar{\theta}^j_k)/c_t$ with c_t such that $\sum_{j=1}^{N_p} \bar{\mu}^j_k = 1$
(3)	Resampling: Evaluate $\widehat{N_{eff}}$: $\widehat{N_{eff}} = \frac{1}{\sum_{j=1}^{N_p}(\bar{\mu}^j_k)^2}$ If $\widehat{N_{eff}} \geq N_{tres}$ $\mu^j_k = \bar{\mu}^j_k$ $(x^j_k, \theta^j_k) = (\bar{x}^j_k, \bar{\theta}^j_k)$ Else if $\widehat{N_{eff}} < N_{tres}$ $\mu^j_k = 1/N_p$ $(x^j_k, \theta^j_k) \sim \sum_{j=1}^{N_p} \bar{\mu}^j_k \chi(\theta, \bar{\theta}^j_k)\delta(x - \bar{x}^j_k)$

6.3 Hybrid Particle filter for a system with state depending on θ_{k-1} and θ_k

The Hybrid Particle filter (HPF) uses N_p/M particles per mode, thus the amount of particles per mode stays the same [Blom & Bloem, 2007; Blom & Bar-Shalom, 2009]. Whereas SIR particle filter could have very few particles in one mode at a certain time, when that mode has very few weight. For the investigation of the conditional densities per mode it is convenient if there are enough particles in every mode at every time step to get a good estimation of the conditional density.

The HPF is an extension of the SIR particle filter with a modified set of particles. That is, the total amount of particles per mode is constant. It seems plausible that for $N_p \to \infty$ the HPF particle filter and the SIR particle filter are the same. The HPF cycle for the model in section 6.1 is given in table 3 [Blom & Bloem, 2007]. Note that the resampling step is applied at each iteration, i.e. N_{thres} is very big.

Table 3: Hybrid Particle Filter (HPF) cycle; state dependant on θ_k and θ_{k+1}.

HPF	$\tilde{p}_{x_{k-1},\theta_{k-1}\|Y_{k-1}} \to \tilde{p}_{x_k,\theta_k\|Y_k}$
(1) Particles	$\left\{\mu_{k-1}^{\theta,j} \in [0,1], x_{k-1}^{\theta,j} \in \mathbb{R}^n, \theta \in \mathbb{M}, ; j = 1, ..., N_p/M\right\}$ $\tilde{p}_{x_{k-1},\theta_{k-1}\|Y_{k-1}}(x,\theta) = \sum_{j=1}^{N_p/M} \mu_{k-1}^{\theta,j} \delta(x - x_{k-1}^{\theta,j})$
(2a) Mode switching:	$u_{k-1}^{\theta,j} \sim p_{u_k}(u)$ $\bar{\theta}_k^{\theta,j} = c(\theta, x_{k-1}^{\theta,j}, u_k^{\theta,j})$
(2b) Prediction:	$w_k^{\theta,j} \sim p_{w_k}(w)$ i.i.d., $\theta \in \mathbb{M}, j \in \{1, ..., N_p/M\}$ $\bar{x}_k^{\theta,j} = a(\bar{\theta}_k^{\theta,j}, x_{k-1}^{\theta,j}, w_k^{\theta,j})$
(2c) Correction:	$\mu_k^{\theta,j} = \mu_{k-1}^{\theta,j} \cdot p_{y_k\|x_k,\theta_k}(y_k\|\bar{x}_k^{\theta,j}, \bar{\theta}_k^{\theta,j})/c_t$ with c_t such that $\sum_{j=1}^{N_p/M} \sum_{\theta\in\mathbb{M}} \mu_k^j = 1$
(3) Resampling:	$\gamma_k(\theta) = \sum_{j=1}^{N_p/M} \sum_{\eta\in\mathbb{M}} \mu_k^{\theta,j} \chi(\bar{\theta}_k^{\eta,j}, \theta)$ $\mu_k^{\theta,j} = \gamma_k(\theta) M/N_p$ $x_k^{\theta,j} \sim \sum_{j=1}^{N_p/M} \sum_{\eta\in\mathbb{M}} \mu_k^{\theta,j} \chi(\theta, \bar{\theta}_k^{\eta,j}) \delta(x - \bar{x}_k^{\theta,j})/\gamma_k(\theta)$ i.i.d for $(\theta, j) \in \mathbb{M} \times \{1, ..., N_p/M\}$ if $\gamma_k(\theta) > 0$

7 Generalized Interacting Multiple Model (IMM) algorithm

7.1 The filtering problem

Following [Blom, 1985; 1986] the filtering problem considered addresses jump linear systems with jumps[1] in x which occur simultaneously with and due to jumps in θ. Let $\{x_k, \theta_k\}$ be a two-component Markov process, with $\{x_k\}$ an Euclidean valued stochastic process and $\{\theta_k\}$ a discrete valued process. The system considered satisfies a hybrid stochastic dynamical model of the form:

$$x_k = A(\theta_k, \theta_{k-1})x_{k-1} + B(\theta_k, \theta_{k-1})w_k + C(\theta_k, \theta_{k-1}) \tag{82}$$

where $\{w_k\}$ is a zero mean, Gaussian white noise process with covariance Q. Further, $\{\theta_k\}$ is an $\mathbb{M}$-valued Markov chain with transition probability matrix Π with components $\pi_{\theta\eta} = p\{\theta_{k+1} = \eta |\ \theta_k = \theta\}$. Let $x \in \mathbb{R}^n$, $\theta \in \mathbb{M}$ and $w \in \mathbb{R}^{n'}$.

Consider the process $\{y_k\}$ which observes the process $\{x_k\}$, according to the following equation:

$$y_k = H(\theta_k)x_k + G(\theta_k)v_k \tag{83}$$

where $\{v_k\}$ is a sequence of i.i.d. standard Gaussian variables of dimension m' and independent of w_k and $y \in \mathbb{R}^m$.

The filtering problem is to estimate the joint conditional density $p_{x_k,\theta_k|Y_k}(x, \theta)$, $x \in \mathbb{R}^n$, $\theta \in \mathbb{M}$, of the pair (x_k, θ_k) given $Y_k = \{y_s; s \leq k\}$, i.e. the realization of the process $\{y_k\}$ up to and including moment k.

7.2 Generalized IMM algorithm for jump linear system with hybrid jumps

Following Blom [1986] it is assumed that for all $j \in \mathbb{M}$ the matrices A, B and C permit the following representation,

$$A(i,j) = A_1(i)A_2(i,j) \tag{84}$$

$$B(i,j) = \begin{bmatrix} A_1(i)B_2(i,j) & B_1(i) \end{bmatrix} \tag{85}$$

$$C(i,j) = \begin{bmatrix} A_1(i)C_2(i,j) & C_1(i) \end{bmatrix} \tag{86}$$

such that for all $i \in \mathbb{M}$ $A_2(i,j)$, $B_1(i,j)B_1(i,j)^T$ and $C_1(i,j)C_1(i,j)^T$ are diagonal matrices.

Using (84), (85) and (86), equation (82) can be decomposed in two equations [Blom, 1986]:

$$x_k = A_1(\theta_k)z_{k-1} + B_1(\theta_k)w_k'' + C_1(\theta_k) \tag{87}$$

$$z_{k-1} = A_2(\theta_k, \theta_{k-1})x_{k-1} + B_2(\theta_k, \theta_{k-1})w_k' + C_2(\theta_k, \theta_{k-1}) \tag{88}$$

[1] [Blom, 1990] (page 74) refers to these jumps as Hybrid jumps.

and $\begin{bmatrix} w'_k & w''_k \end{bmatrix}^T = w_k$.

The generalized IMM algorithm for the filtering problem in section 7.1, with $C = 0$ is described in [Blom, 1986] and [Blom, 1985]. This generalized IMM algorithm for the filtering problem in section 7.1 consists of time extrapolation equations between $k-1$ and k and measurement update equations on moment k. These equations are for the scalars $p_k(i)$, the n dimensional vectors $\hat{x}_k(i)$ and the $n \times n$ dimensional matrices $R_k(i)$, which are for all $i \in \mathbb{M}$ the statistics of approximations of $p_{\theta_k|Y_k}(i)$ and $p_{x_k|\theta_k,Y_k}(x|i)$ in the following way:

$$p_{\theta_k|Y_k}(i) \cong \hat{p}_k(i) \tag{89}$$

$$p_{x_k|\theta_k,Y_k}(x|i) \cong \int_{x \in \mathbb{R}^n} \mathcal{N}_{\hat{x}_k(i),\hat{R}_k(i)}(x)dx \tag{90}$$

where $\mathcal{N}_{E,V}$ is a Gaussian distribution on $\mathbb{R}^n$ with parameters E and V.

The time extrapolation equations from $k-1$ to k are:

Step I. Jump extrapolation equations for all $i \in \mathbb{M}$ follow from (88).

$$\hat{z}_{k-1}(i,j) = A_2(i,j)\hat{x}_{k-1}(j) + C_2(i,j) \tag{91}$$

$$\hat{Z}_{k-1}(i,j) = A_2(i,j)\hat{R}_{k-1}(j)A_2^T(i,j) + B_2(i,j)B_2^T(i,j) \tag{92}$$

$$\bar{p}_k(i) = \sum_{j \in \mathbb{M}} \pi_{ji}\hat{p}_{k-1}(j) \tag{93}$$

$$\bar{z}_{k-1}(i) = \sum_{j \in \mathbb{M}} \pi_{ji}\hat{p}_{k-1}(j)\hat{z}_{k-1}(i,j)/\bar{p}_k(i) \tag{94}$$

$$\bar{Z}_{k-1}(i) = \sum_{j \in \mathbb{M}} \pi_{ji}\hat{p}_{k-1}(j)\{\hat{Z}_{k-1}(i,j) + [\hat{z}_{k-1}(i,j) - \bar{z}_{k-1}(i)].[\hat{z}_{k-1}(i,j) - \bar{z}_{k-1}(i)]^T\}/\bar{p}_k(i) \tag{95}$$

Step II. Kalman time extrapolation equations for all $i \in \mathbb{M}$ follows from equation (87).

$$\bar{x}_k(i) = A_1(i)\bar{z}_{k-1}(i) + C_1(i) \tag{96}$$

$$\bar{R}_k(i) = A_1(i)\bar{Z}_{k-1}(i)A_1^T(i) + B_1(i)B_1(i)^T \tag{97}$$

Step III. Measurement update equations for all $i \in \mathbb{M}$ at moment k.

$$
\begin{aligned}
v_k(i) &= y_k - H(i)\bar{x}_k(i) && (98)\\
Q_k(i) &= H(i)\bar{R}_k(i)H(i)^T + G(i)G(i)^T && (99)\\
K_k(i) &= \bar{R}_k(i)H(i)^T Q_k(i)^{-1} && (100)
\end{aligned}
$$

$$
\begin{aligned}
\hat{x}_k(i) &= \bar{x}_k(i) + K_k(i)v_k(i) && (101)\\
\hat{R}_k(i) &= \bar{R}_k(i) - K_k(i)H(i)\bar{R}_k(i) && (102)\\
\hat{p}_k(i) &= c_k\bar{p}_k(i) \parallel Q_k(i) \parallel^{-\frac{1}{2}} \exp\{-\frac{1}{2}v_k^T(i)Q_k(i)^{-1}v_k(i)\} && (103)
\end{aligned}
$$

with c_k a constant such that $\sum_{i\in\mathbb{M}} \hat{p}_k(i) = 1$.

8 Target motion models

8.1 Target motion model with two modes

We look at a target motion model for one axis of motion. This model describes the dynamics of an object moving on a straight line, i.e. a one-dimensional space. The object's possible movements are considered to be constant speed and acceleration. The acceleration in this case can be positive or negative. The model and parametrization is from [Blom & Bloem, 2007].

Consider the following one-dimensional motion model:

$$x = \begin{bmatrix} s_x & \dot{s}_x & \ddot{s}_x \end{bmatrix}^T \tag{104}$$

with s_x the target position, $\dot{s}_x$ the groundspeed and $\ddot{s}_x$ the target acceleration.

Consider also a two-component Markov process $\{x_k, \theta_k\}$ with $\{x_k\}$ an Euclidean valued stochastic process and $\{\theta_k\}$ a discrete valued process.

The system considered satisfies a hybrid stochastic dynamical model of the form:

$$x_{k+1} = A(\theta_{k+1})x_k + B(\theta_{k+1})w_k \tag{105}$$

where w_k is a sequence of i.i.d. standard Gaussian variables of dimension one.

The process of switching between the different movements is represented by an $\mathbb{M}$-valued Markov chain $\{\theta_k\}$. $\mathbb{M}$ is the set of discrete modes. In this case $\mathbb{M} = \{0, 1\}$. With $\theta_k = 0$ representing the object moves with constant speed and with $\theta_k = 1$ representing the object is accelerating (or decelerating). The Markov chain $\{\theta_k\}$ has transition probability matrix Π with components $\pi_{\theta\eta} = p\{\theta_{k+1} = \eta | \theta_k = \theta\}$. The following transition probability matrix Π will be used for the Markov chain $\{\theta_k\}$:

$$\Pi = \begin{bmatrix} 1 - \frac{t_s}{\tau_1} & \frac{t_s}{\tau_1} \\ \\ \frac{t_s}{\tau_2} & 1 - \frac{t_s}{\tau_2} \end{bmatrix} \tag{106}$$

For $A(\theta)$ we have:

$$A(0) = \begin{bmatrix} 1 & t_s & 0 \\ 0 & 1 & 0 \\ 0 & 0 & 0 \end{bmatrix} \qquad A(1) = \begin{bmatrix} 1 & t_s & \frac{1}{2}t_s^2 \\ 0 & 1 & t_s \\ 0 & 0 & \alpha \end{bmatrix} \tag{107}$$

where t_s is the sampling time interval and the parameter $\alpha \in (0, 1]$ allows the acceleration in mode $\theta = 1$ to vary randomly in time. More information about $A(\theta)$ can be found in

appendix B.

For $B(\theta)$ we have:

$$B(0) = \sigma_a \begin{bmatrix} 0 \\ 0 \\ 1 \end{bmatrix} \qquad B(1) = \sigma_a \sqrt{1-\alpha^2} \begin{bmatrix} 0 \\ 0 \\ 1 \end{bmatrix} \tag{108}$$

where σ_a represents the standard deviation of the acceleration noise.

Consider the process $\{y_k\}$ which observes the state x_k. The process $\{y_k\}$ satisfies the following equation:

$$y_k \quad = \quad Hx_k + \sigma_m v_k \tag{109}$$

where $H = \begin{bmatrix} 1 & 0 & 0 \end{bmatrix}$ and v_k is a sequence of i.i.d. standard Gaussian variables of dimension one independent of w_k. σ_m represents the standard deviation of the measurement error.

8.2 Target motion model with three modes

We look at a target motion model for one axis of motion. This model describes the dynamics of an object moving on a straight line, i.e. a one-dimensional space. The objects possible movements are considered to be constant speed, positive acceleration and negative acceleration. The model is a three modes version of the two modes example in [Blom & Bloem, 2007]. Note that this model makes a distinction between positive and negative acceleration whereas the model in section 8.1 considers positive and negative acceleration as one mode.

Consider the following one-dimensional motion model:

$$x = \begin{bmatrix} s_x & \dot{s}_x & \ddot{s}_x \end{bmatrix}^T \tag{110}$$

with s_x the target position, $\dot{s}_x$ the groundspeed and $\ddot{s}_x$ the target acceleration.

Consider also a two-component Markov process $\{x_k, \theta_k\}$ with $\{x_k\}$ an Euclidean valued stochastic process and $\{\theta_k\}$ a discrete valued process.

The system considered satisfies a hybrid stochastic dynamical model of the form:

$$x_{k+1} = A(\theta_{k+1}, \theta_k)x_k + B(\theta_{k+1}, \theta_k)w_k + C(\theta_{k+1}, \theta_k) \tag{111}$$

where w_k is a sequence of i.i.d. standard Gaussian variables of dimension one.

The process of switching between the different movements is represented by an $\mathbb{M}$-valued Markov chain $\{\theta_k\}$. $\mathbb{M}$ is the set of discrete modes. In this case $\mathbb{M} = \{-1, 0, 1\}$. With $\theta_k = 0$

representing the object moves with constant speed, with $\theta_k = 1$ representing the object is accelerating and with $\theta_k = -1$ representing the object is decelerating. The Markov chain $\{\theta_k\}$ has transition probability matrix Π with components $\pi_{\theta\eta} = p\{\theta_{k+1} = \eta | \theta_k = \theta\}$. The following transition probability matrix Π will be used for the Markov chain $\{\theta_k\}$:

$$\Pi = \begin{bmatrix} 1 - \frac{t_s}{\tau_2} & \frac{t_s}{2\tau_2} & \frac{t_s}{2\tau_2} \\ \frac{t_s}{2\tau_1} & 1 - \frac{t_s}{\tau_1} & \frac{t_s}{2\tau_1} \\ \frac{t_s}{2\tau_2} & \frac{t_s}{2\tau_2} & 1 - \frac{t_s}{\tau_2} \end{bmatrix} \tag{112}$$

For $A(\theta_{k+1}, \theta_k)$ we have:

$$\begin{aligned} A(0,0) &= A(1,0) = A(-1,0) = A(0,1) = A(0,-1) = A(1,-1) = A(-1,1) \\ &= \begin{bmatrix} 1 & t_s & 0 \\ 0 & 1 & 0 \\ 0 & 0 & 0 \end{bmatrix} \end{aligned} \tag{113}$$

$$A(1,1) = A(-1,-1) = \begin{bmatrix} 1 & t_s & \alpha\frac{1}{2}t_s^2 \\ 0 & 1 & \alpha t_s \\ 0 & 0 & \alpha \end{bmatrix} \tag{114}$$

where t_s is the sampling time interval and the parameter $\alpha \in (0, 1]$ allows the acceleration in mode -1 and 1 to vary randomly in time.

For $B(\theta_{k+1}, \theta_k)$ we have:

$$B(0,0) = B(0,1) = B(0,-1) = \begin{bmatrix} 0 \\ 0 \\ 0 \end{bmatrix} \tag{115}$$

$$B(1,0) = B(1,-1) = B(-1,0) = B(-1,1) = \frac{1}{2}\sigma_a \begin{bmatrix} \frac{1}{2}t_s^2 \\ t_s \\ 1 \end{bmatrix} \tag{116}$$

$$B(1,1) = B(-1,-1) = \frac{1}{2}\sigma_a\sqrt{1-\alpha^2} \begin{bmatrix} \frac{1}{2}t_s^2 \\ t_s \\ 1 \end{bmatrix} \tag{117}$$

where σ_a represents the standard deviation of acceleration noise.

For $C(\theta_{k+1}, \theta_k)$ we have:

$$C(0,0) = C(0,1) = C(0,-1) = C(1,1) = C(-1,-1) \quad = \quad \begin{bmatrix} 0 \\ 0 \\ 0 \end{bmatrix} \tag{118}$$

$$C(1,0) = C(1,-1) \quad = \quad \sigma_a \begin{bmatrix} \frac{1}{2}t_s^2 \\ t_s \\ 1 \end{bmatrix} \tag{119}$$

$$C(-1,0) = C(-1,1) \quad = \quad -\sigma_a \begin{bmatrix} \frac{1}{2}t_s^2 \\ t_s \\ 1 \end{bmatrix} \tag{120}$$

After convergence this means

$$Cov(\rho_{k+1}) = \frac{1}{4}\sigma_a^2 \tag{121}$$

where $\rho = \ddot{s}_x$.

$Cov(\rho_{k+1})$ satisfies:

$$\begin{aligned} & Cov(\rho_{k+1}) \\ = & \begin{cases} \frac{1}{4}\sigma_a^2 Cov(w_k) & \text{if } (\theta_{k+1},\theta_k) = (1,0),(1,-1),(-1,0) \text{ or } (-1,1) \\ \alpha^2 Cov(\rho_k) + \frac{1}{4}\sigma_a^2(1-\alpha^2)Cov(w_k) & \text{if } (\theta_{k+1},\theta_k) = (1,1) \text{ or } (-1,-1) \\ 0 & \text{if } (\theta_{k+1},\theta_k) = (0,0),(0,1) \text{ or } (0,-1) \end{cases} \end{aligned} \tag{122}$$

Since $Cov(w_k) = 1$ evaluation of (122) yields:

$$Cov(\rho_{k+1}) \quad = \quad \begin{cases} \frac{1}{4}\sigma_a^2 & \text{if } \theta_{k+1} = 1 \text{ or } -1 \\ 0 & \text{if } \theta_{k+1} = 0 \end{cases} \tag{123}$$

The conditional mean acceleration (or deceleration) of ρ_{k+1} given ρ_k satisfies:

$$\mathbb{E}(\rho_{k+1}|\rho_k) \quad = \quad \begin{cases} \sigma_a & \text{if } (\theta_{k+1},\theta_k) = (1,0) \text{ or } (1,-1) \\ -\sigma_a & \text{if } (\theta_{k+1},\theta_k) = (-1,0) \text{ or } (-1,1) \\ \alpha\rho_k & \text{if } (\theta_{k+1},\theta_k) = (1,1) \\ \alpha\rho_k & \text{if } (\theta_{k+1},\theta_k) = (-1,-1) \\ 0 & \text{if } \theta_{k+1} = 0 \end{cases} \tag{124}$$

Consider the process $\{y_k\}$ which observes the state x_k. The process $\{y_k\}$ satisfies the following equation:

$$y_k = Hx_k + \sigma_m v_k \tag{125}$$

where $H = \begin{bmatrix} 1 & 0 & 0 \end{bmatrix}$ and v_k is a sequence of i.i.d. standard Gaussian variables of dimension one independent of w_k. σ_m represents the standard deviation of the measurement error.

8.3 Representation of the model like representation (84)-(86)

The model in section 8.2 satisfies the following representation:

$$A(\eta, \theta) = A_1 A_2(\eta, \theta) \tag{126}$$

where

$$A_1 = \begin{bmatrix} 1 & t_s & \frac{1}{2}t_s^2 \\ 0 & 1 & t_s \\ 0 & 0 & 1 \end{bmatrix} \tag{127}$$

and

$$A_2(\eta, \theta) = \begin{cases} \begin{bmatrix} 1 & 0 & 0 \\ 0 & 1 & 0 \\ 0 & 0 & \alpha \end{bmatrix} & \text{if } \eta = \theta \neq 0 \\ \begin{bmatrix} 1 & 0 & 0 \\ 0 & 1 & 0 \\ 0 & 0 & 0 \end{bmatrix} & \text{otherwise} \end{cases} \tag{128}$$

Note that for all $\eta, \theta \in \mathbb{M} \times \mathbb{M}$ $A_2(\eta, \theta)$ is a diagonal matrix.

Further,

$$B(\eta, \theta) = A_1 B_2(\eta, \theta) \tag{129}$$

where

$$B_2(\eta, \theta) = \begin{cases} \begin{bmatrix} 0 & 0 & 0 \end{bmatrix}^T & \text{if } (\eta, \theta) = (0,0), (0,1) \text{ or } (0,-1) \\ \begin{bmatrix} 0 & 0 & \frac{1}{2}\sigma_a \end{bmatrix}^T & \text{if } (\eta, \theta) = (1,0), (1,-1), (-1,0) \text{ or } (-1,1) \\ \begin{bmatrix} 0 & 0 & \frac{1}{2}\sigma_a\sqrt{1-\alpha^2} \end{bmatrix}^T & \text{if } (\eta, \theta) = (1,1) \text{ or } (-1,-1) \end{cases} \tag{130}$$

Finally,

$$C(\eta, \theta) = A_1 C_2(\eta, \theta) \tag{131}$$

with

$$C_2(\eta,\theta) = \begin{cases} \begin{bmatrix} 0 & 0 & 0 \end{bmatrix}^T & \text{if } (\eta,\theta) = (0,0),(0,1),(0,-1),(1,1) \text{ or } (-1,-1) \\ \begin{bmatrix} 0 & 0 & \sigma_a \end{bmatrix}^T & \text{if } (\eta,\theta) = (1,0) \text{ or } (1,-1) \\ \begin{bmatrix} 0 & 0 & -\sigma_a \end{bmatrix}^T & \text{if } (\eta,\theta) = (-1,0) \text{ or } (-1,1) \end{cases} \tag{132}$$

Following Blom [1986] the model in equation 111 can now be decomposed as follows:

$$x_k = A_1 z_{k-1} \tag{133}$$

$$z_{k-1} = A_2(\theta_k,\theta_{k-1})x_k + B_2(\theta_k,\theta_{k-1})w_k + C_2(\theta_k,\theta_{k-1}) \tag{134}$$

8.4 One-dimensional target motion with non-Gaussian acceleration noise

The Model in section 8.2 permits the target to have a negative value for $\ddot{s}_x$ while being in acceleration mode $\theta = 1$, and permits the target to have a positive value for $\ddot{s}_x$ while being in deceleration mode $\theta = -1$. This is caused by the acceleration noise w_k which is standard Gaussian. The following model does not permit negative values for $\ddot{s}_x$ while the target is in acceleration mode $\theta = 1$ or the other way around.

The system considered satisfies a hybrid stochastic dynamical model of the form:

$$x_{k+1} = A(\theta_{k+1},\theta_k)x_k + \theta_{k+1} \cdot abs\Big(B(\theta_{k+1},\theta_k)w_k + C(\theta_{k+1},\theta_k)\Big) \tag{135}$$

with x_k, w_k, $A(\theta_{k+1},\theta_k)$, $B(\theta_{k+1},\theta_k)$ and $C(\theta_{k+1},\theta_k)$ given earlier in this section.

9 Monte Carlo Simulations

In this section some Monte Carlo (MC) simulation results are given for HPF and the IMM algorithm. The simulations primarily aim at gaining insight in the behavior and performance of the filters in case of S-turns.

9.1 HPF cycle for the target motion model with M=2 in section 8.1

In this subsection we will discuss how we use the HPF cycle for the model with two modes in section 8.1 in the MC simulations.

At each time step k the output $\hat{x}_k^{HPF}$ of the HPF cycle is given by

$$\hat{x}_k^{HPF} = \sum_{j=1}^{N_p/M} \sum_{\theta \in \mathbb{M}} \mu_k^{\theta,j} x_k^{\theta,j} \tag{136}$$

where $\mu_k^{\theta,j}$ and $x_k^{\theta,j}$ are taken after resampling.

The initial mean and covariance of the HPF state estimate $\hat{x}_0^{HPF}$ are given by the initial state and initial weight of the particles. Similar to [Blom & Bloem, 2007] we start the simulations with initial state of the particles as follows:

$$x_0^{\theta,j} = x_0 + \frac{1}{3}\begin{bmatrix}\sigma_a \nu_1^{\theta,j} & \sigma_m \nu_2^{\theta,j} & \sigma_m \nu_3^{\theta,j}\end{bmatrix}^T \quad \forall \theta, j \tag{137}$$

where x_0 is the exact initial state and $\nu_i^{\theta,j}$, $i = 1, 2, 3$ are i.i.d. standard Gaussian variables of dimension one and independent of θ, j. As initial weight we have

$$\mu_0^{\theta,j} = \frac{M p_0^\theta}{N_p} \quad \forall \theta, j \tag{138}$$

where $\sum_{\theta \in \mathbb{M}} p_0^\theta = 1$ and p_0^θ is the initial mode probability of mode θ. We use the following p_0:

$$p_0^\theta = \begin{cases} 0.9999 & \text{for } \theta = 0 \\ 0.0001 & \text{for } \theta = 1 \end{cases} \tag{139}$$

In this way the initial mean equals the exact initial state probabilities. Since the same initial conditions were used in simulations in [Blom & Bloem, 2007], we can compare results.

In the correction step (2c), we use the following

$$\begin{aligned}
\mu_k^{\theta,j} &= \mu_{k-1}^{\theta,j} \cdot p_{y_k|x_k,\theta_k}(y_k|\bar{x}_k^j, \bar{\theta}_k^j)/c_t \\
&= \mu_{k-1}^{\theta,j} \frac{\exp\left\{-\frac{1}{2}[y_k - h(\bar{\theta}_k^j, \bar{x}_k^j)]^T (g(\bar{\theta}_k^j, \bar{x}_k^j) g(\bar{\theta}_k^j, \bar{x}_k^j)^T)^{-1} [y_k - h(\bar{\theta}_k^j, \bar{x}_k^j)]\right\}}{c_t \text{ Det}\left\{2\pi g(\bar{\theta}_k^j, \bar{x}_k^j) g(\bar{\theta}_k^j, \bar{x}_k^j)^T\right\}^{1/2}} \\
&= \mu_{k-1}^{\theta,j} \frac{\exp\left\{-\frac{1}{2}[y_k - H\bar{x}_k^j]^T (\sigma_m^2)^{-1} [y_k - H\bar{x}_k^j]\right\}}{c_t \text{ Det}\left\{2\pi\sigma_m^2\right\}^{1/2}} \\
&= \exp\left\{\ln\left(\mu_{k-1}^{\theta,j}\right) - \frac{1}{2}[y_k - H\bar{x}_k^j]^T (\sigma_m^2)^{-1} [y_k - H\bar{x}_k^j]\right\} \left(c_t \text{ Det}\left\{2\pi\sigma_m^2\right\}^{1/2}\right)^{-1}
\end{aligned} \tag{140}$$

where $\left(c_t \text{ Det}\left\{2\pi\sigma_m^2\right\}^{1/2}\right)^{-1}$ can be found by normalization. We use equation (140) because the computer rounds off $\exp\{-c\}$ to zero when c is very large. In this way, round off errors are smaller since $\ln\left(\mu_{k-1}^{\theta,j}\right)$ can compensate relatively large $\frac{1}{2}[y_k - H\bar{x}_k^j]^T (\sigma_m^2)^{-1} [y_k - H\bar{x}_k^j]$.

The HPF cycle in table 3 is adapted for the one-dimensional target motion model in section 8.1 in table 4.

Table 4: Hybrid Particle Filter (HPF) cycle adapted from table 3 for one-dimensional target motion model in section 8.1

HPF $\quad \tilde{p}_{x_{k-1},\theta_{k-1}\mid Y_{k-1}} \rightarrow \tilde{p}_{x_k,\theta_k\mid Y_k}$
Initiate: $x_0^{\theta,j} = x_0 + \sigma_m \nu^{\theta,j} \quad \forall \theta, j$ where x_0 is the exact initial state and $\nu^{\theta,j} \sim \mathcal{N}(0,1)$ i.i.d., $\theta \in \mathbb{M}, j \in \{1,...,N_p/2\}$ $\mu_0^{\theta,j} = \frac{2p_0^\theta}{N_p} \quad \forall \theta, j$ with p_0^θ the given initial mode distribution.
For $k = 1$ until $k = k_{end}$
(1) Particles $\quad \left\{\mu_{k-1}^{\theta,j} \in [0,1], x_{k-1}^{\theta,j} \in \mathbb{R}^n, \theta \in \mathbb{M}, ; j = 1,...,N_p/2\right\}$ $\tilde{p}_{x_{k-1},\theta_{k-1}\mid Y_{k-1}}(x,\theta) = \sum_{j=1}^{N_p/2} \mu_{k-1}^{\theta,j} \delta(x - x_{k-1}^{\theta,j})$
(2a) Mode switching: $u_{k-1}^{\theta,j} \sim U(0,1)$ i.i.d., $\theta \in \mathbb{M}, j \in \{1,...,N_p/2\}$ $\bar{\theta}_k^{\theta,j} = \begin{cases} 0 & \text{if } u_k^{\theta,j} \leq \pi_{\theta,0} \\ 1 & \text{if } u_k^{\theta,j} > \pi_{\theta,0} \end{cases}$ (2b) Prediction: $w_k^{\theta,j} \sim \mathcal{N}(0,1)$ i.i.d., $\theta \in \mathbb{M}, j \in \{1,...,N_p/2\}$ $\bar{x}_k^{\theta,j} = A(\bar{\theta}_k^{\theta,j},\theta) x_{k-1}^{\theta,j} + B(\bar{\theta}_k^{\theta,j},\theta) w_k^{\theta,j} + C(\bar{\theta}_k^{\theta,j},\theta)$ (2c) Correction: $\mu_k^{\theta,j} = \exp\left\{\ln\left(\mu_{k-1}^{\theta,j}\right) - \frac{1}{2}[y_k - H\bar{x}_k^j]^T (\sigma_m^2)^{-1} [y_k - H\bar{x}_k^j]\right\} \left(c_t \text{ Det}\left\{2\pi\sigma_m^2\right\}^{1/2}\right)^{-1}$ with c_t such that $\sum_{j=1}^{N_p/2} \sum_{\theta\in\mathbb{M}} \mu_k^{\theta,j} = 1$
(3) Resampling: $\quad \gamma_k(\theta) = \sum_{j=1}^{N_p/2} \sum_{\eta\in\mathbb{M}} \mu_k^{\theta,j} \chi(\bar{\theta}_k^{\eta,j},\theta) \qquad \mu_k^{\theta,j} = \gamma_k(\theta) 2/N_p$ $x_k^{\theta,j} \sim \sum_{j=1}^{N_p/2} \sum_{\eta\in\mathbb{M}} \mu_k^{\theta,j} \chi(\theta,\bar{\theta}_k^{\eta,j}) \delta(x - \bar{x}_k^{\theta,j}) / \gamma_k(\theta)$ i.i.d for $(\theta,j) \in \mathbb{M} \times \{1,...,N_p/2\}$ if $\gamma_k(\theta) > 0$
Output: $\hat{x}_k^{HPF} = \sum_{j=1}^{N_p/2} \sum_{\theta\in\mathbb{M}} \mu_k^{\theta,j} x_k^{\theta,j}$

9.2 IMM cycle for the target motion model with M=2 in section 8.1

This subsection will show how we use the IMM cycle for the model with two modes in section 8.1 in the MC simulations.

The initial mean and covariance of the IMM state estimate $\hat{x}_0^{IMM}$ are given by the initial state estimate $\hat{x}_0(i)$, the initial covariance estimate $\hat{R}_0(i)$ and initial mode probability estimate $\hat{p}_0(i)$ per mode $i \in \mathbb{M}$. Similar to [Blom & Bloem, 2007] we start the simulations with:

$$\begin{aligned}
\hat{x}_0(i) &= x_0 \quad \forall i \in \mathbb{M} && (141)\\
\hat{R}_0(i) &= \frac{1}{9}\begin{bmatrix} \sigma_m^2 & 0 & 0 \\ 0 & \sigma_a^2 & 0 \\ 0 & 0 & \sigma_a^2 \end{bmatrix} \quad \forall i \in \mathbb{M} && (142)\\
\hat{p}_0(i) &= p_0^i \quad \forall i \in \mathbb{M} && (143)
\end{aligned}$$

where x_0 is the exact initial state and p_0^i is the initial mode probability of mode i given in equation (139). We choose to use these initial conditions because the same initial conditions are used in [Blom & Bloem, 2007].

The IMM time extrapolation equations from $k-1$ to k for the one-dimensional target model in section 8.2 are as follows:

Step I. Jump extrapolation equations for all $i \in \mathbb{M}$ are given by (91)-(95) with $A_2(i,j) = I$, $B_2(i,j) = 0$ and $C_2(i,j) = 0$.

$$\begin{aligned}
\hat{z}_{k-1}(i,j) &= \hat{x}_{k-1}(j) && (144)\\
\hat{Z}_{k-1}(i,j) &= \hat{R}_{k-1}(j) && (145)
\end{aligned}$$

$$\begin{aligned}
\bar{p}_k(i) &= \sum_{j\in\mathbb{M}} \pi_{ji}\hat{p}_{k-1}(j) && (146)\\
\bar{z}_{k-1}(i) &= \sum_{j\in\mathbb{M}} \pi_{ji}\hat{p}_{k-1}(j)\hat{z}_{k-1}(i,j)/\bar{p}_k(i) && (147)\\
\bar{Z}_{k-1}(i) &= \sum_{j\in\mathbb{M}} \pi_{ji}\hat{p}_{k-1}(j)\{\hat{Z}_{k-1}(i,j) + [\hat{z}_{k-1}(i,j) - \bar{z}_{k-1}(i)].[\hat{z}_{k-1}(i,j) - \bar{z}_{k-1}(i)]^T\}/\bar{p}_k(i) && (148)
\end{aligned}$$

Step II. Kalman time extrapolation equations for all $i \in \mathbb{M}$ are given by (96)-(97) with $A_1(i) = A(i)$, $B_1(i) = B(i)$ and $C_1(i) = 0$.

$$\bar{x}_k(i) = A(i)\bar{z}_{k-1}(i) \tag{149}$$

$$\bar{R}_k(i) = A(i)\bar{Z}_{k-1}(i)A(i)^T + B(i)B(i)^T \tag{150}$$

Step III. Measurement update equations for all $i \in \mathbb{M}$ at moment k are given by (98)-(103) with $G(i) = \sigma_m$.

$$v_k(i) = y_k - H\bar{x}_k(i) \tag{151}$$

$$Q_k(i) = H\bar{R}_k(i)H^T + \sigma_m^2 \tag{152}$$

$$K_k(i) = \bar{R}_k(i)H^T Q_k(i)^{-1} \tag{153}$$

$$\hat{x}_k(i) = \bar{x}_k(i) + K_k(i)v_k(i) \tag{154}$$

$$\hat{R}_k(i) = \bar{R}_k(i) - K_k(i)\bar{R}_k(i) \tag{155}$$

$$\hat{p}_k(i) = c_k\bar{p}_k(i) \parallel Q_k(i) \parallel^{-\frac{1}{2}} \exp\{-\frac{1}{2}v_k^T(i)Q_k(i)^{-1}v_k(i)\} \tag{156}$$

with c_k a constant such that $\sum_{i\in\mathbb{M}} \hat{p}_k(i) = 1$.

9.3 HPF cycle for the one-dimensional target motion model with three modes in section 8.2

In this subsection we will discuss how we use the HPF cycle for the model with three modes in section 8.2 in the MC simulations.

At each time step k the output $\hat{x}_k^{HPF}$ of the HPF cycle is again given by equation (136).

We start the simulations with initial state of the particles with $x_0^{\theta,j}$ and $\mu_0^{\theta,j}$ given by equations (137) and (138). We use the following p_0:

$$p_0^\theta = \begin{cases} 0.00005 & \text{for } \theta = -1 \\ 0.9999 & \text{for } \theta = 0 \\ 0.00005 & \text{for } \theta = 1 \end{cases} \tag{157}$$

In this way the initial mean equals the exact initial state probabilities. Similar initial conditions were used in simulations in [Blom & Bloem, 2007]. Thus we can compare results in

[Blom & Bloem, 2007] with our simulation results.

Furthermore, we use again equation (140) in the correction step (2c).

The HPF cycle in table 3 is adapted for the one-dimensional target motion model in section 8.2 in table 5.

Table 5: Hybrid Particle Filter (HPF) cycle adapted from table 3 for one-dimensional target motion model in section 8.2

HPF $\quad \tilde{p}_{x_{k-1},\theta_{k-1}|Y_{k-1}} \rightarrow \tilde{p}_{x_k,\theta_k|Y_k}$

Initiate: $x_0^{\theta,j} = x_0 + \sigma_m \nu^{\theta,j} \quad \forall \theta, j$
where x_0 is the exact initial state and $\nu^{\theta,j} \sim \mathcal{N}(0,1)$ i.i.d., $\theta \in \mathbb{M}, j \in \{1, ..., N_p/3\}$
$\mu_0^{\theta,j} = \frac{3p_0^\theta}{N_p} \quad \forall \theta, j$ with p_0^θ the given initial mode distribution.

For $k = 1$ until $k = k_{end}$

(1) Particles $\quad \left\{ \mu_{k-1}^{\theta,j} \in [0,1], x_{k-1}^{\theta,j} \in \mathbb{R}^n, \theta \in \mathbb{M}, ; j = 1, ..., N_p/3 \right\}$

$$\tilde{p}_{x_{k-1},\theta_{k-1}|Y_{k-1}}(x,\theta) = \sum_{j=1}^{N_p/3} \mu_{k-1}^{\theta,j} \delta(x - x_{k-1}^{\theta,j})$$

(2a) Mode switching:

$u_{k-1}^{\theta,j} \sim U(0,1)$ i.i.d., $\theta \in \mathbb{M}, j \in \{1, ..., N_p/3\}$

$$\bar{\theta}_k^{\theta,j} = \begin{cases} -1 & \text{if } u_k^{\theta,j} \leq \pi_{\theta,-1} \\ 0 & \text{if } \pi_{\theta,-1} < u_k^{\theta,j} \leq \pi_{\theta,-1} + \pi_{\theta,0} \\ 1 & \text{if } u_k^{\theta,j} > \pi_{\theta,-1} + \pi_{\theta,0} \end{cases}$$

(2b) Prediction:

$w_k^{\theta,j} \sim \mathcal{N}(0,1)$ i.i.d., $\theta \in \mathbb{M}, j \in \{1, ..., N_p/3\}$

$$\bar{x}_k^{\theta,j} = A(\bar{\theta}_k^{\theta,j}, \theta) x_{k-1}^{\theta,j} + B(\bar{\theta}_k^{\theta,j}, \theta) w_k^{\theta,j} + C(\bar{\theta}_k^{\theta,j}, \theta)$$

(2c) Correction:

$$\mu_k^{\theta,j} = \exp\left\{ \ln\left(\mu_{k-1}^{\theta,j}\right) - \tfrac{1}{2}[y_k - H\bar{x}_k^j]^T (\sigma_m^2)^{-1} [y_k - H\bar{x}_k^j] \right\} \left(c_t \text{ Det}\left\{ 2\pi\sigma_m^2 \right\}^{1/2} \right)^{-1}$$

with c_t such that $\sum_{j=1}^{N_p/3} \sum_{\theta \in \mathbb{M}} \mu_k^{\theta,j} = 1$

(3) Resampling: $\quad \gamma_k(\theta) = \sum_{j=1}^{N_p/3} \sum_{\eta \in \mathbb{M}} \mu_k^{\theta,j} \chi(\bar{\theta}_k^{\eta,j}, \theta) \qquad \mu_k^{\theta,j} = \gamma_k(\theta) 3/N_p$

$$x_k^{\theta,j} \sim \sum_{j=1}^{N_p/3} \sum_{\eta \in \mathbb{M}} \mu_k^{\theta,j} \chi(\theta, \bar{\theta}_k^{\eta,j}) \delta(x - \bar{x}_k^{\theta,j}) / \gamma_k(\theta)$$

i.i.d for $(\theta, j) \in \mathbb{M} \times \{1, ..., N_p/3\}$ if $\gamma_k(\theta) > 0$

Output: $\hat{x}_k^{HPF} = \sum_{j=1}^{N_p/3} \sum_{\theta \in \mathbb{M}} \mu_k^{\theta,j} x_k^{\theta,j}$

9.4 IMM cycle for the target model with M=3 in section 8.2

This subsection will show how we use the IMM cycle for the model with three modes in section 8.2 in the MC simulations.

The initial mean and covariance of the IMM state estimate $\hat{x}_0^{IMM}$ are given by the initial state estimate $\hat{x}_0(i)$, the initial covariance estimate $\hat{R}_0(i)$ and initial mode probability estimate $\hat{p}_0(i)$ per mode $i \in \mathbb{M}$. We start the simulations with

$$\begin{aligned} \hat{x}_0(i) &= x_0 \quad \forall i \in \mathbb{M} && (158)\\ \hat{R}_0(i) &= \frac{1}{9}\begin{bmatrix} \sigma_m^2 & 0 & 0 \\ 0 & \sigma_a^2 & 0 \\ 0 & 0 & \sigma_a^2 \end{bmatrix} \quad \forall i \in \mathbb{M} && (159)\\ \hat{p}_0(i) &= p_0^i \quad \forall i \in \mathbb{M} && (160) \end{aligned}$$

where x_0 is the exact initial state and p_0^i is the initial mode probability of mode i given in equation (157). We choose to use these initial conditions because similar initial conditions are used in [Blom & Bloem, 2007].

The IMM time extrapolation equations from $k-1$ to k for the one-dimensional target model in section 8.2 are as follows:

Step I. Jump extrapolation equations for all $i \in \mathbb{M}$ are given by (91)-(95).

$$\begin{aligned} \hat{z}_{k-1}(i,j) &= A_2(i,j)\hat{x}_{k-1}(j) + C_2(i,j) && (161)\\ \hat{Z}_{k-1}(i,j) &= A_2(i,j)\hat{R}_{k-1}(j)A_2^T(i,j) + B_2(i,j)B_2^T(i,j) && (162) \end{aligned}$$

$$\bar{p}_k(i) = \sum_{j\in\mathbb{M}} \pi_{ji}\hat{p}_{k-1}(j) \quad (163)$$

$$\bar{z}_{k-1}(i) = \sum_{j\in\mathbb{M}} \pi_{ji}\hat{p}_{k-1}(j)\hat{z}_{k-1}(i,j)/\bar{p}_k(i) \quad (164)$$

$$\bar{Z}_{k-1}(i) = \sum_{j\in\mathbb{M}} \pi_{ji}\hat{p}_{k-1}(j)\{\hat{Z}_{k-1}(i,j) + [\hat{z}_{k-1}(i,j) - \bar{z}_{k-1}(i)].[\hat{z}_{k-1}(i,j) - \bar{z}_{k-1}(i)]^T\}/\bar{p}_k(i) \quad (165)$$

Step II. Kalman time extrapolation equations for all $i \in \mathbb{M}$ are given by (96)-(97) with $B_1(i) = 0$ and $C_1(i) = 0$.

$$\bar{x}_k(i) = A_1 \bar{z}_{k-1}(i) \tag{166}$$

$$\bar{R}_k(i) = A_1 \bar{Z}_{k-1}(i) A_1^T \tag{167}$$

Step III. Measurement update equations for all $i \in \mathbb{M}$ at moment k are given by (98)-(103) with $G(i) = \sigma_m$.

$$v_k(i) = y_k - H\bar{x}_k(i) \tag{168}$$

$$Q_k(i) = H\bar{R}_k(i)H^T + \sigma_m^2 \tag{169}$$

$$K_k(i) = \bar{R}_k(i)H^T Q_k(i)^{-1} \tag{170}$$

$$\hat{x}_k(i) = \bar{x}_k(i) + K_k(i)v_k(i) \tag{171}$$

$$\hat{R}_k(i) = \bar{R}_k(i) - K_k(i)\bar{R}_k(i) \tag{172}$$

$$\hat{p}_k(i) = c_k \bar{p}_k(i) \parallel Q_k(i) \parallel^{-\frac{1}{2}} \exp\{-\frac{1}{2} v_k^T(i) Q_k(i)^{-1} v_k(i)\} \tag{173}$$

with c_k a constant such that $\sum_{i \in \mathbb{M}} \hat{p}_k(i) = 1$.

9.5 Filter parameters and target scenarios

The results of the particle filtering simulation for accelerating and decelerating scenarios are shown in this section. The filter parameter values are parameter values used for the filters in MC simulations in [Blom & Bloem, 2007]. Table 6 gives the filter parameter values that are being used for the MC simulations.

In the target scenarios considered the target starts at speed zero and accelerates with σ_a between $40s$ and $60s$. Then decelerates with σ_a between $60s$ and $80s$ and accelerates again with σ_a between $80s$ and $100s$. Figures 1-3 show the position, speed and acceleration of the target in time for the filter scenarios 1-3. Figures 4-6 show the position, speed and acceleration of the target in time for the filter scenarios 4 and 5

Table 6: Parameter values for the filters

Filter Scenario	α	σ_a m/s^2	σ_m m	τ_1 s	τ_2 s	t_s s
1	0.9	50	30	50	5	1
2	0.9	50	30	50	50	1
3	0.9	50	30	5000	5	1
4	0.9	1	30	50	5	1
5	0.9	1	30	5000	500	1

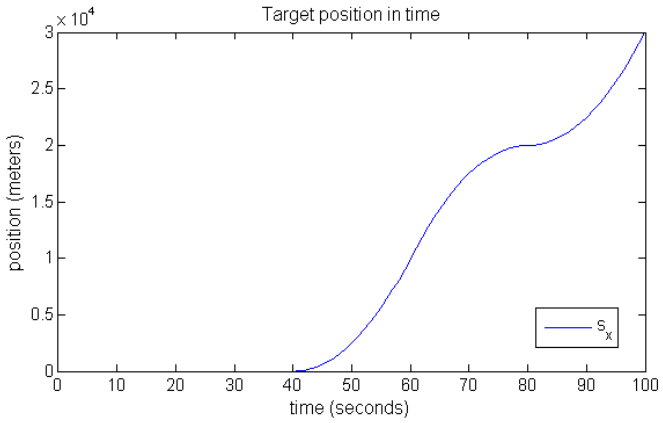

Figure 1: Target position as function of time in the target scenario considered for filter scenarios $1-3$

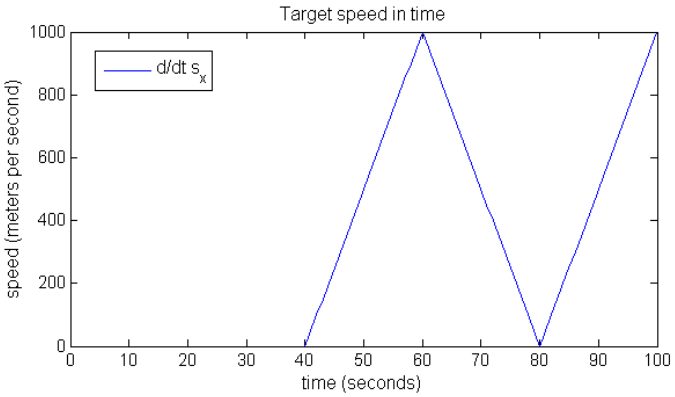

Figure 2: Target speed as function of time in the target scenario considered for filter scenarios $1-3$

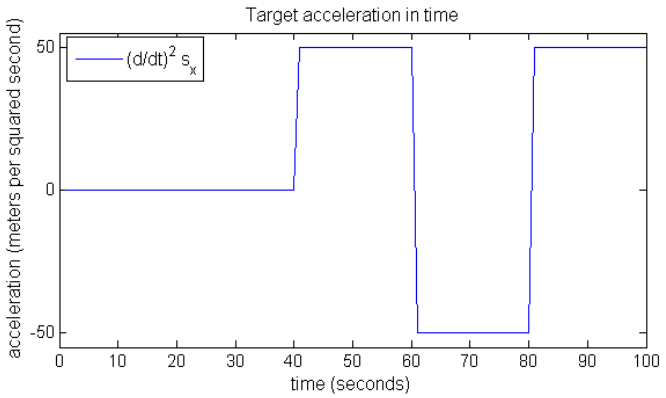

Figure 3: Target acceleration as function of time in the target scenario considered for filter scenarios $1-3$

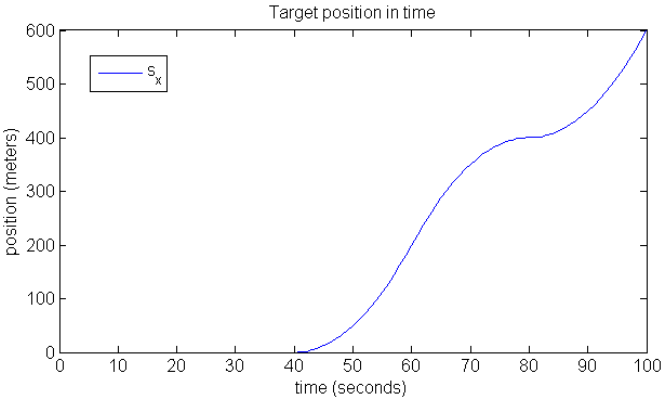

Figure 4: Target position as function of time in the target scenario considered for filter scenarios 4 and 5

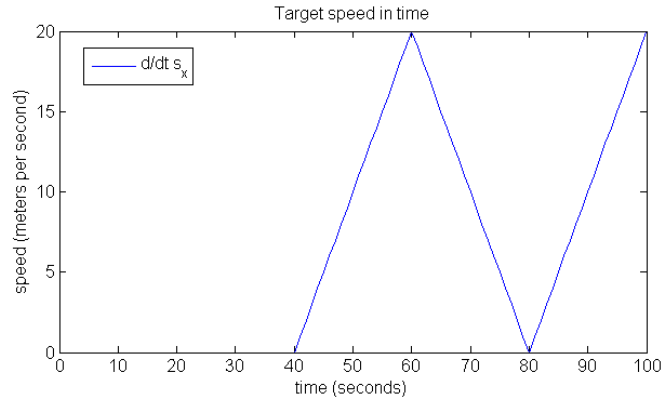

Figure 5: Target speed as function of time in the target scenario considered for filter scenarios 4 and 5

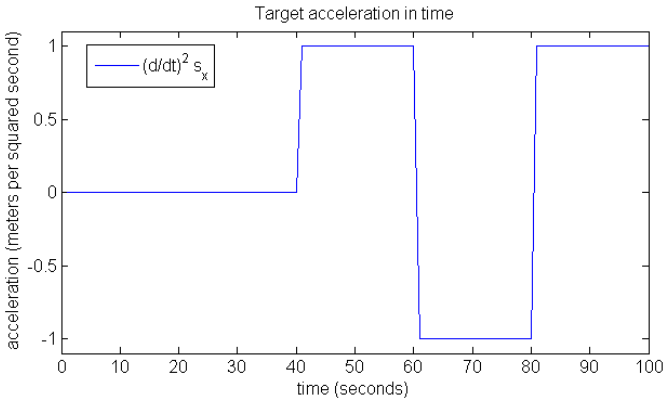

Figure 6: Target acceleration as function of time in the target scenario considered for filter scenarios 4 and 5

To make the comparison between the filters more meaningful, for all filters the same random number streams were used. That is for each target scenario the observation process $\{y_k\}$ per MC simulation run is the same for all filters.

The Root Mean Square (RMS) error of the target position is used to compare the filters. The RMS error of the target position is defined by:

$$\text{position RMS error} = \sqrt{\sum_{i=1}^{r_n} (\hat{x}_{k,i} - x_k)^2 / r_n} \tag{174}$$

where r_n is the amount of simulation runs and $\hat{x}_{k,i}$ is the filter estimation of x_k in run i at moment k.

9.6 Filter scenario I

The particle filter parameters[2] are $\sigma_a = 5g$, $\alpha = 0.9$, $\sigma_m = 30m/s^2$, $\tau_1 = 50s$ and $\tau_2 = 5s$.

First we determine how many particles we should use in the MC simulations. Therefore MC simulations containing 100 runs have been performed for the HPF using the model with two modes (M=2) and three modes (M=3). The number of particles used in these simulations are $N_p = 10^3$, $N_p = 2 \cdot 10^3$, $N_p = 5 \cdot 10^3$ and $N_p = 10^4$. The following figures show the measured RMS error of the target position in time.

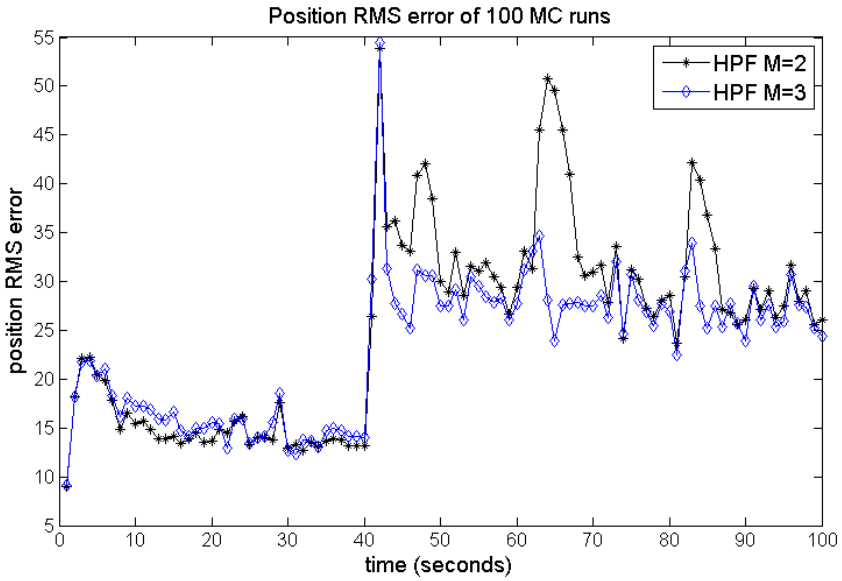

Figure 7: Filter scenario I, 100 MC runs, with $N_p = 10^3$

[2] $5g$ means 5 g-force. $1g$ is equal to $9.80665m/s^2$, meters per second squared

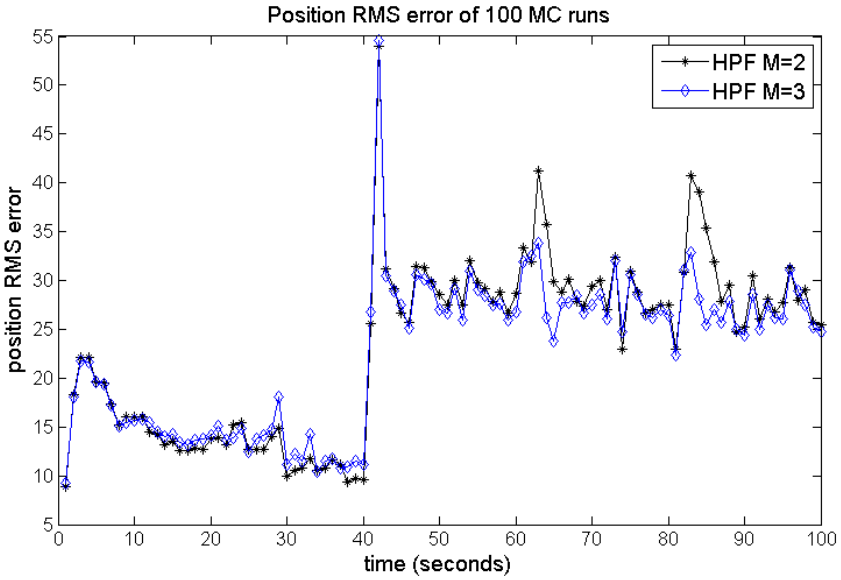

Figure 8: Filter scenario I, 100 MC runs, with $N_p = 2 \cdot 10^3$

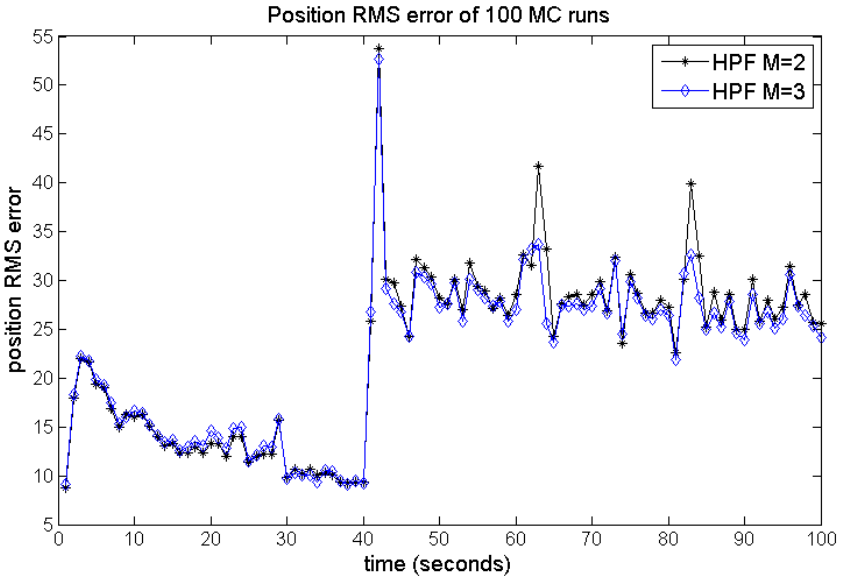

Figure 9: Filter scenario I, 100 MC runs, with $N_p = 5 \cdot 10^3$

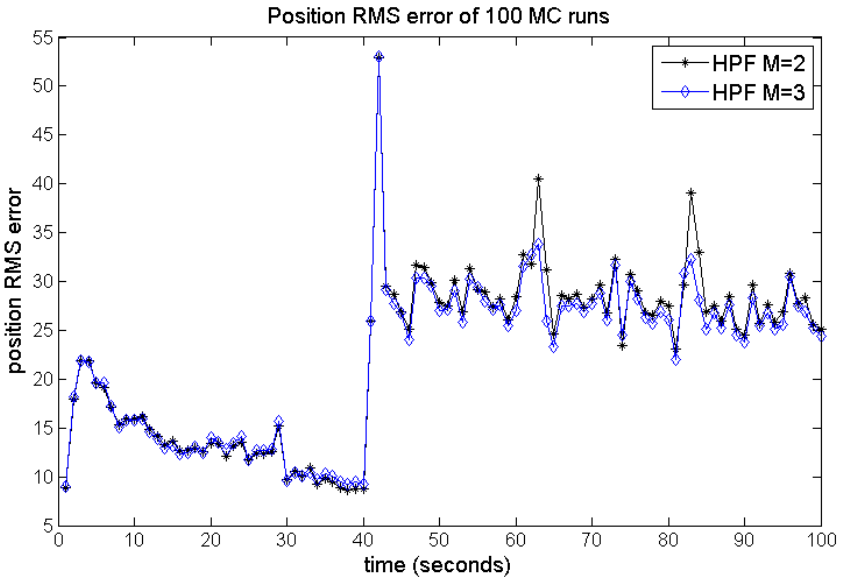

Figure 10: Filter scenario I, 100 MC runs, with $N_p = \cdot 10^4$

Based on figures 7, 8, 9 and 10 we choose to use $N_p = 5 \cdot 10^3$ particles in the MC simulations.

Then we determine how many runs we should use in the MC simulations. Therefore, MC simulations containing 100, 200 and 500 runs have been performed for the IMM filters using the models with $M = 2$ and $M = 3$. The following figures show the Root Mean Square (RMS) error of the target position in time.

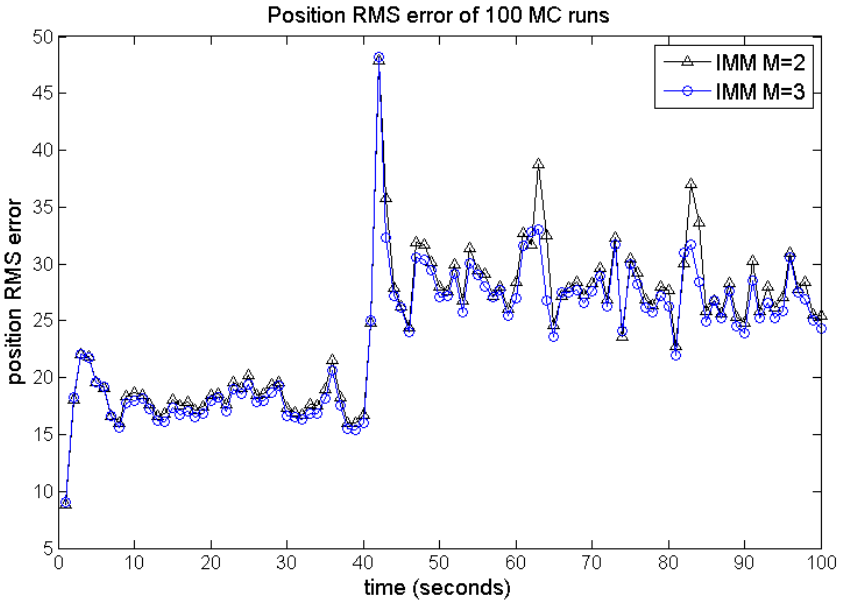

Figure 11: Filter scenario I, 100 MC runs

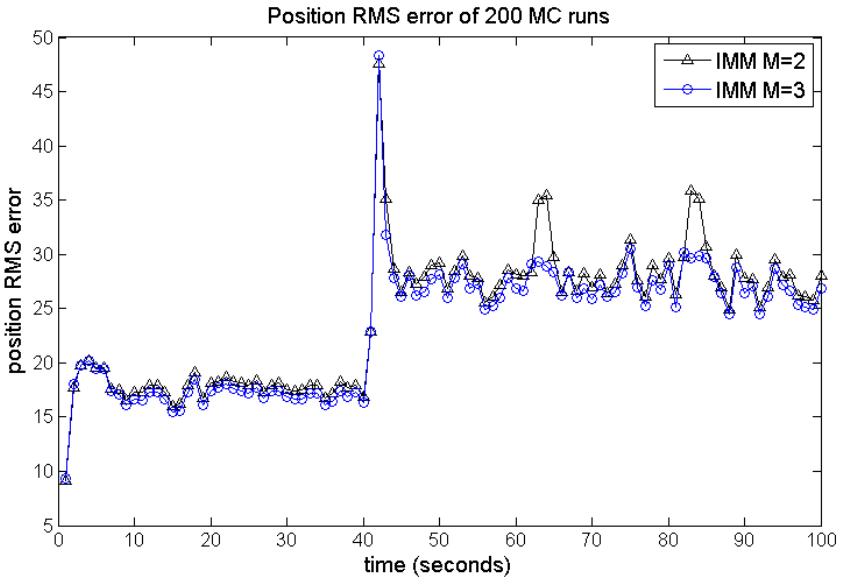

Figure 12: Filter scenario I, 200 MC runs

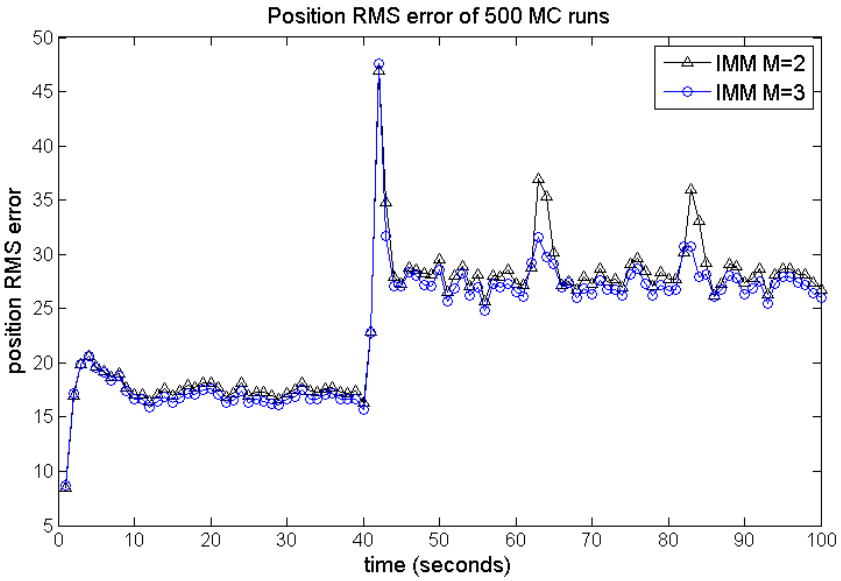

Figure 13: Filter scenario I, 500 MC runs

Based on figures 11, 12 and 13 we choose to use 200 runs in the MC simulations.

MC simulations containing 200 runs have been performed for the IMM filters and the HPF filters using the models with $M = 2$ and $M = 3$. $N_p = 5 \cdot 10^3$ particles are used in these MC simulations for the HPF filters.

Figure 14 shows the target position RMS error in time for HPF with $M = 2$ and $M = 3$. The filters perform equally well except when the target is switching between acceleration and deceleration. This happens after 60 seconds and after 80 seconds. Then the peak RMS error at the start of deceleration is for HPF with $M = 2$ significantly larger than it is for HPF with $M = 3$. However, the peaks of HPF with $M = 2$ after 60 and 80 seconds are significantly smaller than the peak after 40 seconds. Furthermore, HPF with $M = 3$ does not seem to give any significant peak when the target is switching between acceleration and deceleration.

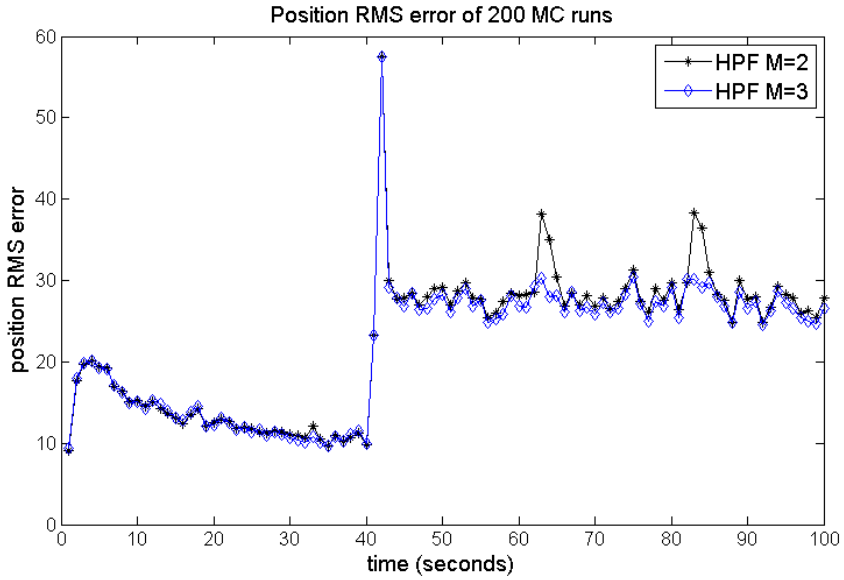

Figure 14: Filter scenario I, 200 MC runs, $N_p = 5 \cdot 10^3$

Figure 15 shows the target position RMS error in time for the IMM filter and the HPF filter with $M = 2$. HPF converges to a lower value during uniform motion than IMM does. As a side effect, the peak RMS error at the start of acceleration is for HPF slightly higher than it is for IMM. The filters perform equally well when the target is switching between acceleration and deceleration. This happens after 60 seconds and after 80 seconds. Both IMM and HPF peak at this point.

Figure 16 shows the target position RMS error in time for the IMM and the HPF with $M = 3$. Again the HPF converges to a lower value during uniform motion than IMM does. As a side effect, the peak RMS error at the start of acceleration is for HPF slightly higher than it is for IMM. The filters perform equally well when the target is switching between acceleration and deceleration. This happens after 60 seconds and after 80 seconds. Both IMM and HPF do not seem to give any significant peak at this point.

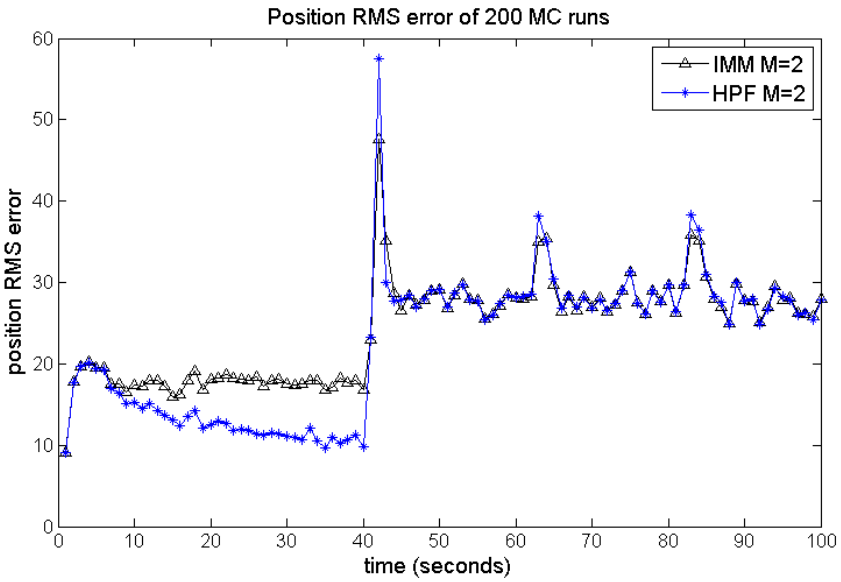

Figure 15: Filter scenario I, 200 MC runs, $N_p = 5 \cdot 10^3$

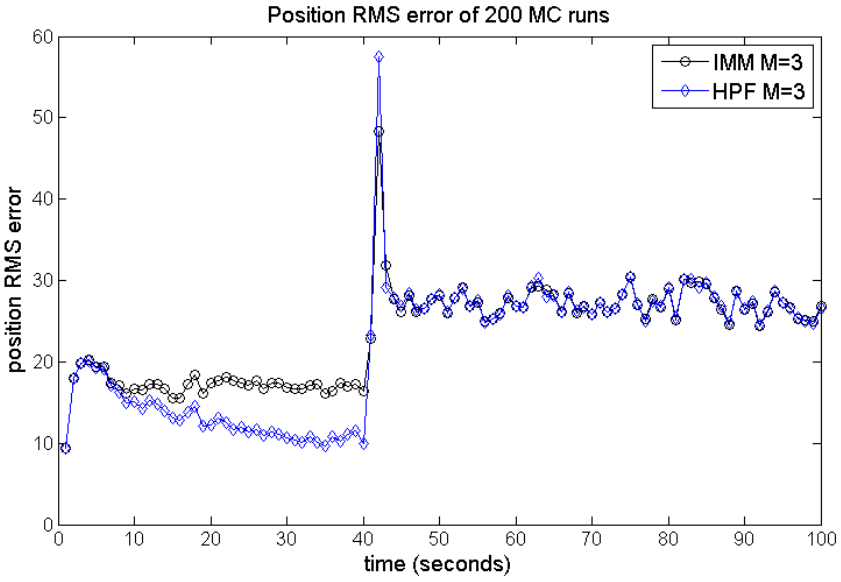

Figure 16: Filter scenario I, 200 MC runs, $N_p = 5 \cdot 10^3$

The HPF filter enables us to make a histogram of the distribution of the particles per time step. A histogram of the position errors $x^j_{error} = x^j_t - x_t,\ j = 1, ..., N_p$ based on an empirical distribution in one Monte Carlo (MC) simulation run of the particles per mode at a specific moment in time, $t = 46$ is shown in figure 17. The mode $\theta = 1$ has the most weight and the histogram of $\theta = 1$ has a Gaussian shape.

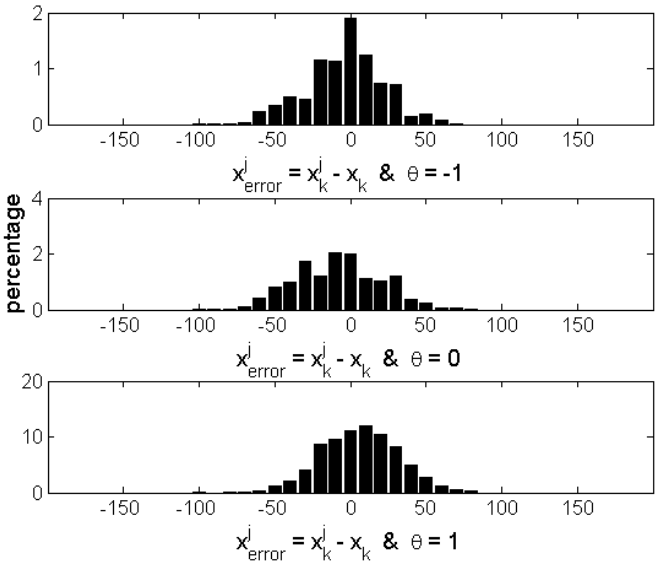

Figure 17: Example of a position histogram based on an empirical density of the particles in one MC simulation run with HPF M=3 at time t=46

A histogram of the speed errors $v^j_{error} = v^j_t - v_t,\ j = 1, ..., N_p$ with $v = \dot{s}_x$, based on an empirical distribution in one Monte Carlo (MC) simulation run of the particles per mode at a specific moment in time, $t = 46$ is shown in figure 18. The histogram of $\theta = -1$ lies the most to the left, the histogram of $\theta = 1$ lies the most to the right and the histogram of $\theta = 0$ lies in between. The horizontal position of a histogram relative to the horizontal position of the other histograms is consistent with the mode value. A particle in mode $\theta = 1$ is accelerating and its speed should therefore increase.

A histogram of the accelerations $\rho^j_t,\ j = 1, ..., N_p$ with $\rho = \ddot{s}_x$, based on an empirical distribution in one MC simulation run of the particles per mode at a specific moment in time, $t = 46$ is shown in figure 19. In figure 19 we see that some particles in deceleration mode $\theta = -1$ have a positive value for $\ddot{s}_x$. Thus, while they are in deceleration mode, they are accelerating. This is a contradiction that is caused by the target motion model. The target motion model permits the target to have a positive acceleration in deceleration mode because the prior deceleration value is assumed to satisfy a Gaussian distribution.
The horizontal position of a histogram relative to the horizontal position of the other histograms is consistent with the mode value. Furthermore, the histogram of the mode $\theta = 0$ is just one bar around zero. Due to the target motion model all particles in mode $\theta = 0$ have zero acceleration.

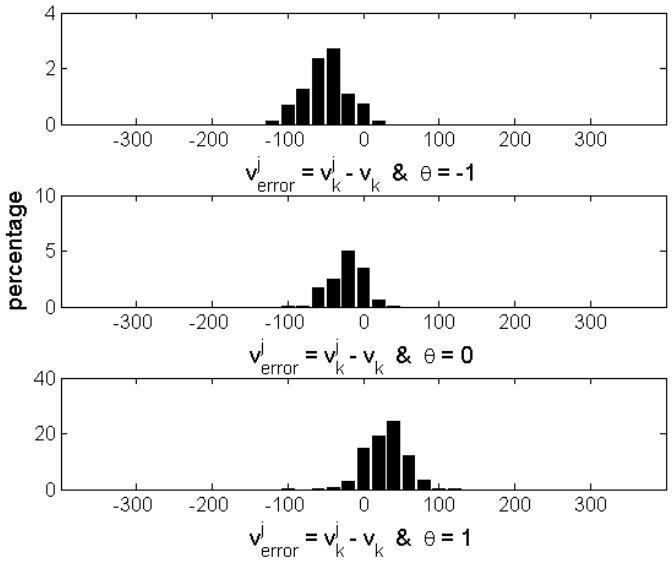

Figure 18: Example of a velocity histogram based on an empirical density of the particles in one MC simulation run with HPF M=3 at time t=46

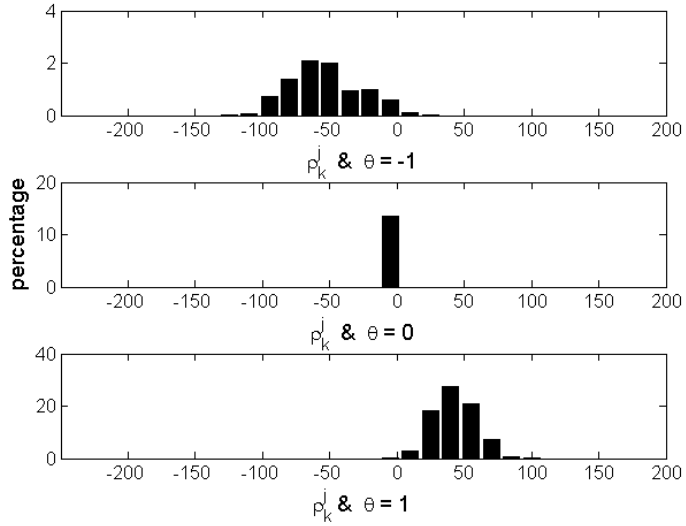

Figure 19: Example of an acceleration histogram based on an empirical density of the particles in one MC simulation run with HPF M=3 at time t=46

Figure 20 shows the target position RMS error in time for the HPF filter with $M = 3$ and the HPF filter using the model with non-Gaussian acceleration noise from section 8.4 (denoted by 'Abs HPF M=3'). The filters perform equally well and do not seem to differ significantly from each other at any moment in time.

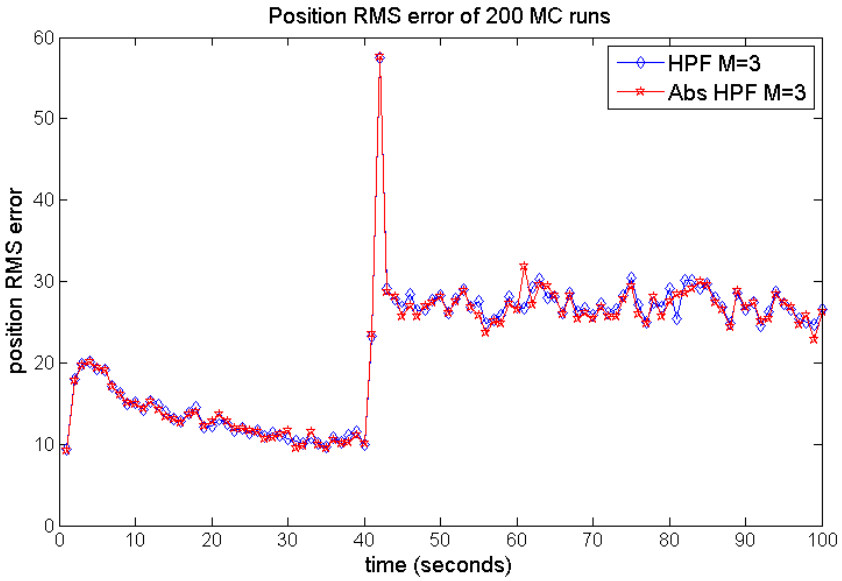

Figure 20: Filter scenario I, 200 MC runs, $N_p = 5 \cdot 10^3$

Figure 21 shows the mode distribution in time for HPF with $M = 2$ in one MC simulation run. The mode distribution seems more stable before the fist switch after $40s$.

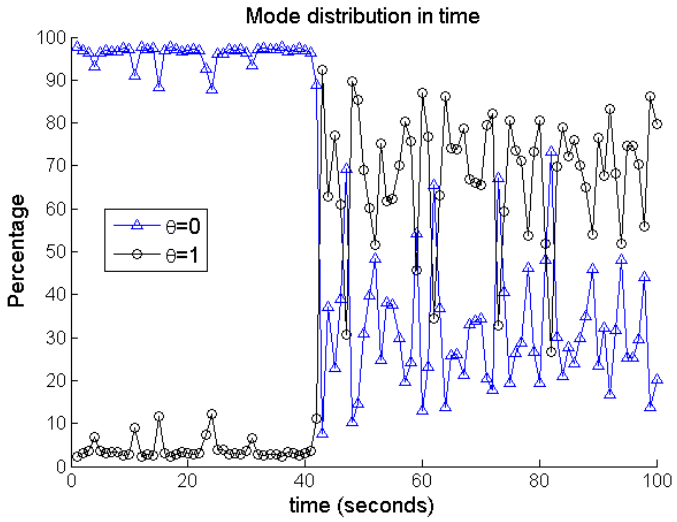

Figure 21: Filter scenario I, HPF $M = 2$, 1 MC run, $N_p = 5 \cdot 10^3$

Figure 22 shows the mode distribution in time for HPF with $M = 3$ in one MC simulation run. The mode distribution seems more stable before the fist switch after $40s$. Furthermore, the mode distribution of HPF with $M = 3$ seems more stable than the mode distribution of HPF with $M = 2$.

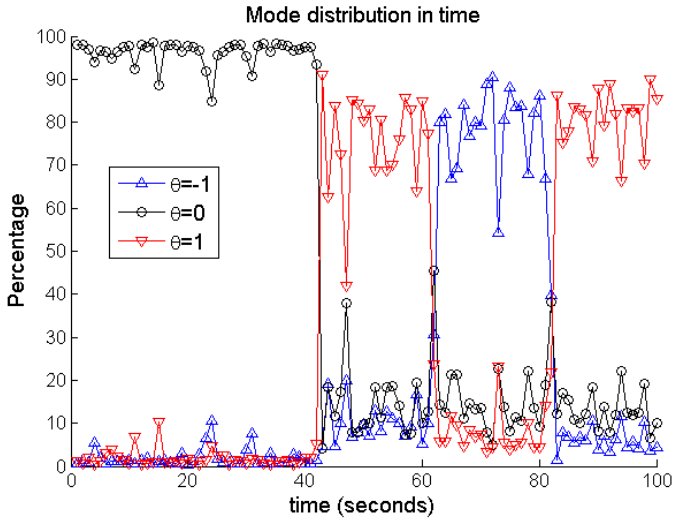

Figure 22: Filter scenario I, HPF $M = 3$, 1 MC run, $N_p = 5 \cdot 10^3$

Figure 23 shows the mode distribution in time for Abs HPF with $M = 3$ in one MC simulation run. The mode distribution seems more stable before the fist switch after $40s$. The mode distribution for HPF with $M = 3$ seems more stable than the mode distribution for Abs HPF.

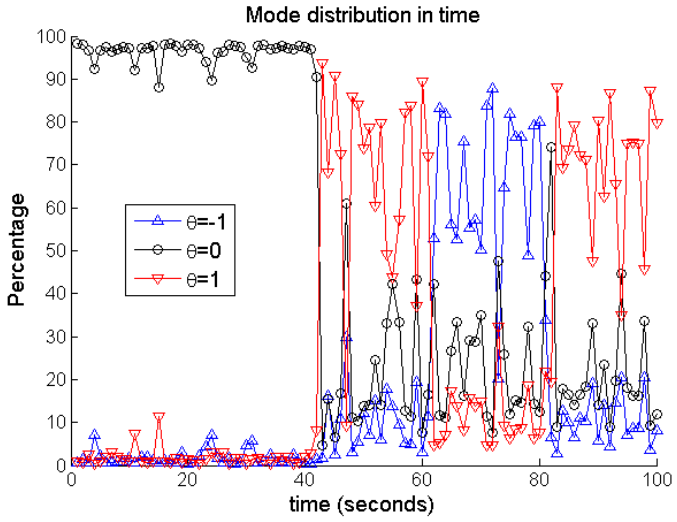

Figure 23: Filter scenario I, Abs HPF $M = 3$, 1 MC run, $N_p = 5 \cdot 10^3$

9.7 Filter scenario II

The particle filter parameters are $\sigma_a = 5g$, $\alpha = 0.9$, $\sigma_m = 30m/s^2$, $\tau_1 = 50$ and $\tau_2 = 50$. MC simulations containing 200 runs have been performed for the IMM filters and the HPF filters using the models with $M = 2$ and $M = 3$. $N_p = 5 \cdot 10^3$ particles are used in these MC simulations for the HPF filters.

Figure 24 shows the target position RMS error in time for the HPF filter with $M = 2$ and $M = 3$. The RMS position error peak after $40s$ is as high as the peak after $40s$ in scenario I. Where in scenario I HPF with $M = 3$ gave no significant peak after $60s$ and after $80s$, in scenario II both filters peak after $60s$ and $80s$. However, the peaks after 60 and 80 seconds are still significantly smaller than the peak after 40 seconds.

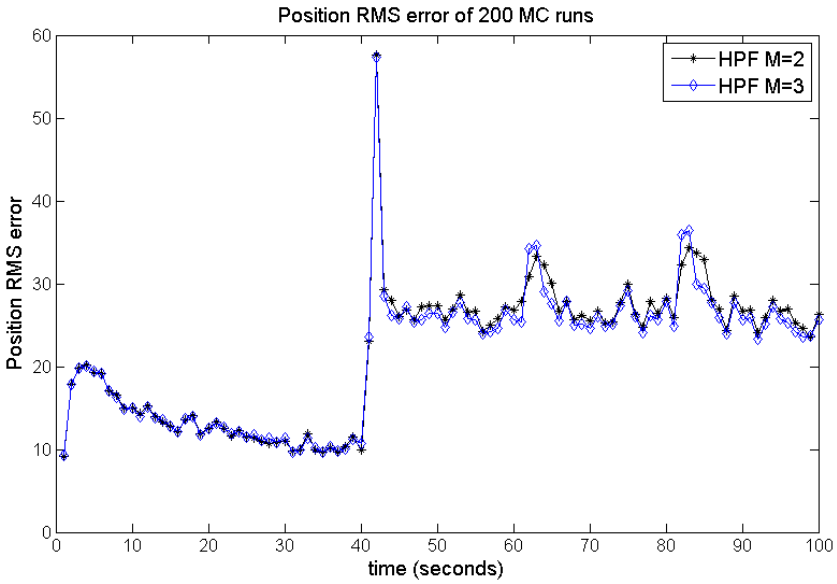

Figure 24: Filter scenario II, 200 MC runs, $N_p = 5 \cdot 10^3$

Figure 25 shows the target position RMS error in time for the IMM filter and the HPF filter with $M = 2$. The peaks after $60s$ and $80s$ of IMM seems to be slightly smaller than the peaks of HPF. Furthermore, the peak after $40s$ of IMM is slightly higher then the peak after $40s$ of IMM with $M = 2$ in scenario I.

Figure 26 shows the target position RMS error in time for the IMM filter and the HPF filter with $M = 3$. Both filters seem to perform equally well after $60s$ and $80s$.

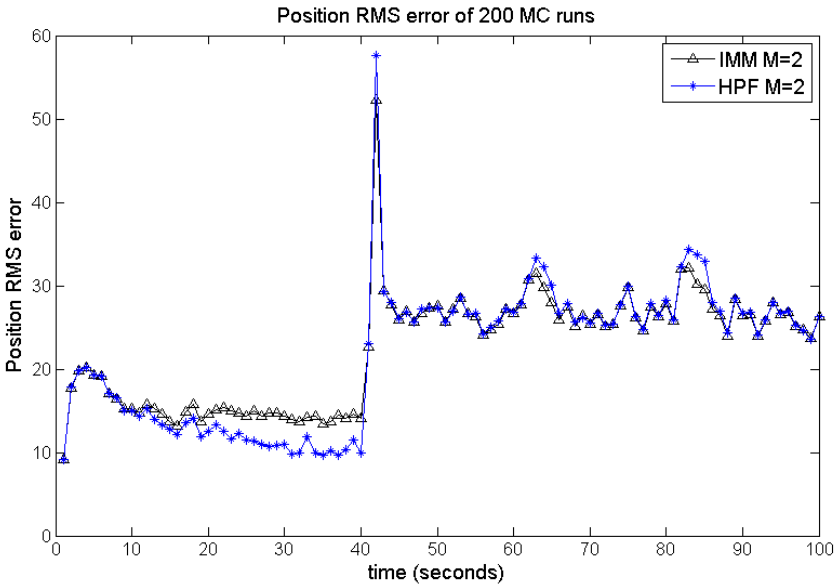

Figure 25: Filter scenario II, 200 MC runs, $N_p = 5 \cdot 10^3$

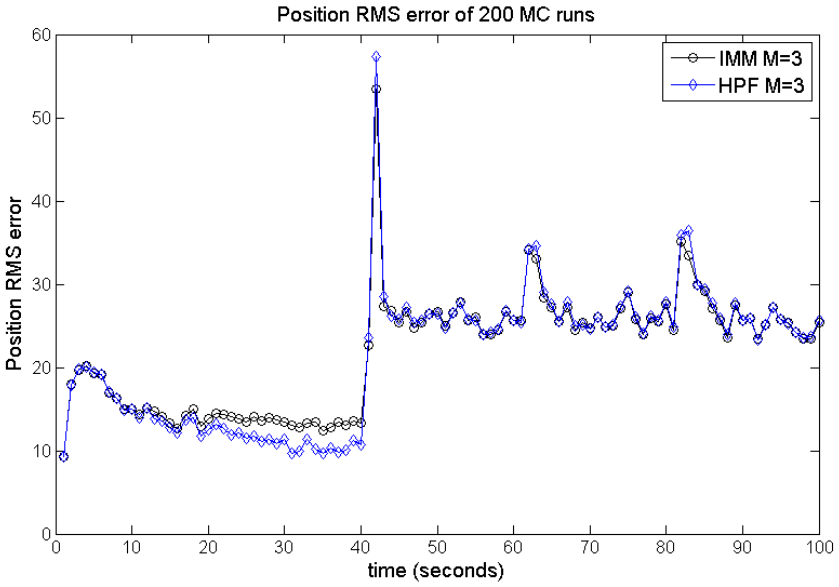

Figure 26: Filter scenario II, 200 MC runs, $N_p = 5 \cdot 10^3$

A histogram of the position errors $x^j_{error} = x^j_t - x_t,\ j = 1, ..., N_p$ based on an empirical distribution in one Monte Carlo (MC) simulation run of the particles per mode at a specific moment in time, $t = 46$ is shown in figure 27. The Gaussian shape we saw in figure 17 is less visible in figure 27.

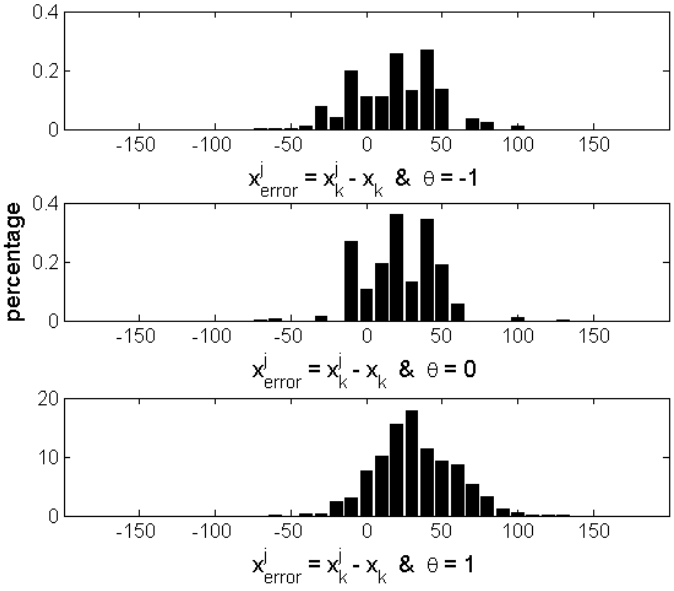

Figure 27: Example of a position histogram based on an empirical density of the particles in one MC simulation run with HPF M=3 at time t=46, $N_p = 5 \cdot 10^3$

A histogram of the speed errors $v^j_{error} = v^j_t - v_t,\ j = 1, ..., N_p$ with $v = \dot{s}_x$, based on an empirical distribution in one Monte Carlo (MC) simulation run of the particles per mode at a specific moment in time, $t = 46$ is shown in figure 28. The horizontal position of a histogram relative to the horizontal position of the other histograms is consistent with the mode value.

A histogram of the accelerations $\rho^j_t,\ j = 1, ..., N_p$ with $\rho = \ddot{s}_x$, based on an empirical distribution in one MC simulation run of the particles per mode at a specific moment in time, $t = 46$ is shown in figure 29. What we saw in figure 19 we see also in figure 29; some particles in deceleration mode $\theta = -1$ have a positive value for $\ddot{s}_x$.

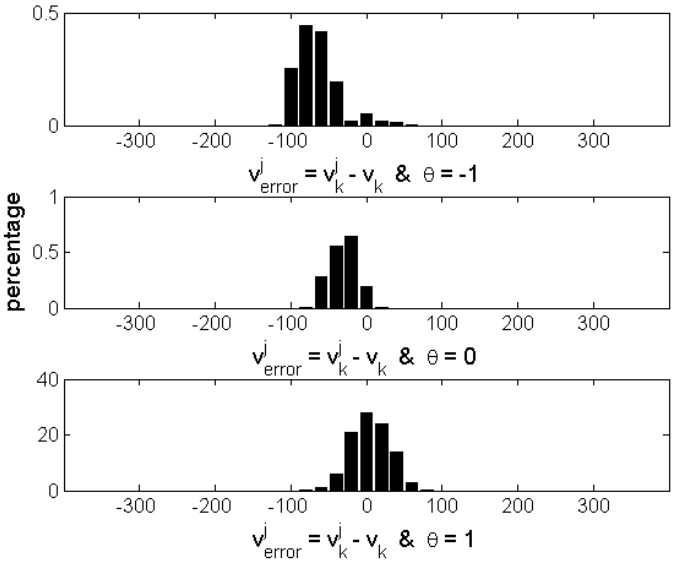

Figure 28: Example of a velocity histogram based on an empirical density of the particles in one MC simulation run with HPF M=3 at time t=46, $N_p = 5 \cdot 10^3$

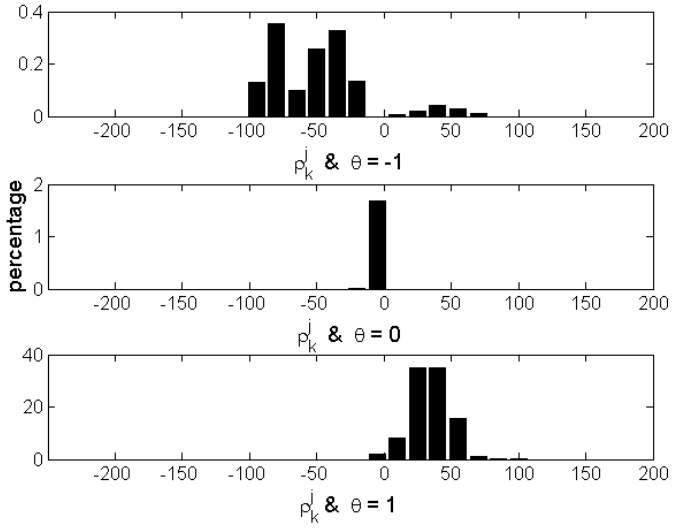

Figure 29: Example of an acceleration histogram based on an empirical density of the particles in one MC simulation run with HPF M=3 at time t=46, $N_p = 5 \cdot 10^3$

The figures 30-32 show histograms of the position, speed and acceleration based on an empirical distribution in one MC simulation run, using the HPF M=3 filter, of the particles per mode at a specific moment in time, $t = 46$. $N_p = 5 \cdot 10^4$ particles are used in this simulation. The Gaussian shape we saw in figure 17 is visible in figure 30. In figure 31 the horizontal position of a histogram is relative to the horizontal position of the other histograms consistent with the mode value. In figure (32) the histogram at mode $\theta = -1$ shows a peak around $\rho = 50$. Thus the mode for deceleration tends to follow the acceleration mode. But the peak around $\rho = -40$ is larger than the one around $\rho = 50$.

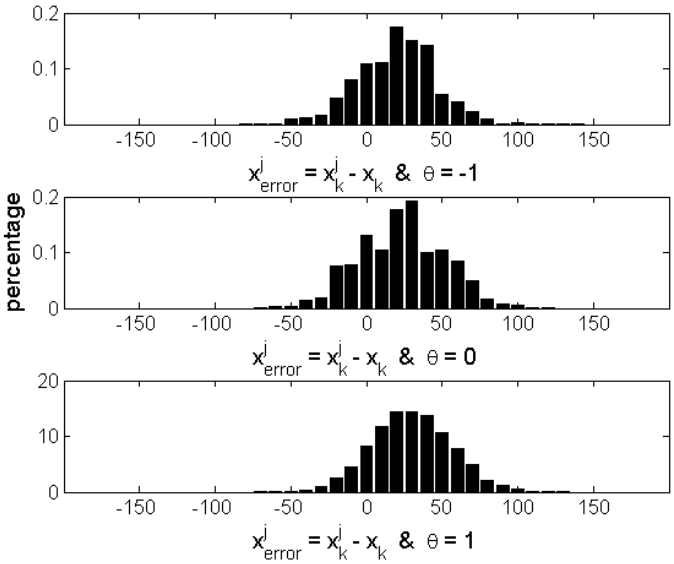

Figure 30: Example of a position histogram based on an empirical density of the particles in one MC simulation run with HPF M=3 at time t=46, $N_p = 5 \cdot 10^4$

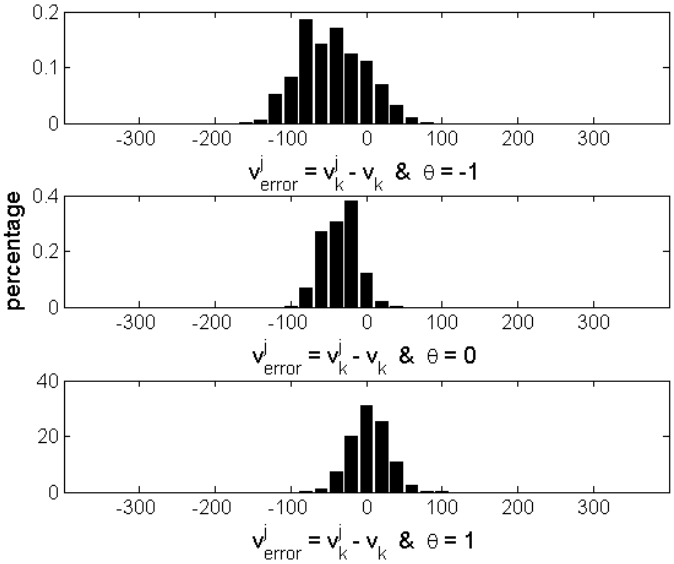

Figure 31: Example of a velocity histogram based on an empirical density of the particles in one MC simulation run with HPF M=3 at time t=46, $N_p = 5 \cdot 10^4$

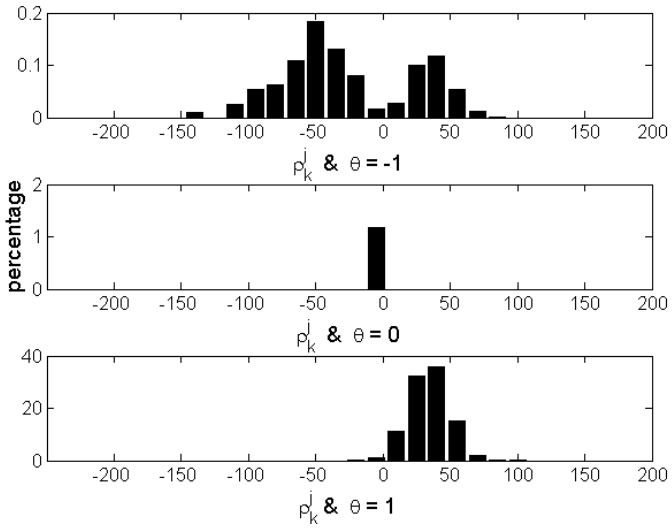

Figure 32: Example of an acceleration histogram based on an empirical density of the particles in one MC simulation run with HPF M=3 at time t=46, $N_p = 5 \cdot 10^4$

Let us look at the histograms just after the mode switch after $60s$. The following figures show histograms of the accelerations ρ_t^j, $j = 1, ..., N_p$ with $\rho = \ddot{s}_x$, based on an empirical distribution in one MC simulation run of the particles per mode at some specific moments in time, $t = 60$, $t = 61$, $t = 62$, $t = 63$ and $t = 64$. $N_p = 5 \cdot 10^4$ particles are used in this simulation.

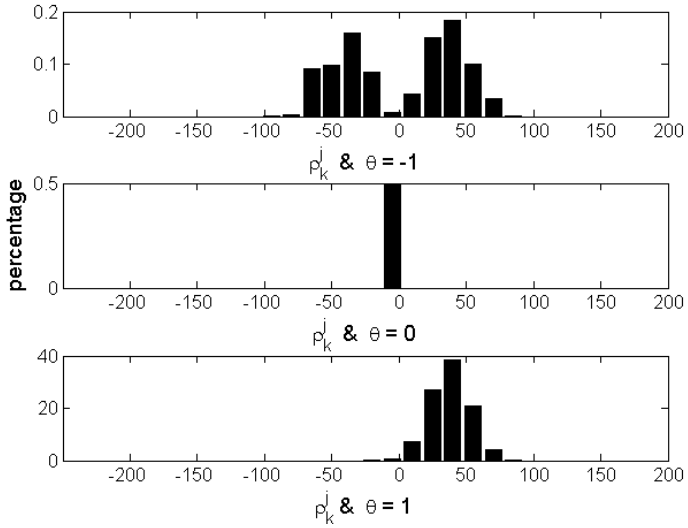

Figure 33: Example of an acceleration histogram based on an empirical density of the particles in one MC simulation run with HPF M=3 at time t=60, $N_p = 5 \cdot 10^4$

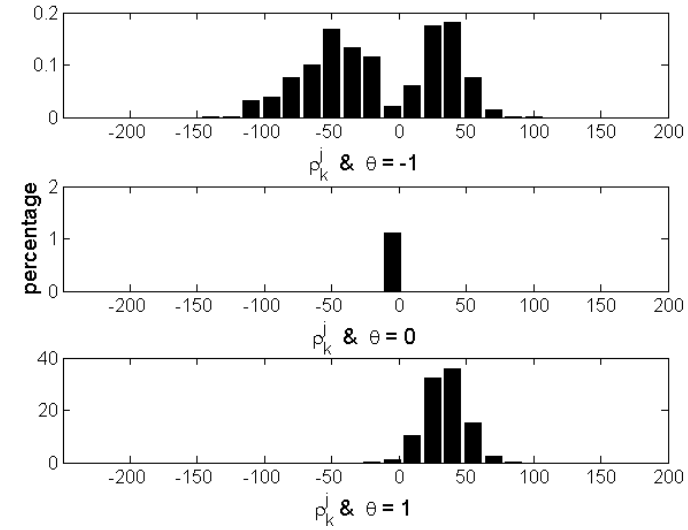

Figure 34: Example of an acceleration histogram based on an empirical density of the particles in one MC simulation run with HPF M=3 at time t=61, $N_p = 5 \cdot 10^4$

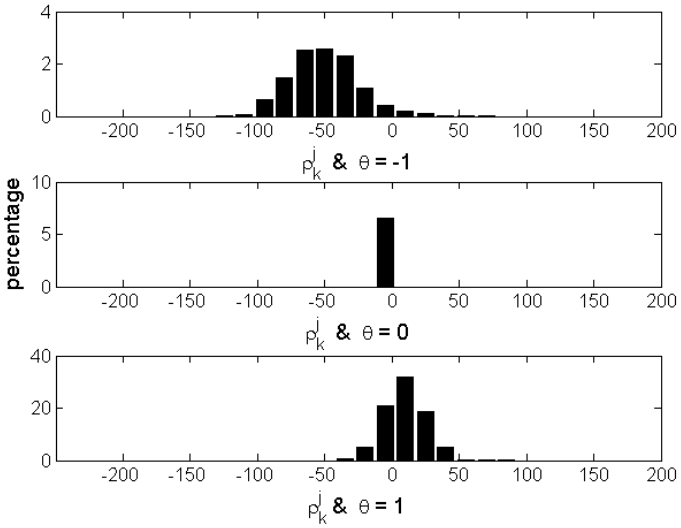

Figure 35: Example of an acceleration histogram based on an empirical density of the particles in one MC simulation run with HPF M=3 at time t=62, $N_p = 5 \cdot 10^4$

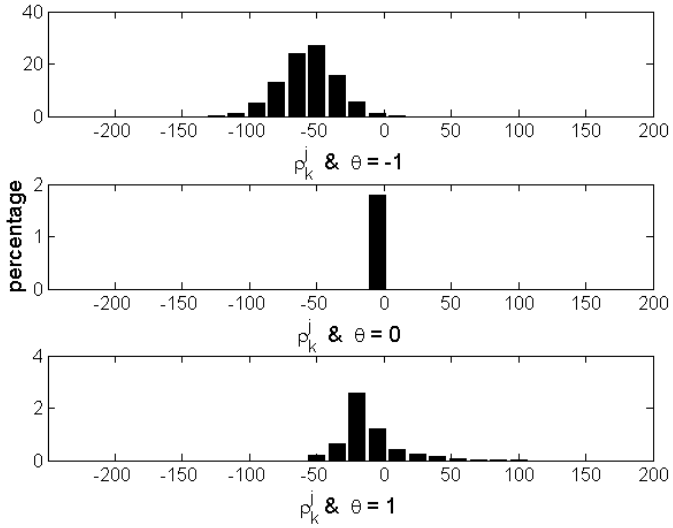

Figure 36: Example of an acceleration histogram based on an empirical density of the particles in one MC simulation run with HPF M=3 at time t=63, $N_p = 5 \cdot 10^4$

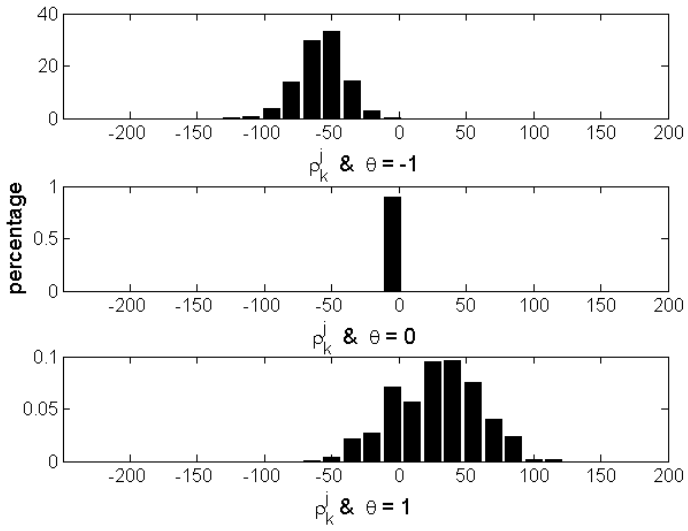

Figure 37: Example of an acceleration histogram based on an empirical density of the particles in one MC simulation run with HPF M=3 at time t=64, $N_p = 5 \cdot 10^4$

In figures 33-37 we see how the histograms change as time progresses. At $t = 60$ the histogram for the mode $\theta = -1$ is shaped by two peaks. One with negative values and one with positive values. But the weight of mode $\theta = 1$ is much larger than the weight of mode $\theta = -1$. As time progresses, first the peak in the histogram for mode $\theta = -1$ with positive values disappears and the histogram of mode $\theta = 1$ shifts to the left. Then the weight shifts to mode $\theta = -1$ and the histogram of mode $\theta = 1$ shifts more to the left. Finally, the histogram of mode $\theta = 1$ shifts back to the right and we end with two histograms shaped by one peak. The histogram of mode $\theta = -1$ with negative values and the histogram of mode $\theta = 1$ with positive values.

Figure 38 shows the target position RMS error in time for the HPF filter with $M = 3$ and the HPF filter using the model with non-Gaussian acceleration noise from section 8.4 (denoted by 'Abs HPF M=3'). The filters perform equally well, except when the target is switching between acceleration and deceleration. The peaks after $60s$ and $80s$ of Abs HPF seem to be slightly earlier then the peaks of HPF. Further, the peak after $80s$ of Abs HPF is slightly smaller than the peak of HPF after $80s$.

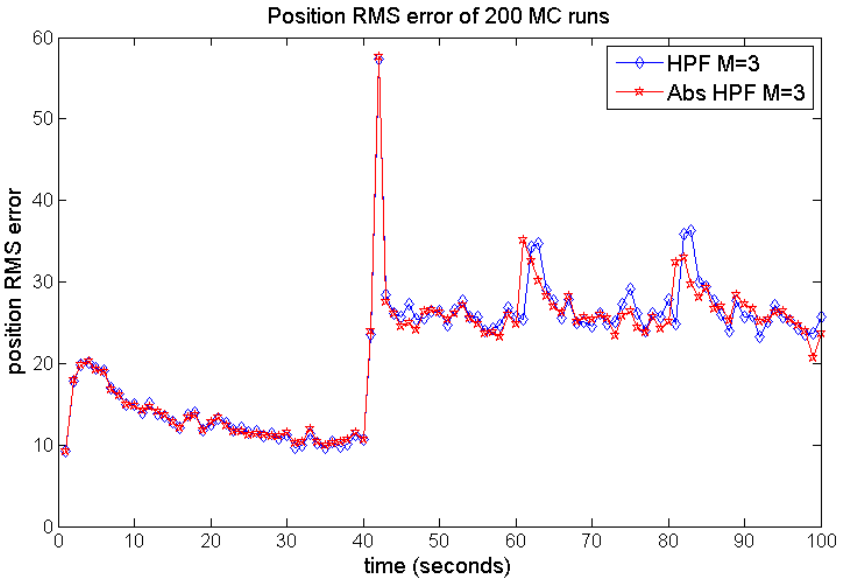

Figure 38: Filter scenario II, 200 MC runs, $N_p = 5 \cdot 10^3$

Figures 39-41 show histograms of the position, speed and acceleration based on an empirical distribution in one MC simulation run using the Abs HPF M=3 filter, of the particles per mode at a specific moment in time, $t = 46$. $N_p = 5 \cdot 10^4$ particles are used in this simulation. The Gaussian shape we saw in figure 17 and 30 is visible in figure 39. Furthermore, the horizontal position of the histogram of mode $\theta = 1$ in figure 39 seems more to the right than the histogram of mode $\theta = -1$. In figure 40 we see again that the horizontal position of a histogram relative to the horizontal position of the other histograms is consistent with the mode value.
The target motion model does not permit the target to have a positive acceleration value in deceleration mode. In figure 41 we see no particles in deceleration mode $\theta = -1$ that have a positive value for $\ddot{s}_x$.

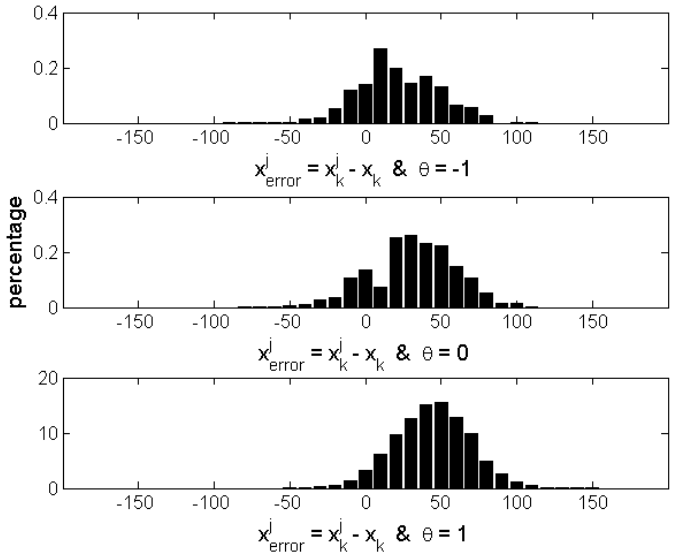

Figure 39: Example of a position histogram based on an empirical density of the particles in one MC simulation run with Abs HPF M=3 at time t=46, $N_p = 5 \cdot 10^4$

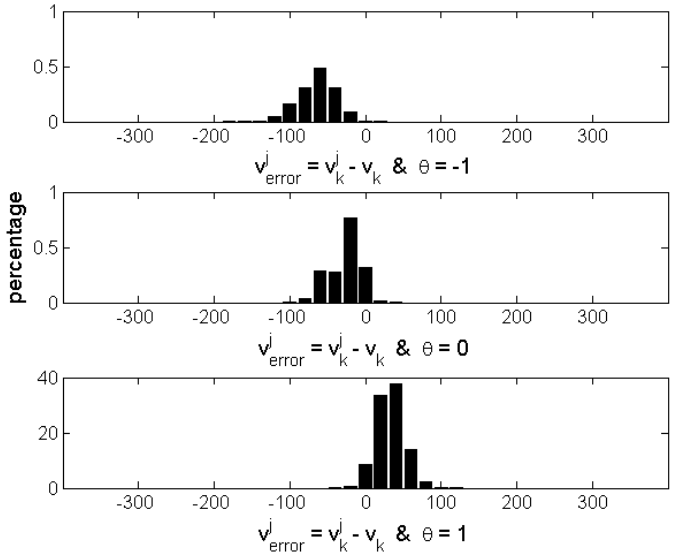

Figure 40: Example of a velocity histogram based on an empirical density of the particles in one MC simulation run with Abs HPF M=3 at time t=46, $N_p = 5 \cdot 10^4$

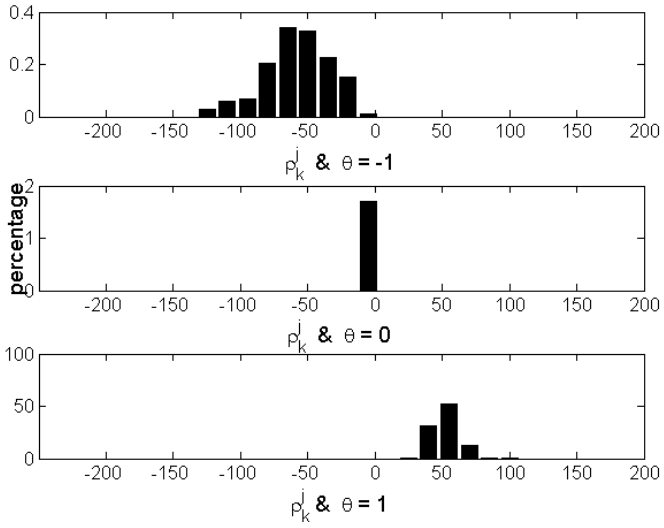

Figure 41: Example of an acceleration histogram based on an empirical density of the particles in one MC simulation run with Abs HPF M=3 at time t=46, $N_p = 5 \cdot 10^4$

Figure 42 shows the mode distribution in time for the HPF with $M = 2$ in one MC simulation run. The mode distribution seems more stable than the mode distribution in scenario I figure 21.

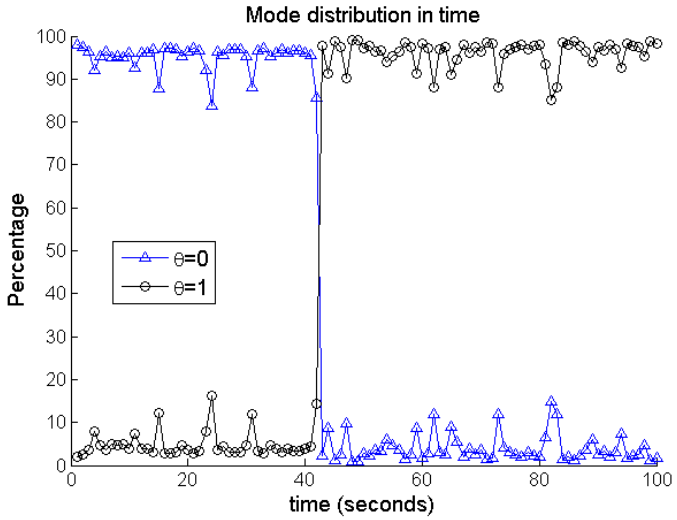

Figure 42: Filter scenario II, HPF $M = 2$, 1 MC run, $N_p = 5 \cdot 10^3$

Figure 43 shows the mode distribution in time for the HPF with $M = 3$ in one MC simulation run. The mode distribution of figure 43 seems more stable than the mode distribution in scenario I figure 21. Furthermore, the mode distribution of HPF with $M = 3$ in figure 43 seems more stable than the mode distribution of HPF with $M = 2$ in figure 42.

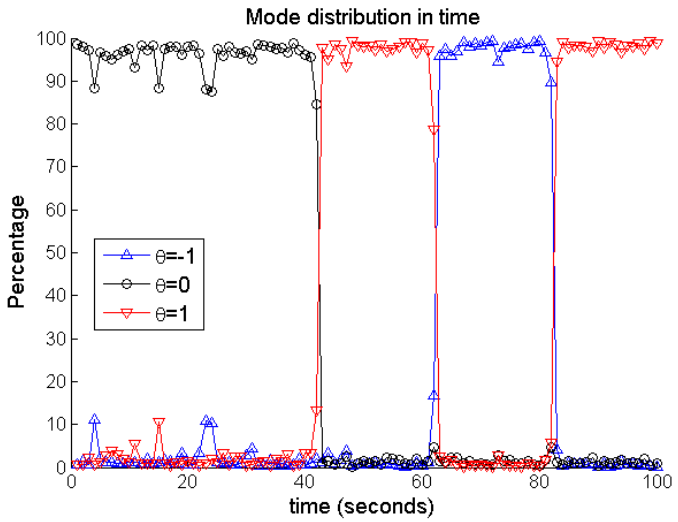

Figure 43: Filter scenario II, HPF $M = 3$, 1 MC run, $N_p = 5 \cdot 10^3$

Figure 44 shows the mode distribution in time for the Abs HPF with $M = 3$ in one MC simulation run. The mode distribution for the HPF $M = 3$ seems more stable than the mode distribution for the Abs HPF. But, the mode distribution of Abs HPF in figure 44 seems more stable than the mode distribution of Abs HPF in scenario II figure 23.

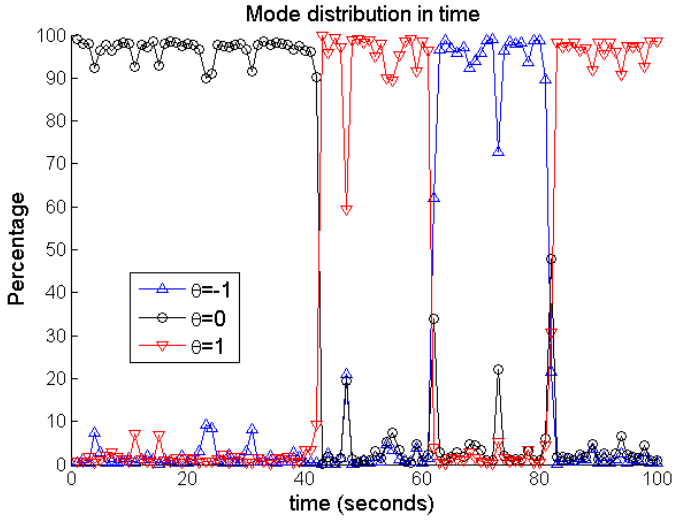

Figure 44: Filter scenario II, Abs HPF $M = 3$, 1 MC run, $N_p = 5 \cdot 10^3$

9.8 Filter scenario III

The particle filter parameters are $\sigma_a = 5g$, $\alpha = 0.9$, $\sigma_m = 30m/s^2$, $\tau_1 = 5000$ and $\tau_2 = 5$. MC simulations containing 200 runs have been performed for the IMM filters and the HPF filters using the models with $M = 2$ and $M = 3$. $N_p = 5 \cdot 10^3$ particles are used in these MC simulations for the HPF filters.

Figure 45 shows the target position RMS error in time for the HPF filter with $M = 2$ and $M = 3$. The RMS position error peak after 40s is higher than the peak after 40s in scenarios I and II. Unlike in scenarios I and II, in scenario III HPF with $M = 2$ seems to perform worse than HPF with $M = 3$. Furthermore, HPF with $M = 3$ does not seem to give any significant peak when the target is switching between acceleration and deceleration. Figure 45 shows the target position RMS error in time for the HPF filter with $M = 2$ and $M = 3$.

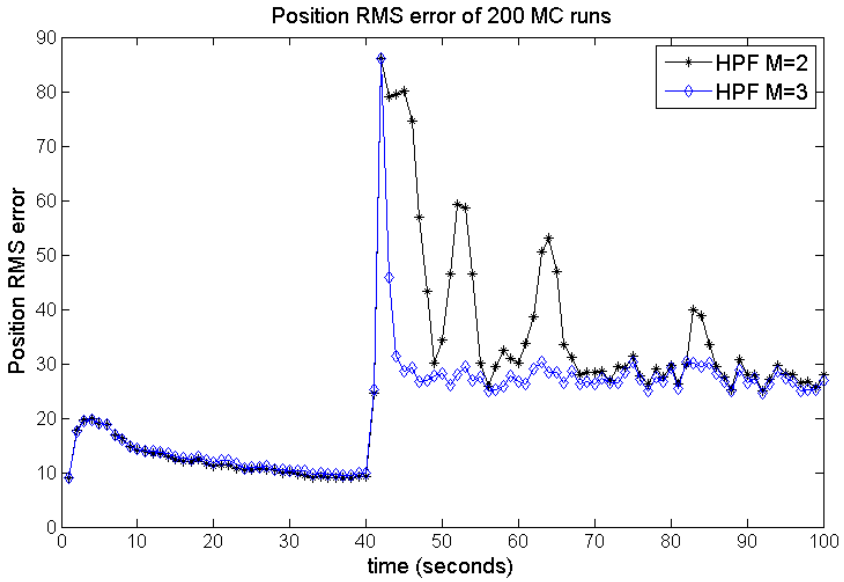

Figure 45: Filter scenario III, 200 MC runs, $N_p = 5 \cdot 10^3$

Figure 46 shows the target position RMS error in time for the IMM filter and the HPF filter with $M = 2$. IMM seems to be more stable than HPF. Furthermore, the peak after 40s of IMM is higher than the peak after 40s of IMM with $M = 2$ in scenarios I and II. IMM with $M = 2$ peaks when the target is switching between acceleration and deceleration. The peaks in scenario III are slightly higher than in scenarios I and II.

Figure 47 shows the target position RMS error in time for the IMM filter and the HPF filter with $M = 3$. Both filters seem to perform equally well. IMM gives a higher peak after $40s$ than HPF.

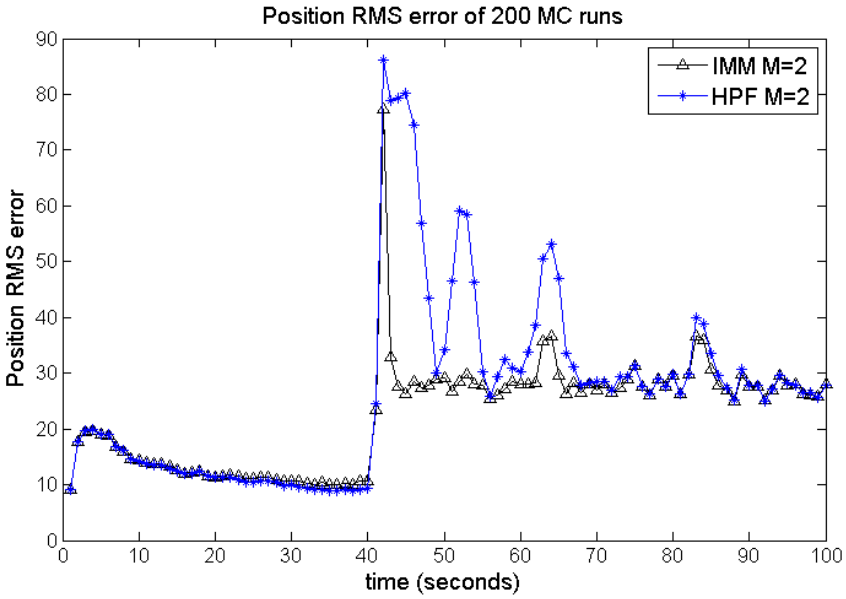

Figure 46: Filter scenario III, 200 MC runs, $N_p = 5 \cdot 10^3$

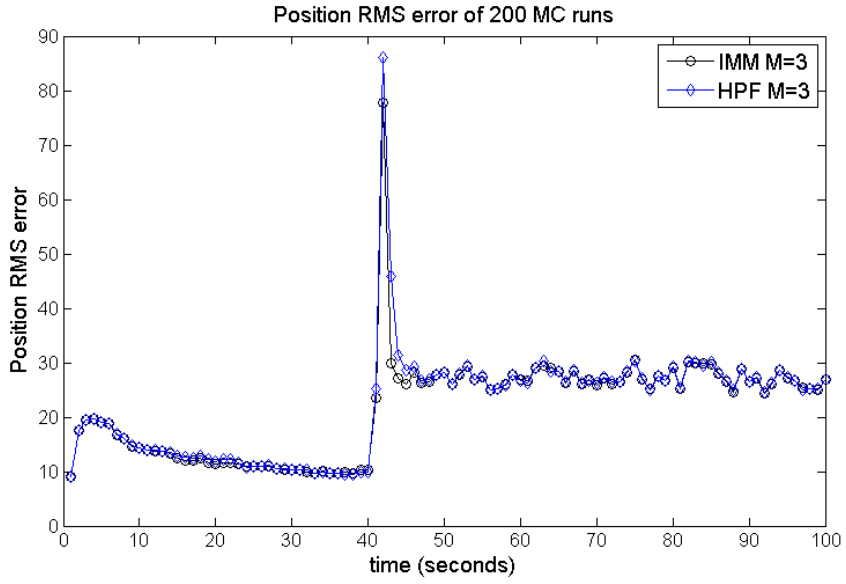

Figure 47: Filter scenario III, 200 MC runs, $N_p = 5 \cdot 10^3$

Figure 48 shows the target position RMS error in time for the IMM filter with $M = 2$ and $M = 3$. IMM with $M = 3$ performs better than IMM with $M = 2$.

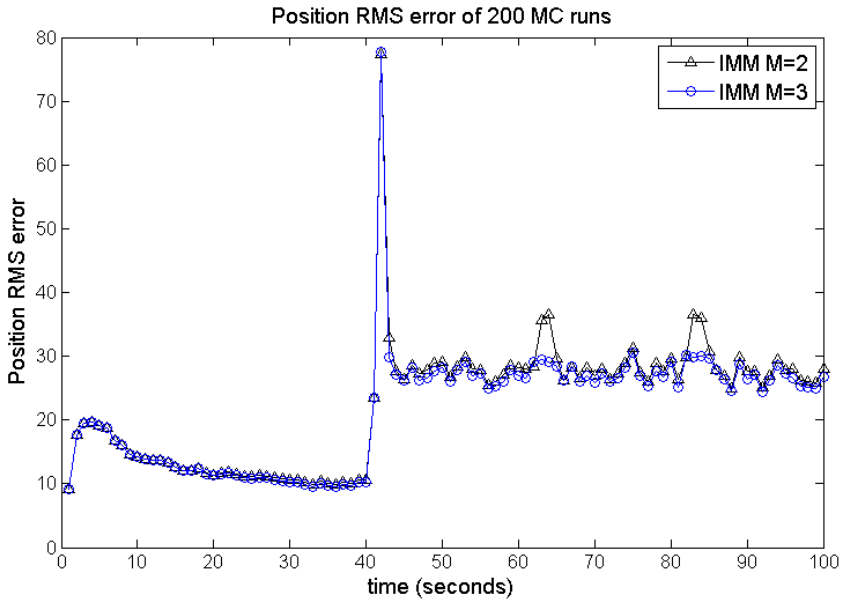

Figure 48: Filter scenario V, 200 MC runs, $N_p = 5 \cdot 10^3$

Figure 49 shows the target position RMS error in time for the HPF filter with $M = 3$ and the HPF filter using the model with non-Gaussian acceleration noise from section 8.4 (denoted by 'Abs HPF M=3'). Both filters perform equally well.

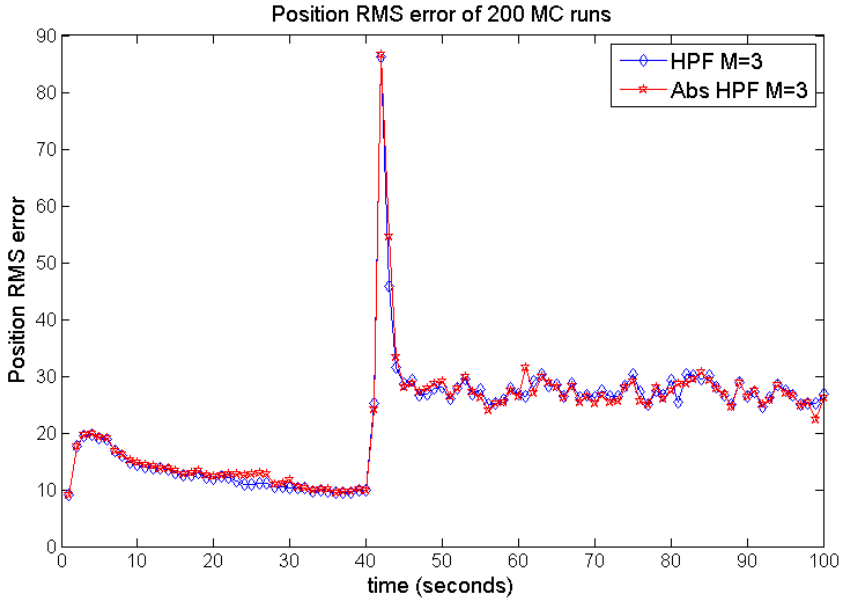

Figure 49: Filter scenario III, 200 MC runs, $N_p = 5 \cdot 10^3$

9.9 Filter scenario IV

The particle filter parameters are $\sigma_a = 0.1g$, $\alpha = 0.9$, $\sigma_m = 30m/s^2$, $\tau_1 = 50$ and $\tau_2 = 5$. MC simulations containing 200 runs have been performed for the IMM filters and the HPF filters using the models with $M = 2$ and $M = 3$. $N_p = 5 \cdot 10^3$ particles are used in these MC simulations for the HPF filters.

Figure 50 shows the target position RMS error in time for HPF with $M = 2$ and $M = 3$. Both filters seem to perform equally well, but when the target is switching between acceleration and deceleration HPF with $M = 3$ seems to perform slightly better than HPF with $M = 2$.

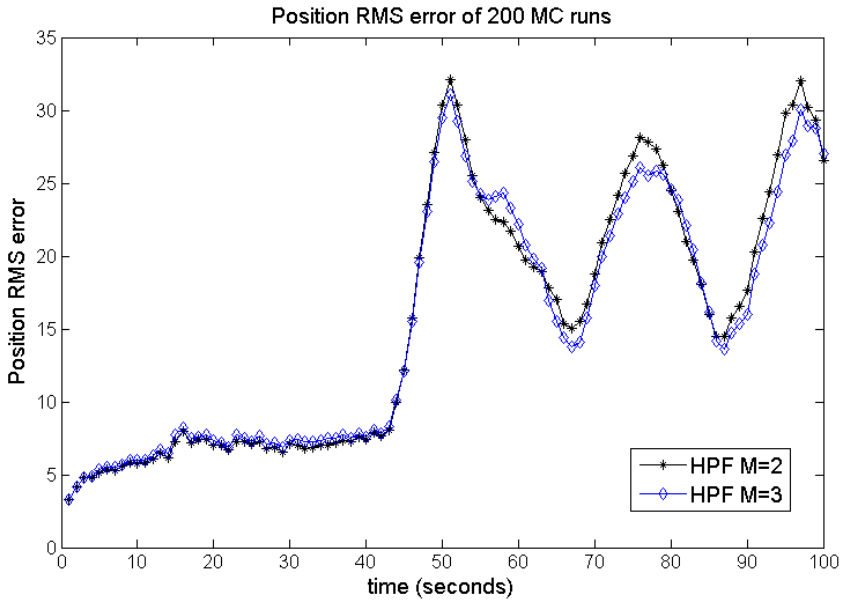

Figure 50: Filter scenario IV, 200 MC runs, $N_p = 5 \cdot 10^3$

Figure 51 shows the target position RMS error in time for the IMM filter and the HPF filter with $M = 2$. The peaks of IMM seem to be later than the peaks of HPF. Furthermore, HPF converges to a lower value during uniform motion than IMM does.

Figure 52 shows the target position RMS error in time for the IMM filter and the HPF filter with $M = 3$. The first peak after $40s$ of IMM is later than the first peak of HPF. When the target is switching between acceleration and deceleration the filters seem to perform equally well. HPF converges to a lower value during uniform motion than IMM does.

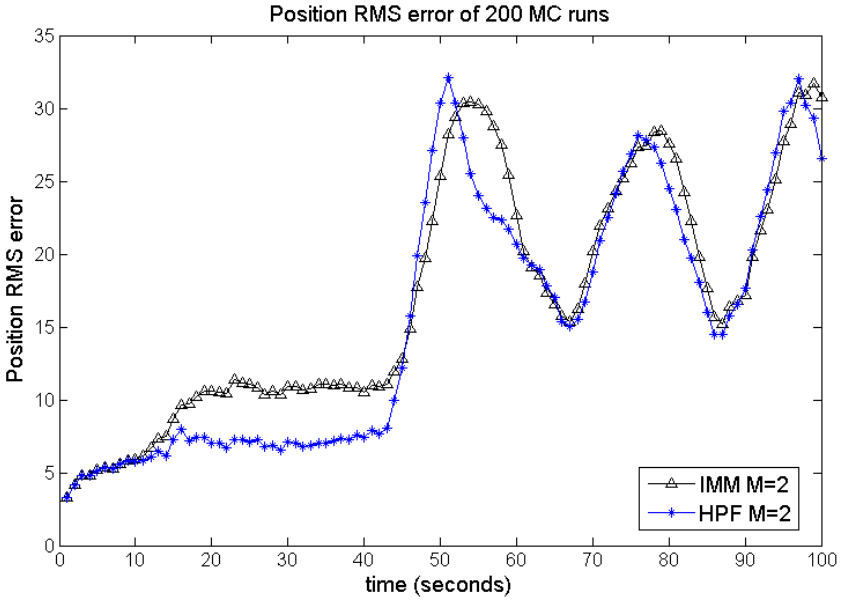

Figure 51: Filter scenario IV, 200 MC runs, $N_p = 5 \cdot 10^3$

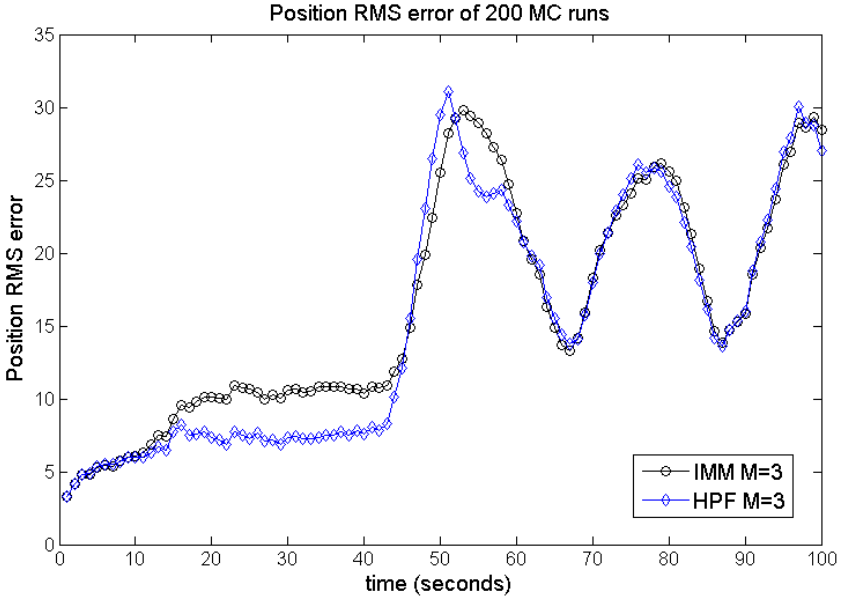

Figure 52: Filter scenario IV, 200 MC runs, $N_p = 5 \cdot 10^3$

Figure 53 shows the target position RMS error in time for the IMM filter with $M = 2$ and $M = 3$. IMM with $M = 3$ performs better than IMM with $M = 2$. Both filters peak at the same moments in time.

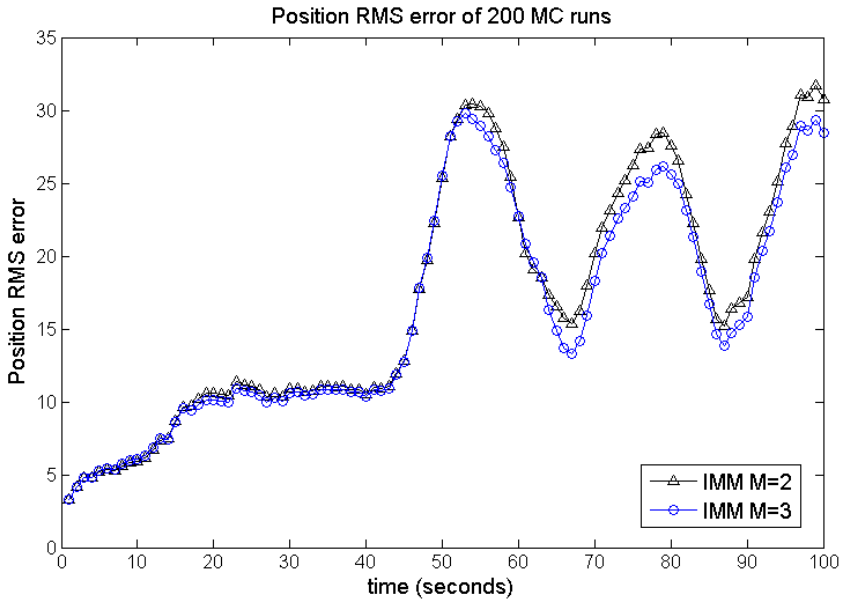

Figure 53: Filter scenario IV, 200 MC runs, $N_p = 5 \cdot 10^3$

Figure 54 shows the target position RMS error in time for the HPF filter with $M = 3$ and the HPF filter using the model with non-Gaussian acceleration noise from section 8.4 (denoted by 'Abs HPF M=3'). When the target is switching between acceleration and deceleration, Abs HPF seems more stable than HPF. The position RMS peaks of Abs HPF are smaller but Abs HPF converges less when the target is switching between acceleration and deceleration.

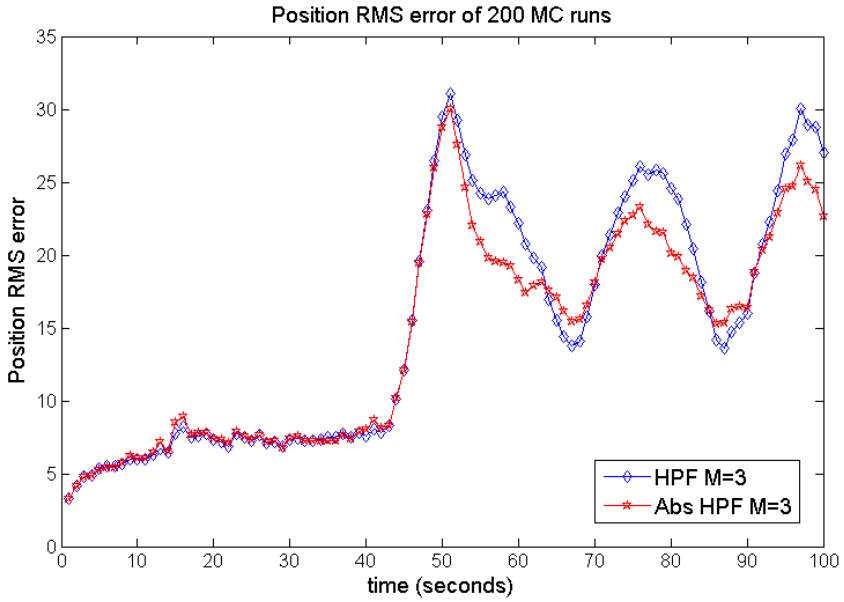

Figure 54: Filter scenario IV, 200 MC runs, $N_p = 5 \cdot 10^3$

9.10 Filter scenario V

The particle filter parameters are $\sigma_a = 0.1g$, $\alpha = 0.9$, $\sigma_m = 30m/s^2$, $\tau_1 = 5000$ and $\tau_2 = 500$. MC simulations containing 200 runs have been performed for the IMM filters and the HPF filters using the models with $M = 2$ and $M = 3$. $N_p = 5 \cdot 10^3$ particles are used in these MC simulations for the HPF filters.

Figure 55 shows the target position RMS error in time for HPF with $M = 2$ and $M = 3$. Both filters show an equally large peak after $40s$. When the target is switching between acceleration and deceleration, HPF with $M = 2$ seems more stable than HPF with $M = 3$.

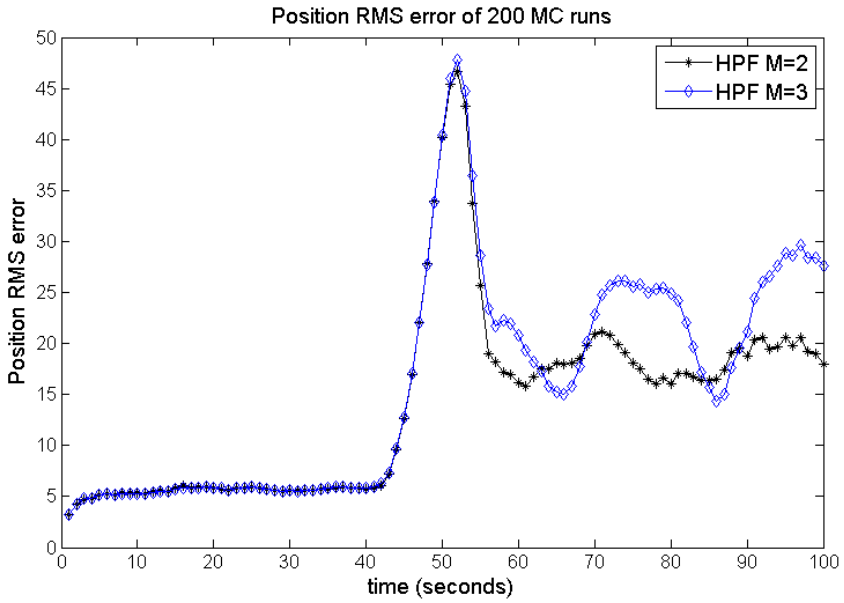

Figure 55: Filter scenario V, 200 MC runs, $N_p = 5 \cdot 10^3$

Figure 56 shows the target position RMS error in time for the IMM filter and the HPF filter with $M = 2$. Both filters seem to perform equally well.

Figure 57 shows the target position RMS error in time for the IMM filter and the HPF filter with $M = 3$. IMM seems to perform better than HPF. When the target is switching between acceleration and deceleration IMM shows smaller peaks than HPF.

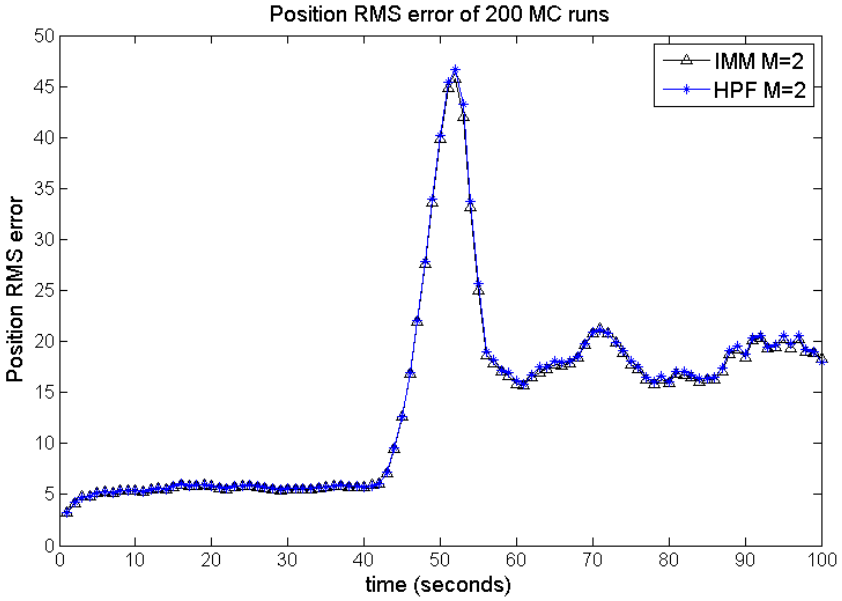

Figure 56: Filter scenario V, 200 MC runs, $N_p = 5 \cdot 10^3$

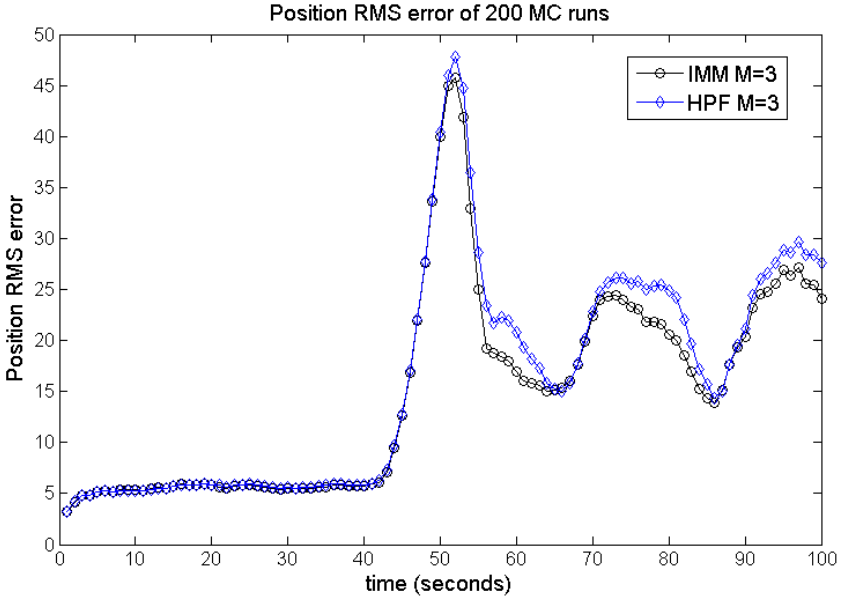

Figure 57: Filter scenario V, 200 MC runs, $N_p = 5 \cdot 10^3$

Figure 58 shows the target position RMS error in time for the IMM filter with $M = 2$ and $M = 3$. When the target is switching between acceleration and deceleration IMM with $M = 2$ seems more stable than IMM with $M = 3$.

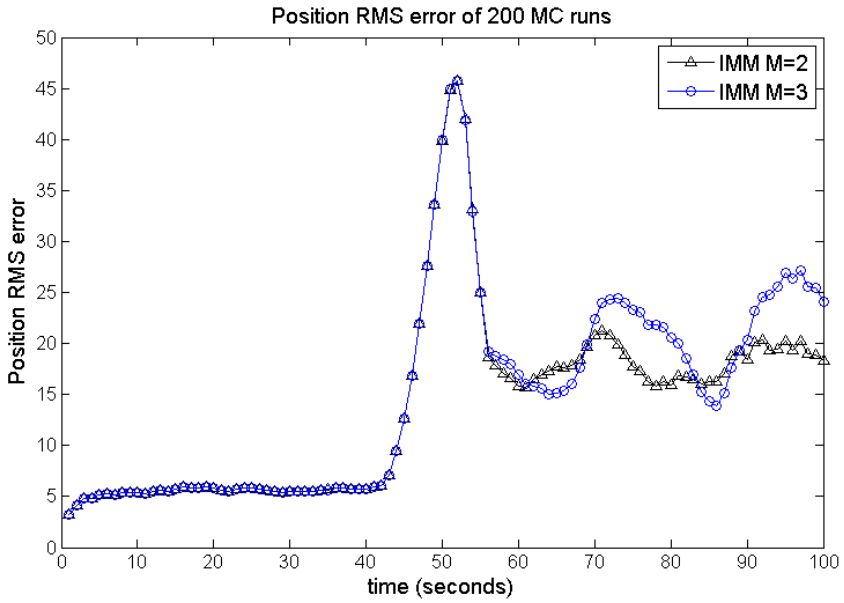

Figure 58: Filter scenario V, 200 MC runs, $N_p = 5 \cdot 10^3$

Figure 59 shows the target position RMS error in time for the HPF filter with $M = 3$ and the HPF filter using the model with non-Gaussian acceleration noise from section 8.4 (denoted by 'Abs HPF M=3'). HPF seems to perform much better than Abs HPF. Furthermore, when the target is switching between acceleration and deceleration Abs HPF peaks when HPF has a low point and HPF peaks when Abs HPF has a low point.

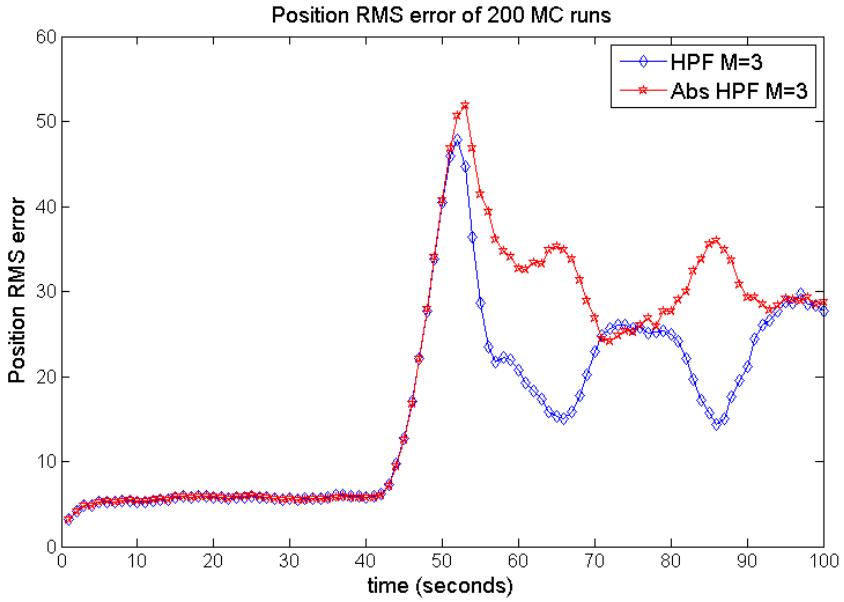

Figure 59: Filter scenario V, 200 MC runs, $N_p = 5 \cdot 10^3$

10 Conclusions and recommendations

In this thesis we investigated the influence of a target motion model on the exact Bayesian filter recursion. The research question is; 'How does the choice for a certain motion model affect the exact Bayesian filter equations?'

10.1 Conclusions

In this thesis we derived the exact Bayesian filter recursions for several target motion models. We used particle filtering to evaluate the Bayesian filter equations numerically. The results of MC simulations were compared with results of IMM MC simulations. In the MC simulations we used several target motion models, several target scenarios and several filter scenarios.

All filters perform relatively well when the target is switching between acceleration and deceleration. That is, the largest peak in position RMS error of all filters in all filter scenarios appears after the target switches from uniform mode to acceleration. The results show no effects of the tracking problems caused by S-turns which we expected.

For all five filter scenarios IMM performs better than HPF. In the first four target scenarios IMM and HPF using the target motion model with three modes perform better than IMM and HPF using the target motion model with two modes. Furthermore, with frequent mode switching and relatively large target acceleration noise (filter scenario I and III), the filters using the model with three modes gave no significant peak in position RMS error when the target was switching between acceleration and deceleration. However, with infrequent mode switching and relatively few target acceleration noise (filter scenario V), the filters using the model with two modes perform better than the filters using the model with three modes.

Then, we showed histograms of accelerations based on an empirical distribution in one Monte Carlo (MC) simulation run with HPF using the model with three modes, of the particles per mode at a specific moment in time. These histograms showed that some particles in deceleration mode have a positive acceleration value. The target motion model permits the target to have a positive acceleration in deceleration mode because the prior deceleration value is assumed to satisfy a Gaussian distribution. Therefore, we tested the HPF filter with another model. This model does not permit the target to have a positive acceleration in deceleration mode (section 8.4). We compared the results of MC simulations of the HPF filter using these two models. In the first four target scenarios the HPF filter using the model of section 8.4 (Abs HPF) performs better than HPF. However, in scenario V Abs HPF performs worse than HPF.

10.2 Recommendations

In this project we used a simple target motion model of three modes that does not permit the target to have a positive acceleration in deceleration mode. We recommend to do further research to make a better target motion model that does not permit the target to have a positive acceleration in deceleration mode.

This project showed that a filter using the target motion model with three modes performs better than a filter using the target motion model with two modes. Future work could be done to increase the amount of modes in the target motion model to increase the performance of the filters.

All scenarios showed the largest peak in position RMS error after $40s$. More research could be done to decrease the hight of this peak. For example by making sure that the position RMS error cannot converge below a certain low value. This could decrease the peak after $40s$.

A Appendix

A.1 Derivation of the formula in equation (23)

$$\begin{aligned}
L &= Q^{-1} - Q^{-1}FS^{-1}F^TQ^{-1} + H^T(GG^T)^{-1}H \\
&= Q^{-1} - Q^{-1}F[F^TQ^{-1}F + \Sigma^{-1}]^{-1}F^TQ^{-1} + H^T(GG^T)^{-1}H \\
&= Q^{-1} - Q^{-1}F\Sigma[F^TQ^{-1}F\Sigma + I]^{-1}F^TQ^{-1} + H^T(GG^T)^{-1}H \\
&= Q^{-1} - Q^{-1}F\Sigma F^TQ^{-1}[F\Sigma F^TQ^{-1} + I]^{-1} + H^T(GG^T)^{-1}H \\
&= \left(Q^{-1}[F\Sigma F^TQ^{-1} + I] - Q^{-1}F\Sigma F^TQ^{-1}\right)[F\Sigma F^TQ^{-1} + I]^{-1} + H^T(GG^T)^{-1}H \\
&= Q^{-1}[F\Sigma F^TQ^{-1} + I]^{-1} + H^T(GG^T)^{-1}H \\
&= [F\Sigma F^T + Q]^{-1} + H^T(GG^T)^{-1}H
\end{aligned} \tag{175}$$

A.2 Derivation of the formula in equation (24)

$$\begin{aligned}
Q^{-1}FS^{-1}\Sigma^{-1}\mu &= Q^{-1}F[F^TQ^{-1}F + \Sigma^{-1}]^{-1}\Sigma^{-1}\mu \\
&= Q^{-1}F\Sigma[F^TQ^{-1}F\Sigma + I]^{-1}\Sigma^{-1}\mu \\
&= Q^{-1}[F\Sigma F^TQ^{-1} + I]^{-1}F\mu \\
&= [F\Sigma F^T + Q]^{-1}F\mu
\end{aligned} \tag{176}$$

A.3 Derivation of the recursive formula in equation (47)

$$\begin{aligned}
& p_{x_{k+1},\theta_{k+1}|Y_{k+1}}(x,\eta) \\
= & \frac{\exp\left\{-\frac{1}{2}[y_{k+1} - h(\eta,x)]^T(g(\eta,x)g(\eta,x)^T)^{-1}[y_{k+1} - h(\eta,x)]\right\}}{c_t\ \mathrm{Det}\left\{2\pi g(x,\eta)g(x,\eta)^T\right\}^{1/2}} \\
& \cdot \int\limits_{x'\in\mathbb{R}^4} \frac{\exp\left\{-\frac{1}{2}[x - a(\eta,x')]^T(b(\eta)Qb(\eta)^T)^{-1}[x - a(\eta,x')]\right\}}{\mathrm{Det}\left\{2\pi b(\eta)Qb(\eta)^T\right\}^{1/2}} \sum_{\theta\in\mathbb{M}} \pi_{\theta\eta}\ \ p_{x_k,\theta_k|Y_k}(x',\theta)dx' \\
= & \int\limits_{x'\in\mathbb{R}^4} \frac{\exp\left\{-\frac{1}{2}[y_{k+1} - h(\eta,x)]^T(g(\eta,x)g(\eta,x)^T)^{-1}[y_{k+1} - h(\eta,x)]\right\}}{c_t\ \mathrm{Det}\left\{2\pi g(x,\eta)g(x,\eta)^T\right\}^{1/2}} \\
& \cdot \frac{\exp\left\{-\frac{1}{2}[x - a(\eta,x')]^T(b(\eta)Qb(\eta)^T)^{-1}[x - a(\eta,x')]\right\}}{\mathrm{Det}\left\{2\pi b(\eta)Qb(\eta)^T\right\}^{1/2}} \sum_{\theta\in\mathbb{M}} \pi_{\theta\eta}\ \ p_{x_k,\theta_k|Y_k}(x',\theta)dx' \\
= & \int\limits_{x'\in\mathbb{R}^4} \frac{\exp\left\{-\frac{1}{2}(r_1 + r_2)\right\}}{c_t\left(\mathrm{Det}\left\{2\pi g(x,\eta)g(x,\eta)^T\right\}\mathrm{Det}\left\{2\pi b(\eta)Qb(\eta)^T\right\}\right)^{1/2}} \sum_{\theta\in\mathbb{M}} \pi_{\theta\eta}\ \ p_{x_k,\theta_k|Y_k}(x',\theta)dx'
\end{aligned} \tag{177}$$

where

$$r_1 = [y_{k+1} - h(\eta, x)]^T (g(\eta, x) g(\eta, x)^T)^{-1} [y_{k+1} - h(\eta, x)] \quad (178)$$

$$r_2 = [x - a(\eta, x')]^T (b(\eta) Q b(\eta)^T)^{-1} [x - a(\eta, x')] \quad (179)$$

B One-dimensional target motion model

Consider the following one-dimensional motion model:

$$x = \begin{bmatrix} s_x & \dot{s}_x & \ddot{s}_x \end{bmatrix}^T \tag{180}$$

with s_x the target position, $\dot{s}_x$ the groundspeed and $\ddot{s}_x$ the target acceleration.

The model will presume that the target moves with (nearly) constant acceleration. Thus $\ddot{s}_x = \rho$ and $\dddot{s}_x = 0$.

When we assume that acceleration $\ddot{s}_x$ is time-invariant, then

$$\dot{x} = \begin{bmatrix} \dot{s}_x & \ddot{s}_x & 0 \end{bmatrix}^T = \begin{bmatrix} 0 & 1 & 0 \\ 0 & 0 & 1 \\ 0 & 0 & 0 \end{bmatrix} x \tag{181}$$

In the discrete-time setting we have:

$$x_k = \begin{bmatrix} s_x(kt_s) & \dot{s}_x(kt_s) & \ddot{s}_x(kt_s) \end{bmatrix} \tag{182}$$

with t_s the sampling time interval. Now x_{k+1} satisfies:

$$x_{k+1} = x_k + \int_{kt_s}^{(k+1)t_s} \dot{x} dt \tag{183}$$

Since $\ddot{s}_x(t) = \rho$, $\dot{s}_x$ satisfies $\dot{s}_x(t) = \dot{s}_x(t_0) + (t - t_0)\rho$.

The difference between x_k and x_{k+1} equals:

$$\begin{aligned} x_{k+1} - x_k &= \int_{kt_s}^{(k+1)t_s} \dot{x}(t) dt \\ &= \int_{kt_s}^{(k+1)t_s} \begin{bmatrix} t_s \dot{s}_x(t_0) + (t - t_0)\rho \\ \rho \\ 0 \end{bmatrix} dt \\ &= \begin{bmatrix} t_s \dot{s}_x(kt_s) + \frac{1}{2} t_s^2 \rho \\ t_s \rho \\ 0 \end{bmatrix} \\ &= \begin{bmatrix} t_s \dot{s}_x(kt_s) + \frac{1}{2} t_s^2 \ddot{s}_x(kt_s) \\ t_s \ddot{s}_x(kt_s) \\ 0 \end{bmatrix} \\ &= \begin{bmatrix} 0 & t_s & \frac{1}{2} t_s^2 \\ 0 & 0 & t_s \\ 0 & 0 & 0 \end{bmatrix} x_k \end{aligned} \tag{184}$$

Now (183) yields:

$$x_{k+1} = x_k + \begin{bmatrix} 0 & t_s & \frac{1}{2}t_s^2 \\ 0 & 0 & t_s \\ 0 & 0 & 0 \end{bmatrix} x_k \tag{185}$$

which we can write as:

$$x_{k+1} = \begin{bmatrix} 1 & t_s & \frac{1}{2}t_s^2 \\ 0 & 1 & t_s \\ 0 & 0 & 1 \end{bmatrix} x_k \tag{186}$$

Define A as:

$$A = \begin{bmatrix} 1 & t_s & \frac{1}{2}t_s^2 \\ 0 & 1 & t_s \\ 0 & 0 & 1 \end{bmatrix} \tag{187}$$

x_{k+1} can now be written as:

$$x_{k+1} = Ax_k \tag{188}$$

In order to represent influence of wind and other uncertainties we add noise. We write $\ddot{s}_x(kt_s) = \rho_k$.

$$\rho_{k+1} = \alpha\rho_k + \frac{1}{2}\sigma_a\sqrt{1-\alpha^2}w_k \tag{189}$$

where w_k is a sequence of i.i.d. standard Gaussian variables of dimension one.

In this way for the mean and covariance of ρ_{k+1} holds:

$$\mathbb{E}(\rho_{k+1}) = \alpha\mathbb{E}(\rho_k) \tag{190}$$

$$Cov(\rho_{k+1}) = \alpha^2 Cov(\rho_k) + \sigma_a^2(1-\alpha^2)Cov(w_k) \tag{191}$$

References

Bagchi, A. [1993]. *Optimal Control of Stochastic Systems*, Prentice Hall.

Berzuini, C., Best, N. G., Gilks, W. R. & Larizza, C. [1997]. Dynamic conditional independence mondels and markov chain monte carlo methods, *Journal of the American Statistical Association* **92**(440): 1403–1412.

Blom, H. A. P. [1985]. An efficient decision-making-free filter for processes with abrupt changes, *Technical report*, National Aerospace Laboratory NLR, 1006 BM Amsterdam, The Netherlands. Presented at the 7th IFAC Symposium on Identification and System Parameter Estimation, York, United Kingdom.

Blom, H. A. P. [1986]. Overlooked potential of systems with markovian coefficients, *IEEE 25th Conference on Decision and Control*, 1006 BM Amsterdam, The Netherlands.

Blom, H. A. P. [1990]. *Bqyesian estimation for decision-directed stochastic control*, PhD thesis, Delft University of Technology, ISBN 90-9003366-1.

Blom, H. A. P. & Bar-Shalom, Y. [2009]. Bayesian filtering of stochastic hybrid systems in discrete-time and interacting multiple model. Eds. B. Rozovsky and D. Crisan, Oxford Handbook on Nonlinear Filtering, Forthcoming.

Blom, H. A. P. & Bloem, E. A. [2007]. Exact Bayesian and particle filtering of stochastic hybrid systems, *IEEE Transactions on aerospace and electronic systems* **43**: 55–70.

Doucet, A. [1998]. On sequential simulation-based methods for bayesian filtering, *Technical Report CUED/F-INFENG/TR.310*, Cambridge University, Cambridge, UK. Signal Processing Group, Department of Engineering.

Gordon, N. J., Salmond, D. J. & Smith, A. [1993]. Novel approach to nonlinear/non-gaussian bayesian state estimation, *IEE Proceedings F* **140**: 107–113.

Ross, S. M. [1996]. *Stochastic Processes*, second edn, John Wiley and sons, inc.

van der Merwe, R., Doucet, A., de Freitas, N. & Wan, E. [2000]. The unscented particle filter, *in* T. G. Dietterich, T. K. Leen & V. Tresp (eds), *Advances in Neural Information Processing*, ...

van der Valk, J. J. [2009]. Modelling of target movement. Report of internship at National Aerospace Laboratory in Amsterdam, the Netherlands.